

GEORG-AUGUST-UNIVERSITÄT GÖTTINGEN

On the influence of morphological operators
on testing for a region of interest

A THESIS SUBMITTED FOR THE DEGREE OF MASTER OF
SCIENCE IN MATHEMATICS

Author:

Dominik BLANK

Examiners:

Prof. Dr. Axel MUNK

Dr. Robin RICHTER

Göttingen, September 3, 2020

Abstract

Morphological operations play an important role in fingerprint recognition. In this thesis, we quantify their impact for a simplified statistical model.

Contents

List of symbols	2
1 Introduction	3
2 Testing for a rectangular region of interest	9
2.1 Definitions	9
2.2 Statistical model	11
2.3 Bound for the probability of a type I error	14
2.4 Analysis of the probability of a type II error	21
3 Binary morphological operations	28
3.1 Definition of opening & closing	29
3.2 Examples	36
4 Main results	38
5 Simulation results	51
6 Discussion	59
References	60
A Additional proofs	62
B Simulations	68
C Algorithms	75

List of symbols

$\mathbb{R}^{m \times n}$	Set of real m -by- n matrices
$\{0, 1\}^{m \times n}$	Set of binary m -by- n matrices
$\mathcal{V}_c^{m,n}$	Set of matrices in $\{-c, 0, +c\}^{m \times n}$, that contain a rectangular region of interest with a chessboard pattern
$\mathcal{H}_0(i, j)$	Set of matrices in $\mathcal{V}_c^{m,n}$, such that the null hypothesis at (i, j) is true
$\mathcal{H}_1(i, j)$	Set of matrices in $\mathcal{V}_c^{m,n}$, such that the alternative hypothesis at (i, j) is true
Δ^+, Δ^-	Forward and backward discrete derivative operator
F, V, \dots	Matrices in $\mathbb{R}^{m \times n}$
$\mathfrak{I}, \mathfrak{K}, \dots$	Matrices in $\{0, 1\}^{m \times n}$
$\Omega, \Lambda, \Theta, \dots$	Subsets of \mathbb{Z}^2
Ψ, Φ, \dots	Structuring elements, subsets of \mathbb{Z}^2
$\ \cdot\ $	Euclidean norm, ℓ^2 -norm
\ominus, \oplus	Morphological erosion & dilation operator
\circ, \bullet	Morphological opening & closing operator

1 Introduction

Fingerprint analysis has played an important role in biometric identification for more than a century with a variety of applications ranging from border control to smartphone development [Hen00]. By comparing the characteristic features of two fingerprints, called minutiae, the likelihood of them originating from the same individual can be determined. Complementary to the study of matching algorithms, the usage of image preprocessing techniques to improve the performance of these matching algorithms has become a beneficial field of study. One important preprocessing step of many automated matching algorithms is the extraction of the so-called *region of interest* (ROI) of the fingerprint aiming at dividing a given fingerprint image into the ROI or foreground, that contains the fingerprint and thus the minutia, and the background containing no information about the fingerprint, see [Mal+09]. Automated extraction of the ROI is often achieved by the use of thresholding methods, see [THG16], and morphological operators, see [THG16; BG01; Liu+11]. While the thresholding methods provide a binarization of the image to categorize pixels into ROI and background, the use of morphological operators aims at minimizing errors, such as falsely classifying a background pixel as ROI or vice versa. The usage of these morphological operators relies on prior information of the fingerprint image, such as convexity and oscillatory behaviour within the ROI.

We interpret the thresholding techniques via statistical testing. When thresholding, one usually applies an operator to the image and compares the outcome to a threshold, for an example see [AB96]. This is the same procedure as calculating a test statistic and performing a one- or two-sided hypothesis test. In this sense, falsely classifying a background pixel as a foreground pixel and vice versa can be seen as a type I and II error of a statistical test. Considering this interpretation, the application of morphological operators is an attempt to lower the error rates of the statistical test.

The interplay of thresholding techniques with post-processing via morphological operators, incorporating prior knowledge, has, to the best of the author's knowledge, not been addressed. This thesis aims at providing a first step to-

wards understanding this interplay by assessing the change of error rates through application of morphological operators.

In a simplified scenario, we analyze the impact of morphological operators on the upper bounds for the error probabilities. The focus lies on the probabilities of misclassifying a single pixel. We restrict our assessment to the application of morphological opening and closing, since these operators only rely on a neighbourhood of the specific pixel we are considering, making their effect easy to understand.

The model is given by an image with constant gray background and a rectangular region of interest with a chessboard pattern, see Figure 1. The model exhibits convexity of the ROI and an oscillatory pattern within the ROI, as in a fingerprint image, and thus can be viewed as a toy example of a fingerprint. Notably, we are interested in the change of the error probabilities for a specific pixel. Hence, we do not consider methods to test for the whole rectangle, but develop a test for each pixel to decide whether or not it is part of the rectangular region of interest. As an example, testing for the corners of the rectangle might offer better power, when trying to determine the rectangular ROI, but such an approach does not generalize to fingerprint images.

The statistical model Let $m, n \in \mathbb{N}$ and $c \in \mathbb{R} \setminus \{0\}$. We assume a noisy image following the statistical model

$$F(i, j) = \underbrace{c + V(i, j)}_{=: \tilde{V}(i, j)} + \varepsilon_{i, j} \quad (1.1)$$

for all $(i, j) \in \Omega := \{1, \dots, m\} \times \{1, \dots, n\}$. The values of V alternate between c and $-c$ along the rows and columns of the region of interest. The noise terms $\varepsilon_{i, j} \sim \mathcal{N}(0, \sigma^2)$ are assumed to be i.i.d. normally distributed random variables for some $\sigma > 0$.

For visualization we use grayscale images and set $c = 127.5$. Then the values of the image \tilde{V} alternate between 0 (black) and 255 (white) within the region of interest. This gives the region of interest of \tilde{V} a classical chessboard pattern, see Figure 1 for an example.

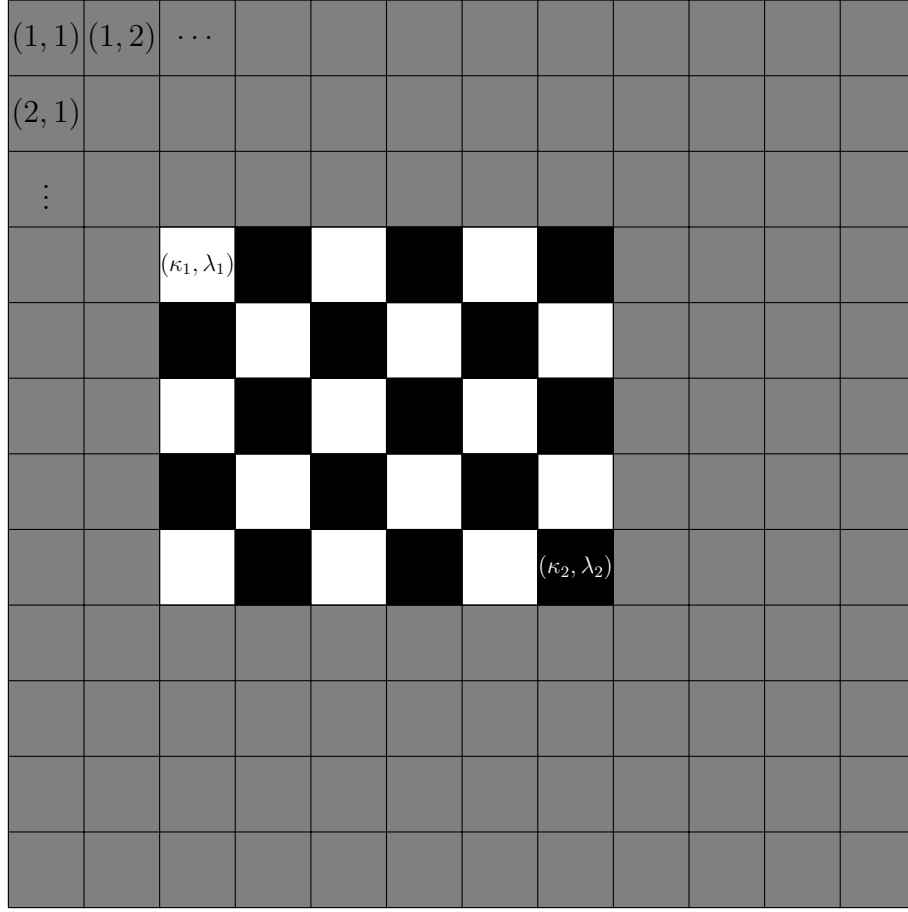


Figure 1: Example of a matrix \tilde{V} as in the statistical model 1.1, that contains a ROI with a chessboard pattern. The top left corner of the ROI is $(4, 3)$ and the bottom right corner is $(8, 8)$. Here we have $m = n = 12$.

Notably, we make two simplifications in our statistical model. First, we assume the variance σ of the noise terms to be known beforehand. Second, we ignore the limitations of grayscale images and let the images in our model take all values in the real numbers. When trying to restore a ROI from an actual grayscale fingerprint image, the image, and thus the observed data F , would only take values in $\{0, \dots, 255\}$.

The goal is to develop a statistical test for every pixel to determine whether or not the pixel belongs to the region of interest of V and as such reconstructing the unknown V from the noisy data. Choosing a chessboard pattern admits the use of the discrete derivative operator for the statistical test.

As shown in Section 2.2, the pixel (i, j) belonging to the ROI is equivalent to $\min\{\|\Delta^+ V(i, j)\|, \|\Delta^- V(i, j)\|\} \neq 0$, where $\|\cdot\|$ is the Euclidean norm and Δ^+ and Δ^- denote the forward and backward discrete derivative operator, respectively. Based on this observation, we use

$$T(i, j) := \min\{\|\Delta^+ F(i, j)\|, \|\Delta^- F(i, j)\|\}$$

as a test statistic to test the null hypothesis $H_0(i, j)$, stating that (i, j) does not belong to the ROI of V , against the alternative hypothesis $H_1(i, j)$, stating that (i, j) does belong to the ROI of V . We reject the null hypothesis, if the test statistic is greater than or equal to a given threshold. This is done for each pixel $(i, j) \in \Omega$.

In Section 2.3 we study the choice of a suitable threshold t_α , that bounds the probability of a type I error in this testing procedure below a given statistical significance $\alpha \in (0, 1)$. We achieve this by bounding the distribution of the test statistic under the null hypothesis by the cumulative distribution function of a non-central Chi distributed random variable with normally distributed non-centrality parameter, see Lemma 2.6. This yields a compound probability distribution, which we compute in Theorem 2.8. By employing a trial and error algorithm, we find a threshold t_α , such that the probability of falsely categorizing a background pixel as a foreground pixel is smaller than a given statistical significance $\alpha \in (0, 1)$.

Furthermore, we numerically generate bounds for the probability of a type II error in Section 2.4.

Main results We aim at researching the changes of the upper bounds of the error probabilities under morphological opening and closing. These morphological operations require the choice of a subset of \mathbb{Z}^2 , called a *structuring element*, see [Shi10]. As the region of interest in our case is rectangular, we use a square structuring element.

In Theorem 4.1 we show, that using such a square structuring element yields an exponential improvement of the upper bound of the probability of a type I error after morphological opening compared to the upper bound before

opening is applied, see inequality (4.1). Applying morphological closing after opening will worsen this bound, but only polynomially, see inequality (4.3). On the other hand, the upper bound, when only applying closing to the outcome of the statistical test, becomes a multiple of the upper bound before closing, see inequality (4.2). Overall, we obtain a better upper bound for the probability of a type I error, when applying morphological opening or opening and closing. When applying morphological closing, the upper bound worsens. These results allow us to adjust the statistical significance used for the statistical test, such that the probability of a type I error after morphological operations have been applied, is bounded below a given statistical significance $\alpha \in (0, 1)$ in any of these cases. Details on these adjustments as well as simulation results can be found in Section 5.

The question of bounding the probability of a type II error after morphological opening and closing also arises. Upper bounds are given in Theorem 4.4. It turns out, morphological opening increases the upper bound of this probability polynomially, see (4.4). The application of morphological closing, when applied after opening, does not improve the upper bound, since independence of the pixels is not guaranteed anymore, see (4.6). When only morphological closing is applied, the upper bound does not change, see (4.5). Note, that all upper bounds in these theorems are independent of the specific (i, j) . This means, that the bounds also hold for the worst case, i.e. pixels directly at the transition from background to foreground.

These results are only upper bounds for the error probabilities. To examine the actual change of the probabilities, we perform a simulation to calculate empiric error rates in Section 5. We simulate six different positions of (i, j) with respect to the region of interest, see Figure 10, and use adjusted statistical significances as described above.

Outlook The region of interest in this simplified model is convex and has an oscillatory pattern, similar to a fingerprint image. We use the discrete derivative operator to binarize the image and proceed by applying morphological opening and closing.

The results presented in this thesis do not simply carry over to fingerprints.

How the error probabilities can be bounded as well as how a structuring element should be chosen are questions that need to be explored.

Furthermore, we only consider bounds for single pixels. A next step should involve methods from the field of multiple testing to consider the simultaneous test of all pixels in the image.

Outline of the thesis In Section 2.1 we introduce definitions and notation of the aforementioned images and properties. With the introduced terminology we develop a statistical test for every pixel determining whether or not it is part of the region of interest in Section 2.2. After having established the statistical test, we proof in Section 2.3 that we can bound the probability of a type I error by a given statistical significance and analyze the probability of a type II error in the statistical test in Section 2.4. In Section 3 the two morphological operators, that we study in this thesis, are introduced, along with some examples of their application. From there, we proceed to proof the main theorems of this thesis in Section 4. We compare our theoretical results to simulations in Section 5 and discuss possible further research in Section 6.

2 Testing for a rectangular region of interest

2.1 Definitions

Assume that the noise-free image V in our statistical model has a rectangular region of interest with a chessboard pattern, cf. equation (1.1) and Figure 1. In the following we give a formal definition of this setup.

Definition 2.1. Let $m, n \in \mathbb{N}$, $c \in \mathbb{R} \setminus \{0\}$ and $V \in \{-c, 0, +c\}^{m \times n}$. We say that V contains a *rectangular region of interest with a chessboard pattern*, if

$$V(i, j) = \begin{cases} c, & \text{if } (i, j) \in \{\kappa_1, \dots, \kappa_2\} \times \{\lambda_1, \dots, \lambda_2\} \text{ and } i + j \equiv \kappa_1 + \lambda_1 \pmod{2} \\ -c, & \text{if } (i, j) \in \{\kappa_1, \dots, \kappa_2\} \times \{\lambda_1, \dots, \lambda_2\} \text{ and } i + j \not\equiv \kappa_1 + \lambda_1 \pmod{2} \\ 0, & \text{if } (i, j) \notin \{\kappa_1, \dots, \kappa_2\} \times \{\lambda_1, \dots, \lambda_2\} \end{cases} \quad (2.1)$$

for some $(\kappa_1, \lambda_1), (\kappa_2, \lambda_2) \in \mathbb{N}^2$ with $1 < \kappa_1 \leq \kappa_2 < m$ and $1 < \lambda_1 \leq \lambda_2 < n$ and all $(i, j) \in \{1, \dots, m\} \times \{1, \dots, n\}$. The set of all such V is denoted by $\mathcal{V}_c^{m,n}$.

We call $\Lambda = \{\kappa_1, \dots, \kappa_2\} \times \{\lambda_1, \dots, \lambda_2\}$ a *rectangular region of interest (ROI)* and say that V contains the ROI Λ .

Furthermore, we call (κ_1, λ_1) the *top left corner* and (κ_2, λ_2) the *bottom right corner* of Λ .

Hence, the top left corner of the region of interest of V takes the value c and then the values of V alternate between $+c$ and $-c$ along the rows and columns of the region of interest. This is similar to the classical chessboard pattern.

Remark 2.2. Any matrix $V \in \mathcal{V}_c^{m,n}$ is uniquely defined by the top left and bottom right corner of Λ .

Remark 2.3. To adjust for boundary issues, we use a periodic boundary condition, i.e. we extend V to all of \mathbb{Z}^2 by setting $V(i, j) = V(i \bmod m, j \bmod n)$ for all $(i, j) \in \mathbb{Z}^2$. We also require there to be at least one pixel distance between the ROI and the edge of the image.

In Figure 1 we see an example of such a matrix. To visualize these types of matrices, we would have $c = 127.5$ and plot the grayscale image $V + c$. Thus, gray pixels represent $V = 0$, white pixels represent $V = c$ and black pixels represent $V = -c$. We use notation from the field of image processing and start indexing at the top left corner of the image.

We also need the forward and backward discrete derivative operator, whose definitions we give below, to establish our statistical test.

Definition 2.4. Let $m, n \in \mathbb{N}$ and let $V \in \mathbb{R}^{m \times n}$. Define the set of possible indices $\Omega := \{1, \dots, m\} \times \{1, \dots, n\}$. Let $(i, j) \in \Omega$. The *forward and backward discrete derivative of V evaluated at (i, j)* are defined as

$$\Delta^+ V(i, j) = \begin{pmatrix} V(i+1, j) - V(i, j) \\ V(i, j+1) - V(i, j) \end{pmatrix} \quad (2.2)$$

and

$$\Delta^- V(i, j) = \begin{pmatrix} V(i-1, j) - V(i, j) \\ V(i, j-1) - V(i, j) \end{pmatrix}, \quad (2.3)$$

respectively.

The following lemma shows, that the Euclidean norm of these operators evaluated at a pixel $(i, j) \in \Omega$ for matrices $V \in \mathcal{V}_c^{m,n}$ can only take specific values.

Lemma 2.5. Let $m, n \in \mathbb{N}$ and $c \in \mathbb{R} \setminus \{0\}$. Let $V \in \mathcal{V}_c^{m,n}$. For any $(i, j) \in \Omega$ we have

$$\|\Delta^+ V(i, j)\|, \|\Delta^- V(i, j)\| \in \{0, c, \sqrt{2}c, \sqrt{5}c, \sqrt{8}c\}, \quad (2.4)$$

where $\|\cdot\|$ denotes the ℓ^2 -norm.

Proof. Let $(i, j) \in \Omega$. By assumption, $V \in \mathcal{V}_c^{m,n}$. Thus, V only takes values in $\{-c, 0, +c\}$ and we obtain $\Delta^+ V(i, j), \Delta^- V(i, j) \in \{-2c, -c, 0, +c, +2c\}^2$. Taking the Euclidean norm of all possible combinations yields

$$\|\Delta^+ V(i, j)\|, \|\Delta^- V(i, j)\| \in \{0, c, 2c, \sqrt{2}c, \sqrt{5}c, \sqrt{8}c\}.$$

Position of pixels $(i, j), (i+1, j), (i, j+1)$	$ V(i+1, j) - V(i, j) $	$ V(i, j+1) - V(i, j) $	$\ \Delta^+ V(i, j)\ $
$(i, j), (i+1, j), (i, j+1) \notin \Lambda$	0	0	0
$(i, j), (i+1, j) \notin \Lambda$ and $(i, j+1) \in \Lambda$	0	c	c
$(i, j), (i, j+1) \notin \Lambda$ and $(i+1, j) \in \Lambda$	c	0	c
$(i, j) \in \Lambda$ and $(i+1, j), (i, j+1) \notin \Lambda$	c	c	$\sqrt{2}c$
$(i, j), (i+1, j) \in \Lambda$ and $(i, j+1) \notin \Lambda$	$2c$	c	$\sqrt{5}c$
$(i, j), (i, j+1) \in \Lambda$ and $(i+1, j) \notin \Lambda$	c	$2c$	$\sqrt{5}c$
$(i, j), (i+1, j), (i, j+1) \in \Lambda$	$2c$	$2c$	$\sqrt{8}c$

Table 1: Possible locations of the pixels (i, j) , $(i+1, j)$, $(i, j+1)$ and the corresponding values of $|V(i+1, j) - V(i, j)|$, $|V(i, j+1) - V(i, j)|$ and $\|\Delta^+ V(i, j)\|$, respectively. See Figure 2 for a visualization of these cases.

We can narrow this list down even more. By assumption, V contains a rectangular region of interest Λ with a chessboard pattern. This only allows for the combinations of $|V(i+1, j) - V(i, j)|$ and $|V(i, j+1) - V(i, j)|$ listed in Table 1.

Other cases are not possible and thus $\|\Delta^+ V(i, j)\| \in \{0, c, \sqrt{2}c, \sqrt{5}c, \sqrt{8}c\}$. By analogous deduction, we also obtain $\|\Delta^- V(i, j)\| \in \{0, c, \sqrt{2}c, \sqrt{5}c, \sqrt{8}c\}$.

□

2.2 Statistical model

Let $m, n \in \mathbb{N}$, $c \in \mathbb{R} \setminus \{0\}$ and $\Omega = \{1, \dots, m\} \times \{1, \dots, n\}$. Assume we are given noisy data

$$F(i, j) = c + V(i, j) + \varepsilon_{i,j} \quad (2.5)$$

for all $(i, j) \in \Omega$, where $V \in \mathcal{V}_c^{m,n}$ is unknown and $\varepsilon_{i,j} \sim \mathcal{N}(0, \sigma^2)$ are i.i.d. normal distributed random variables for some $\sigma > 0$.

Let Λ be the rectangular region of interest contained in the above V . In the following we specify a statistical test to determine for each individual pixel whether $(i, j) \in \Lambda$ or $(i, j) \notin \Lambda$.

By the assumption, that V contains a rectangular ROI, it follows, that $V(i, j) = 0$ if and only if $(i, j) \notin \Lambda$. Let (κ_1, λ_1) and (κ_2, λ_2) be the top left and bottom right corner of Λ , respectively. Now, if $(i, j) \notin \Lambda$, it follows that $i \notin \{\kappa_1, \dots, \kappa_2\}$ or $j \notin \{\lambda_1, \dots, \lambda_2\}$. We have to distinguish four cases here, which are visualized in Figure 3:

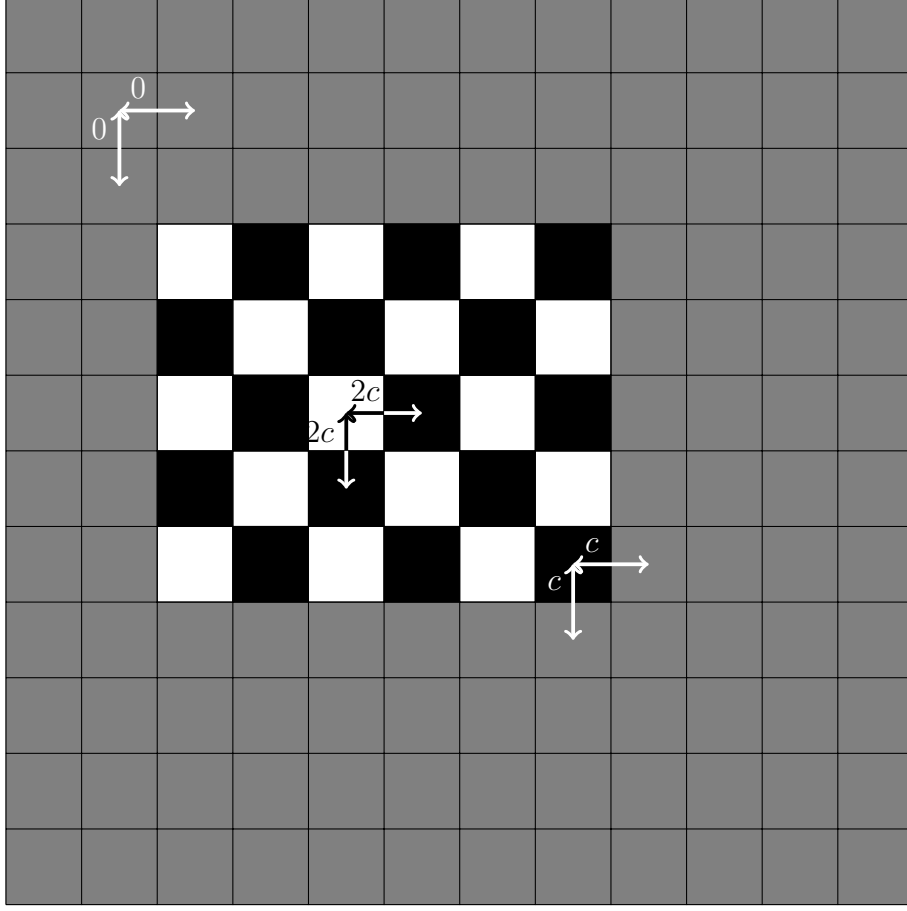


Figure 2: Possible values of $|V(i+1, j) - V(i, j)|$ and $|V(i, j+1) - V(i, j)|$ as listed in Table 1.

- (I) $i < \kappa_1 \Rightarrow (i, j-1) \notin \Lambda$ and $(i-1, j) \notin \Lambda$
 $\Rightarrow V(i, j-1) = V(i-1, j) = 0$
- (II) $j < \lambda_1 \Rightarrow (i-1, j) \notin \Lambda$ and $(i, j-1) \notin \Lambda$
 $\Rightarrow V(i-1, j) = V(i, j-1) = 0$
- (III) $i > \kappa_2 \Rightarrow (i, j+1) \notin \Lambda$ and $(i+1, j) \notin \Lambda$
 $\Rightarrow V(i, j+1) = V(i+1, j) = 0$
- (IV) $j > \lambda_2 \Rightarrow (i+1, j) \notin \Lambda$ and $(i, j+1) \notin \Lambda$
 $\Rightarrow V(i+1, j) = V(i, j+1) = 0$

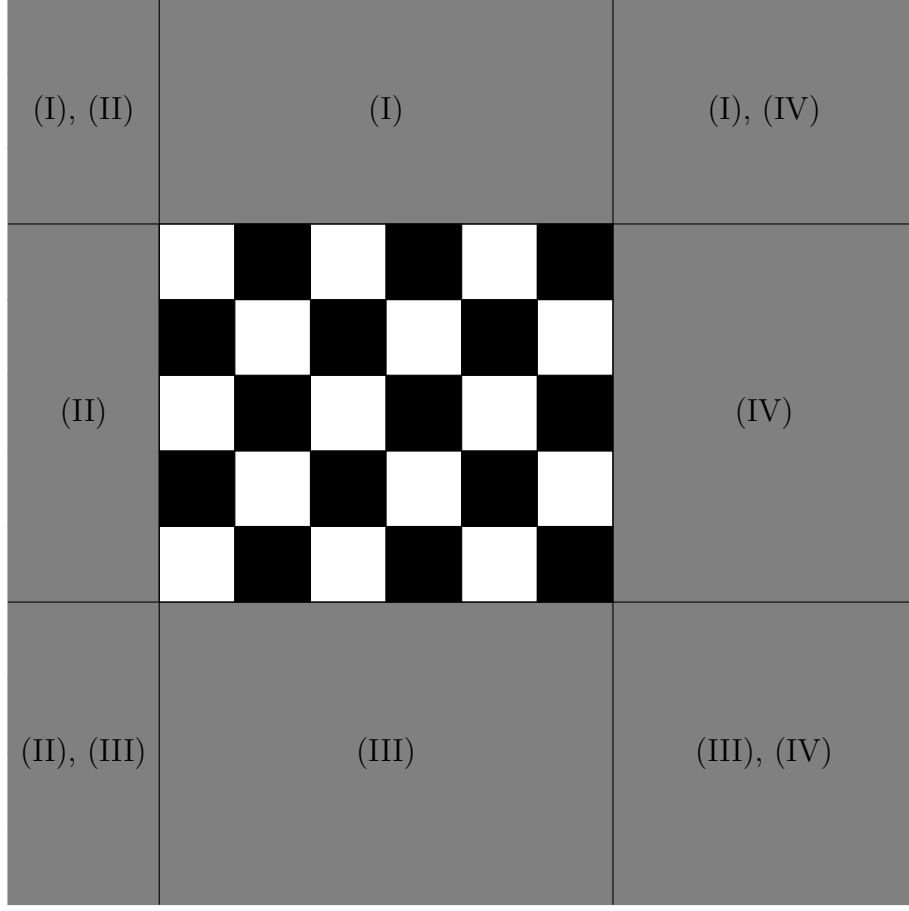


Figure 3: Depiction of the regions, for which the cases (I) - (IV) hold. Every background pixel belongs to at least one of these regions.

From now on, $\|\cdot\|$ always denotes the ℓ^2 -norm. We have $\|\Delta^-V(i, j)\| = 0$ in the first two cases and $\|\Delta^+V(i, j)\| = 0$ in the latter two cases. Thus, $(i, j) \notin \Lambda$ implies $\min\{\|\Delta^+V(i, j)\|, \|\Delta^-V(i, j)\|\} = 0$.

On the other hand, we have assumed, that Λ has a chessboard pattern. Thus $\|\Delta^-V(i, j)\|, \|\Delta^+V(i, j)\| \neq 0$ for $(i, j) \in \Lambda$. This yields the equivalence

$$(i, j) \notin \Lambda \Leftrightarrow \min\{\|\Delta^+V(i, j)\|, \|\Delta^-V(i, j)\|\} = 0.$$

Using this equivalence, we test for each individual pixel (i, j) the null hypothesis

$$H_0(i, j) : (i, j) \notin \Lambda \tag{2.6}$$

against the alternative hypothesis

$$H_1(i, j) : (i, j) \in \Lambda \quad (2.7)$$

using the test statistic

$$T(i, j) := \min\{\|\Delta^+ F(i, j)\|, \|\Delta^- F(i, j)\|\}, \quad (2.8)$$

which is based on the given noisy data.

To extract the ROI, we classify pixels as foreground, if we reject the null hypothesis, i.e. if $T(i, j) \geq t$ for some threshold $t \in \mathbb{R}^+$. The choice of the threshold is examined in Section 2.3.

For convenience, we want to define some subsets of $\mathcal{V}_c^{m,n}$, such that $(i, j) \notin \Lambda$. For every $(i, j) \in \Omega$ we define the set of images, for which the null hypothesis $H_0(i, j)$ is true as

$$\mathcal{H}_0(i, j) := \left\{ V \in \mathcal{V}_c^{m,n} \mid \min\{\|\Delta^+ V(i, j)\|, \|\Delta^- V(i, j)\|\} = 0 \right\}. \quad (2.9)$$

Then $H_0(i, j)$ is true, if and only if $V \in \mathcal{H}_0(i, j)$. Furthermore, we define two subsets of this set as

$$\mathcal{H}_0^+(i, j) := \left\{ V \in \mathcal{V}_c^{m,n} \mid \|\Delta^+ V(i, j)\| = 0 \right\}, \quad (2.10)$$

$$\mathcal{H}_0^-(i, j) := \left\{ V \in \mathcal{V}_c^{m,n} \mid \|\Delta^- V(i, j)\| = 0 \right\}. \quad (2.11)$$

Then $\mathcal{H}_0(i, j) = \mathcal{H}_0^+(i, j) \cup \mathcal{H}_0^-(i, j)$, where the union is usually not disjoint, except for pixels on the boundary of the ROI.

2.3 Bound for the probability of a type I error

Having established our hypotheses and test statistic, we want to examine the choice of the threshold $t \in \mathbb{R}^+$ in the testing procedure. We reject the null hypothesis, if $T(i, j) \geq t$ for some threshold $t \in \mathbb{R}^+$. We want to choose t such, that the probability of falsely classifying a background pixel as foreground is bounded from above by a given statistical significance

$\alpha \in (0, 1)$. Such a threshold will be denoted as t_α .

We use the notation $\mathbb{P}_V(\dots)$ for the probability of an event for some *fixed* image V . This will allow us to analyze the probabilities of falsely categorizing a pixel. Using this notation, we want to find a threshold t_α , such that $\mathbb{P}_V(T(i, j) \geq t_\alpha) \leq \alpha$ for every $V \in \mathcal{H}_0(i, j)$. A first step towards finding such a threshold is the following lemma.

Lemma 2.6. *Let $(i, j) \in \Omega$ and $t \in \mathbb{R}^+$. Assume that F follows the statistical model given in (2.5) and let $T(i, j)$ be defined as in (2.8). Let $V \in \mathcal{V}_c^{m,n}$. Then*

$$\mathbb{P}_V(T(i, j) \geq t) \leq \min \left\{ \mathbb{P}_V(\|\Delta^+ F(i, j)\| \geq t), \mathbb{P}_V(\|\Delta^- F(i, j)\| \geq t) \right\}. \quad (2.12)$$

Proof. Let $t \in \mathbb{R}^+$. We have

$$\begin{aligned} \mathbb{P}_V(T(i, j) \geq t) &= \mathbb{P}_V(\min\{\|\Delta^+ F(i, j)\|, \|\Delta^- F(i, j)\|\} \geq t) \\ &= \mathbb{P}_V(\{\|\Delta^+ F(i, j)\| \geq t\} \cap \{\|\Delta^- F(i, j)\| \geq t\}) \\ &\leq \mathbb{P}_V(\|\Delta^+ F(i, j)\| \geq t). \end{aligned}$$

Analogously, we obtain

$$\mathbb{P}_V(T(i, j) \geq t) \leq \mathbb{P}_V(\|\Delta^- F(i, j)\| \geq t).$$

Combining these two inequalities yields the result and thus finishes the proof of the lemma. \square

The second step is given in the following theorem, where we calculate the cumulative distribution functions of $\mathbb{P}_V(\|\Delta^+ F(i, j)\| \leq t)$ for $V \in \mathcal{H}_0^+(i, j)$ and $\mathbb{P}_V(\|\Delta^- F(i, j)\| \leq t)$ for $V \in \mathcal{H}_0^-(i, j)$, which turn out to be the same. This cumulative distribution function involves the Marcum Q -function. For $M \geq 1$, it is defined as

$$Q_M(a, b) = \int_b^\infty x \left(\frac{x}{a}\right)^{M-1} \exp\left(-\frac{x^2 + a^2}{2}\right) I_{M-1}(ax) dx.$$

Remark 2.7. The cumulative distribution function of a non-central chi dis-

tributed random variable with k degrees of freedom and non-centrality parameter λ is given by $1 - Q_{\frac{k}{2}}(\lambda, x)$.

Theorem 2.8. *Let $(i, j) \in \Omega$ and $t \in \mathbb{R}^+$. Assume that F follows the statistical model given in (2.5). Let $V_1 \in \mathcal{H}_0^+(i, j)$ and $V_2 \in \mathcal{H}_0^-(i, j)$. Then*

$$\mathbb{P}_{V_1}(\|\Delta^+ F(i, j)\| \leq t) = p_\sigma(t) = \mathbb{P}_{V_2}(\|\Delta^- F(i, j)\| \leq t) \quad (2.13)$$

where

$$\begin{aligned} p_\sigma(t) := & \frac{1}{\sqrt{3}} \left(\frac{3}{2} - \frac{3}{2} \exp\left(-\frac{t^2}{3\sigma^2}\right) I_0\left(\frac{t^2}{6\sigma^2}\right) \right) - \sqrt{3} \\ & - \frac{2 - \sqrt{3}}{2} Q_1\left(\sqrt{\frac{2 - \sqrt{3}}{6}} \frac{t}{\sigma}, \sqrt{\frac{2 + \sqrt{3}}{6}} \frac{t}{\sigma}\right) \\ & + \frac{2 + \sqrt{3}}{2} Q_1\left(\sqrt{\frac{2 + \sqrt{3}}{6}} \frac{t}{\sigma}, \sqrt{\frac{2 - \sqrt{3}}{6}} \frac{t}{\sigma}\right) \end{aligned} \quad (2.14)$$

with I_0 being the modified Bessel function of the first kind [GR07, p. 910-911] and Q_1 denoting the Marcum Q_1 -function [Nut74].

Proof. We start by proving the first equality of equation (2.13). By assumption, $V_1 \in \mathcal{H}_0^+(i, j)$ and thus $\|\Delta^+ V_1(i, j)\| = 0$. By definition of Δ^+ we get the equivalence

$$\|\Delta^+ V_1(i, j)\| = 0 \Leftrightarrow V_1(i + 1, j) - V_1(i, j) = V_1(i, j + 1) - V_1(i, j) = 0.$$

We expand the term $\mathbb{P}_{V_1}(\|\Delta^+ F(i, j)\| \leq t)$, which we call $q(t)$, and use the equivalence above to obtain

$$\begin{aligned} q(t) &:= \mathbb{P}_{V_1}(\|\Delta^+ F(i, j)\| \leq t) \\ &= \mathbb{P}_{V_1}\left((c + V_1(i + 1, j) + \varepsilon_{i+1,j} - c - V_1(i, j) - \varepsilon_{i,j})^2 \right. \\ &\quad \left. + (c + V_1(i, j + 1) + \varepsilon_{i,j+1} - c - V_1(i, j) - \varepsilon_{i,j})^2 \leq t^2\right) \\ &= \mathbb{P}_{V_1}\left((\varepsilon_{i+1,j} - \varepsilon_{i,j})^2 + (\varepsilon_{i,j+1} - \varepsilon_{i,j})^2 \leq t^2\right) \\ &= \mathbb{P}\left((\varepsilon_{i+1,j} - \varepsilon_{i,j})^2 + (\varepsilon_{i,j+1} - \varepsilon_{i,j})^2 \leq t^2\right) \\ &= \mathbb{P}\left(\sqrt{(\varepsilon_{i+1,j} - \varepsilon_{i,j})^2 + (\varepsilon_{i,j+1} - \varepsilon_{i,j})^2} \leq t\right) \end{aligned}$$

where we dropped the index V_1 , since the probability does no longer depend on the chosen V_1 .

To proceed, we need to determine the distribution of the random variable $\sqrt{(\varepsilon_{i+1,j} - \varepsilon_{i,j})^2 + (\varepsilon_{i,j+1} - \varepsilon_{i,j})^2}$ conditioned on $\varepsilon_{i,j} = \epsilon$ for some fixed $\epsilon \in \mathbb{R}$. We define the random variables

$$\begin{aligned} X_1 &= \varepsilon_{i+1,j} - \epsilon \sim \mathcal{N}(-\epsilon, \sigma^2), \\ X_2 &= \varepsilon_{i,j+1} - \epsilon \sim \mathcal{N}(-\epsilon, \sigma^2) \end{aligned}$$

and obtain

$$\begin{aligned} &\mathbb{P}\left(\sqrt{(\varepsilon_{i+1,j} - \varepsilon_{i,j})^2 + (\varepsilon_{i,j+1} - \varepsilon_{i,j})^2} \leq t \mid \varepsilon_{i,j} = \epsilon\right) \\ &= \mathbb{P}\left(\sqrt{(\varepsilon_{i+1,j} - \epsilon)^2 + (\varepsilon_{i,j+1} - \epsilon)^2} \leq t\right) \\ &= \mathbb{P}\left(\sqrt{\left(\frac{X_1}{\sigma}\right)^2 + \left(\frac{X_2}{\sigma}\right)^2} \leq \frac{t}{\sigma}\right). \end{aligned}$$

Since X_1 and X_2 are independent, the square root inside has a non-central Chi distribution with two degrees of freedom and non-centrality parameter

$$\lambda = \sqrt{\left(\frac{-\epsilon}{\sigma}\right)^2 + \left(\frac{-\epsilon}{\sigma}\right)^2} = \frac{\sqrt{2}|\epsilon|}{\sigma}.$$

This yields

$$\sqrt{\left(\frac{X_1}{\sigma}\right)^2 + \left(\frac{X_2}{\sigma}\right)^2} \sim \chi_2\left(\frac{\sqrt{2}|\epsilon|}{\sigma}\right)$$

and consequently

$$\frac{\sqrt{(\varepsilon_{i+1,j} - \varepsilon_{i,j})^2 + (\varepsilon_{i,j+1} - \varepsilon_{i,j})^2}}{\sigma} \mid \varepsilon_{i,j} = \epsilon \sim \chi_2\left(\frac{\sqrt{2}|\epsilon|}{\sigma}\right).$$

Up to this point, we assumed $\varepsilon_{i,j}$ to be fixed, however it is itself a normal distributed random variable with zero mean and standard deviation σ . Thus, we have a compound probability distribution. We can calculate the density of this non-central Chi-distributed random variable with normally distributed

non-centrality parameter $\varepsilon_{i,j}$ by marginalizing over $\varepsilon_{i,j}$ and obtain

$$\begin{aligned}
q(t) &= \mathbb{P} \left(\frac{\sqrt{(\varepsilon_{i+1,j} - \varepsilon_{i,j})^2 + (\varepsilon_{i,j+1} - \varepsilon_{i,j})^2}}{\sigma} \leq \frac{t}{\sigma} \right) \\
&= \int_0^{\frac{t}{\sigma}} \int_0^\infty \underbrace{x \exp \left(-\frac{x^2}{2} - \frac{\eta^2}{\sigma^2} \right) I_0 \left(\frac{\sqrt{2}\eta}{\sigma} x \right)}_{\text{pdf of } \chi_2 \left(\frac{\sqrt{2}\eta}{\sigma} \right) \text{ for fixed } \eta} \underbrace{\frac{2}{\sqrt{2\pi\sigma^2}} \exp \left(-\frac{\eta^2}{2\sigma^2} \right)}_{\text{pdf of absolute value of } \mathcal{N}(0, \sigma^2)} d\eta dx \\
&= \frac{2}{\sqrt{2\pi\sigma^2}} \int_0^{\frac{t}{\sigma}} x \exp \left(-\frac{x^2}{2} \right) \int_0^\infty \exp \left(-\frac{3}{2\sigma^2} \eta^2 \right) I_0 \left(\frac{\sqrt{2}x}{\sigma} \eta \right) d\eta dx,
\end{aligned}$$

where I_0 is the modified Bessel function of the first kind. We can solve the inner integral first. Equality (A.1) from Theorem A.1 states, that

$$\int_0^\infty \exp(-\alpha\eta^2) I_0(\beta\eta) d\eta = \frac{\sqrt{\pi}}{2\sqrt{\alpha}} \exp\left(\frac{\beta^2}{8\alpha}\right) I_0\left(\frac{\beta^2}{8\alpha}\right)$$

for $\alpha, \beta > 0$. In our case, we have $\alpha = \frac{3}{2\sigma^2} > 0$ and $\beta = \frac{\sqrt{2}x}{\sigma} > 0$, which yields

$$\begin{aligned}
\int_0^\infty \exp\left(-\frac{3}{2\sigma^2} \eta^2\right) I_0\left(\frac{\sqrt{2}x}{\sigma} \eta\right) d\eta &= \frac{\sqrt{\pi}}{2\sqrt{\frac{3}{2\sigma^2}}} \exp\left(\frac{\frac{2x^2}{\sigma^2}}{8\frac{3}{2\sigma^2}}\right) I_0\left(\frac{\frac{2x^2}{\sigma^2}}{8\frac{3}{2\sigma^2}}\right) \\
&= \frac{\sqrt{\pi}\sigma}{\sqrt{6}} \exp\left(\frac{x^2}{6}\right) I_0\left(\frac{x^2}{6}\right).
\end{aligned}$$

Plugging this in, we obtain

$$\begin{aligned}
q(t) &= \frac{2}{\sqrt{2\pi\sigma^2}} \int_0^{\frac{t}{\sigma}} x \exp\left(-\frac{x^2}{2}\right) \frac{\sqrt{\pi}\sigma}{\sqrt{6}} \exp\left(\frac{x^2}{6}\right) I_0\left(\frac{x^2}{6}\right) dx \\
&= \frac{1}{\sqrt{3}} \int_0^{\frac{t}{\sigma}} x \exp\left(-\frac{x^2}{2}\right) \exp\left(\frac{x^2}{6}\right) I_0\left(\frac{x^2}{6}\right) dx \\
&= \frac{1}{\sqrt{3}} \int_0^{\frac{t}{\sigma}} x \exp\left(-\frac{x^2}{3}\right) I_0\left(\frac{x^2}{6}\right) dx.
\end{aligned}$$

To proceed, we need to integrate by parts to replace the modified Bessel function I_0 of order zero by a modified Bessel function I_1 of order one [Olv+10,

p. 251].

$$\begin{aligned} q(t) &= \frac{1}{\sqrt{3}} \left[-\frac{3}{2} \exp\left(-\frac{x^2}{3}\right) I_0\left(\frac{x^2}{6}\right) \right]_0^{\frac{t}{\sigma}} + \frac{1}{2\sqrt{3}} \int_0^{\frac{t}{\sigma}} \exp\left(-\frac{x^2}{3}\right) x I_1\left(\frac{x^2}{6}\right) dx \\ &= \frac{1}{\sqrt{3}} \left(\frac{3}{2} - \frac{3}{2} \exp\left(-\frac{t^2}{3\sigma^2}\right) I_0\left(\frac{t^2}{6\sigma^2}\right) \right) + \frac{1}{2\sqrt{3}} \int_0^{\frac{t}{\sigma}} \exp\left(-\frac{x^2}{3}\right) x I_1\left(\frac{x^2}{6}\right) dx \end{aligned}$$

In the next step we substitute $y = x^2$ in the remaining integral, which leaves us with

$$q(t) = \frac{1}{\sqrt{3}} \left(\frac{3}{2} - \frac{3}{2} \exp\left(-\frac{t^2}{3\sigma^2}\right) I_0\left(\frac{t^2}{6\sigma^2}\right) \right) + \frac{1}{4\sqrt{3}} \int_0^{\frac{t^2}{\sigma^2}} \exp\left(-\frac{y}{3}\right) I_1\left(\frac{y}{6}\right) dy.$$

We want to solve the remaining integral. Let $p \neq b$ and $s = \sqrt{p^2 - b^2}$, $u = \sqrt{a(p-s)}$ and $v = \sqrt{a(p+s)}$. Then [Nut74]

$$\int_0^a \exp(-px) I_M(bx) dx = \frac{1}{sb^M} \left((p-s)^M (1 - Q_M(u, v)) - (p+s)^M (1 - Q_M(v, u)) \right), \quad (2.15)$$

where Q_M denotes the Marcum Q -function. The Marcum Q -function is only defined for $M \geq 1$, which made the integration by parts necessary. Applying this equation with $M = 1$ to the integral yields

$$\begin{aligned} \int_0^{\frac{t^2}{\sigma^2}} \exp\left(-\frac{y}{3}\right) I_1\left(\frac{y}{6}\right) dy &= 2\sqrt{3}(2 - \sqrt{3}) \left(1 - Q_1\left(\sqrt{\frac{2 - \sqrt{3}}{6}} \frac{t}{\sigma}, \sqrt{\frac{2 + \sqrt{3}}{6}} \frac{t}{\sigma}\right) \right) \\ &\quad - 2\sqrt{3}(2 + \sqrt{3}) \left(1 - Q_1\left(\sqrt{\frac{2 + \sqrt{3}}{6}} \frac{t}{\sigma}, \sqrt{\frac{2 - \sqrt{3}}{6}} \frac{t}{\sigma}\right) \right). \end{aligned}$$

Plugging this in, we obtain the final result

$$\begin{aligned} q(t) &= \frac{1}{\sqrt{3}} \left(\frac{3}{2} - \frac{3}{2} \exp\left(-\frac{t^2}{3\sigma^2}\right) I_0\left(\frac{t^2}{6\sigma^2}\right) \right) + \frac{1}{4\sqrt{3}} \int_0^{\frac{t^2}{\sigma^2}} \exp\left(-\frac{y}{3}\right) I_1\left(\frac{y}{6}\right) dy \\ &= \frac{1}{\sqrt{3}} \left(\frac{3}{2} - \frac{3}{2} \exp\left(-\frac{t^2}{3\sigma^2}\right) I_0\left(\frac{t^2}{6\sigma^2}\right) \right) \\ &\quad + \frac{2\sqrt{3}}{4\sqrt{3}} (2 - \sqrt{3}) \left(1 - Q_1\left(\sqrt{\frac{2 - \sqrt{3}}{6}} \frac{t}{\sigma}, \sqrt{\frac{2 + \sqrt{3}}{6}} \frac{t}{\sigma}\right) \right) \end{aligned}$$

$$\begin{aligned}
& -\frac{2\sqrt{3}}{4\sqrt{3}}(2+\sqrt{3}) \left(1 - Q_1 \left(\sqrt{\frac{2+\sqrt{3}}{6}} \frac{t}{\sigma}, \sqrt{\frac{2-\sqrt{3}}{6}} \frac{t}{\sigma} \right) \right) \\
&= \frac{1}{\sqrt{3}} \left(\frac{3}{2} - \frac{3}{2} \exp \left(-\frac{t^2}{3\sigma^2} \right) I_0 \left(\frac{t^2}{6\sigma^2} \right) \right) - \sqrt{3} \\
& \quad - \frac{2-\sqrt{3}}{2} Q_1 \left(\sqrt{\frac{2-\sqrt{3}}{6}} \frac{t}{\sigma}, \sqrt{\frac{2+\sqrt{3}}{6}} \frac{t}{\sigma} \right) \\
& \quad + \frac{2+\sqrt{3}}{2} Q_1 \left(\sqrt{\frac{2+\sqrt{3}}{6}} \frac{t}{\sigma}, \sqrt{\frac{2-\sqrt{3}}{6}} \frac{t}{\sigma} \right) \\
&= p_\sigma(t).
\end{aligned}$$

This finishes the proof of the first equality of equation (2.14). Analogously, we can proof $\mathbb{P}_{V_2}(\|\Delta^- F(i, j)\| \leq t) = p_\sigma(t)$, finishing the proof of Theorem 2.8. \square

Corollary 2.9. *Let $(i, j) \in \Omega$ and $t \in \mathbb{R}^+$. Assume that F follows the statistical model given in (2.5) and let $T(i, j)$ be defined as in (2.8). Then*

$$\mathbb{P}_V(T(i, j) \geq t) \leq 1 - p_\sigma(t) \quad (2.16)$$

for every $V \in \mathcal{H}_0(i, j)$.

Proof. Since $V \in \mathcal{H}_0(i, j)$, we have $V \in \mathcal{H}_0^+(i, j)$ or $V \in \mathcal{H}_0^-(i, j)$. In the first case, by Lemma 2.6 and Theorem 2.8 we have

$$\begin{aligned}
\mathbb{P}_V(T(i, j) \geq t) &\leq \min \left\{ \mathbb{P}_V \left(\|\Delta^+ F(i, j)\| \geq t \right), \mathbb{P}_V \left(\|\Delta^- F(i, j)\| \geq t \right) \right\} \\
&\leq \mathbb{P}_V \left(\|\Delta^+ F(i, j)\| \geq t \right) \\
&= 1 - p_\sigma(t).
\end{aligned}$$

The second case is proven analogously. \square

Let $\alpha \in (0, 1)$ be given. According to Corollary 2.9 any threshold t_α with $1 - p_\sigma(t_\alpha) \leq \alpha$ bounds the probability of a type I error in our statistical test below the given statistical significance α . Since the function $p_\sigma(t)$ does not depend on V , the threshold is independent of the specific V .

Note, that finding inverse functions of the modified Bessel function of the first kind I_ν and of the Marcum Q -function Q_M is not feasible and consequently there is no way to compute an inverse function of $p_\sigma(t)$. Thus, we cannot provide a closed form to calculate the threshold, but we can compute a threshold t_α numerically with a trial and error algorithm, see Algorithm 1. To this end, we note, that $p_\sigma(t_\alpha \cdot \sigma) = p_1(t_\alpha)$. Hence, it is sufficient to calculate a threshold t_α for $\sigma = 1$. The function $p_1(t)$ is strictly monotone, as it is the cumulative distribution function of a continuous random variable. The used algorithm steadily increases a guess for a suitable threshold, until one is found. The monotonicity of $p_1(t)$ assures, that the computed threshold suffices the inequality $\mathbb{P}_V(T(i, j) \geq t_\alpha) \leq \alpha$. Other algorithms, e.g. quasi-Newton methods, likely use less computation time, but a threshold calculated with these methods will not necessarily suffice this inequality. As we only need to compute a threshold for $\sigma = 1$, we ignore the additional computation time of our algorithm in favor of adhering to the inequality.

A *MATLAB* implementation of this algorithm can be found in Appendix C. In Figure 4 the cumulative distribution function $p_1(t)$ is plotted. For $\alpha = 0.05$ and $\alpha = 0.01$ the thresholds have been numerically computed.

Algorithm 1: Computation of a threshold for a given statistical significance

Input: $\alpha \in (0, 1)$

Output: t_α and α_{real} , s.t. $p_1(t_\alpha) = 1 - \alpha_{real} \geq 1 - \alpha$

```

1  $t_\alpha = 0$ ;
2  $t_{inc} = 0.0001$ ;
3 while  $p_1(t_\alpha) < 1 - \alpha$  do
4    $t_\alpha = t_\alpha + t_{inc}$ ;
5    $\alpha_{real} = 1 - p_1(t_\alpha)$ ;
6 end while
```

2.4 Analysis of the probability of a type II error

Through Corollary (2.9) we bound the probability of falsely classifying a background pixel as a foreground pixel below a given statistical significance.

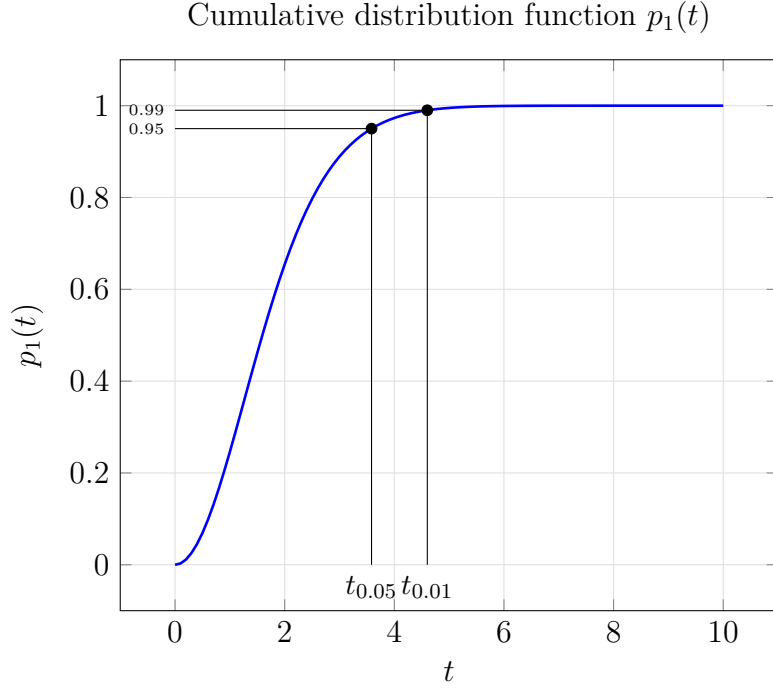


Figure 4: Plot of the cumulative distribution function $p_1(t)$. The numerically computed thresholds $t_{0.05} = 3.5844$ and $t_{0.01} = 4.6017$ are marked.

In the following, we are interested in upper and lower bounds for the probability of a type II error, that is falsely classifying a foreground pixel as a background pixel.

To this end, we define a subset of $\mathcal{V}_c^{m,n}$ for every pixel. Let $(i, j) \in \Omega$. We define the set of images, for which the alternative hypothesis $H_1(i, j)$ is true as

$$\mathcal{H}_1(i, j) := \left\{ V \in \mathcal{V}_c^{m,n} \mid \min\{\|\Delta^+ V(i, j)\|, \|\Delta^- V(i, j)\|\} \neq 0 \right\}. \quad (2.17)$$

A first step towards bounds for the probability of a type II error is achieved in the following lemma.

Lemma 2.10. *Let $(i, j) \in \Omega$ and $t \in \mathbb{R}^+$. Assume that F follows the statistical model given (2.5) and let $T(i, j)$ and $H_1(i, j)$ be defined as in (2.8) and (2.7). Let $V, V_1, V_2 \in \mathcal{H}_1(i, j)$. Assume V_1 is such, that $\|\Delta^+ V_1(i, j)\| = \sqrt{2}c$*

and V_2 such, that $\|\Delta^+ V_2(i, j)\| = \sqrt{8}c$. Then the following inequalities hold:

$$\mathbb{P}_V(T(i, j) \leq t) \leq 2 \cdot \mathbb{P}_{V_1}(\|\Delta^+ F(i, j)\| \leq t) \quad (2.18)$$

$$\mathbb{P}_V(T(i, j) \leq t) \geq \mathbb{P}_{V_2}(\|\Delta^+ F(i, j)\| \leq t) \quad (2.19)$$

Proof. By assumption $V \in \mathcal{H}_1(i, j) \subseteq \mathcal{V}_c^{m,n}$. By design of our statistical test, if $H_1(i, j)$ is true, then $(i, j) \in \Lambda$, where Λ denotes the ROI contained in V . As can be seen from Table 1 in the proof of Lemma 2.5, $(i, j) \in \Lambda$ implies

$$\|\Delta^+ V(i, j)\|, \|\Delta^- V(i, j)\| \in \{\sqrt{2}c, \sqrt{5}c, \sqrt{8}c\}.$$

Hence, we can rewrite the set $\mathcal{H}_1(i, j)$ as

$$\mathcal{H}_1(i, j) = \{V \in \mathcal{V}_c^{m,n} \mid \|\Delta^+ V(i, j)\|, \|\Delta^- V(i, j)\| \in \{\sqrt{2}c, \sqrt{5}c, \sqrt{8}c\}\}.$$

Furthermore, we note, that for any $\bar{V}, \tilde{V} \in \mathcal{V}_c^{m,n}$ with $\Delta^+ \bar{V}(i, j) \geq \Delta^+ \tilde{V}(i, j)$, we have

$$\mathbb{P}_{\bar{V}}(\|\Delta^+ F(i, j)\| \leq t) \leq \mathbb{P}_{\tilde{V}}(\|\Delta^+ F(i, j)\| \leq t).$$

Using this knowledge, we can start bounding the probability of a type II error in our testing procedure, which we call β_V , from above by

$$\begin{aligned} \beta_V(t) &:= \mathbb{P}_V(T(i, j) \leq t) \\ &= \mathbb{P}_V(\min\{\|\Delta^+ F(i, j)\|, \|\Delta^- F(i, j)\|\} \leq t) \\ &= \mathbb{P}_V(\{\|\Delta^+ F(i, j)\| \leq t\} \cup \{\|\Delta^- F(i, j)\| \leq t\}) \\ &\leq \mathbb{P}_V(\|\Delta^+ F(i, j)\| \leq t) + \mathbb{P}_V(\|\Delta^- F(i, j)\| \leq t). \end{aligned}$$

This upper bound depends on the actual value of $\|\Delta^+ V(i, j)\|$, which is unknown. In both terms we take a $V^* \in \mathcal{H}_1(i, j)$ that maximizes the probability and obtain

$$\begin{aligned} \beta_V(t) &\leq \max_{V^* \in \mathcal{H}_1(i, j)} \mathbb{P}_{V^*}(\|\Delta^+ F(i, j)\| \leq t) + \max_{V^* \in \mathcal{H}_1(i, j)} \mathbb{P}_{V^*}(\|\Delta^- F(i, j)\| \leq t) \\ &= 2 \cdot \max_{V^* \in \mathcal{H}_1(i, j)} \mathbb{P}_{V^*}(\|\Delta^+ F(i, j)\| \leq t) \end{aligned}$$

where we used the equality

$$\max_{V^* \in \mathcal{H}_1(i,j)} \mathbb{P}_{V^*} \left(\|\Delta^+ F(i,j)\| \leq t \right) = \max_{V^* \in \mathcal{H}_1(i,j)} \mathbb{P}_{V^*} \left(\|\Delta^- F(i,j)\| \leq t \right).$$

Using the above observation, we see, that the maximum is attained, if $\|\Delta^+ V^*(i,j)\|$ is minimal. Thus, exploiting $\|\Delta^+ V_1(i,j)\| = \sqrt{2}c$, we obtain

$$\begin{aligned} \beta_V(t) &\leq 2 \cdot \max_{V^* \in \mathcal{H}_1(i,j)} \mathbb{P}_{V^*} \left(\|\Delta^+ F(i,j)\| \leq t \right) \\ &= 2 \cdot \mathbb{P}_{V_1} \left(\|\Delta^+ F(i,j)\| \leq t \right), \end{aligned}$$

which proves inequality (2.18).

For the lower bound consider

$$\begin{aligned} \beta_V(t) &= \mathbb{P}_V (T(i,j) \leq t) \\ &= \mathbb{P}_V \left(\min\{\|\Delta^+ F(i,j)\|, \|\Delta^- F(i,j)\|\} \leq t \right) \\ &\geq \mathbb{P}_V \left(\|\Delta^+ F(i,j)\| \leq t \right). \end{aligned}$$

Again, this lower bound depends on the value of $\|\Delta^+ V(i,j)\|$, which is unknown, and we bound this further by

$$\begin{aligned} \beta_V(t) &\geq \mathbb{P}_V \left(\|\Delta^+ F(i,j)\| \leq t \right) \\ &\geq \min_{V^* \in \mathcal{H}_1(i,j)} \mathbb{P}_{V^*} \left(\|\Delta^+ F(i,j)\| \leq t \right). \end{aligned}$$

Similar to the proof of the first inequality, the minimum is attained, if $\|\Delta^+ V^*(i,j)\|$ is maximal. Hence, by $\|\Delta^+ V^*(i,j)\| = \sqrt{8}c$, we obtain

$$\begin{aligned} \beta_V(t) &\geq \min_{V^* \in \mathcal{H}_1(i,j)} \mathbb{P}_{V^*} \left(\|\Delta^+ F(i,j)\| \leq t \right) \\ &= \mathbb{P}_{V_2} \left(\|\Delta^+ F_2(i,j)\| \leq t \right) \end{aligned}$$

which proves inequality (2.19) and finishes the proof. \square

The previous theorem is the equivalent to Lemma 2.6 for the probability of a type II error. We would like to write these bounds in terms of well-known

functions like we did in Theorem 2.8. This would require more generalized versions of equalities (A.1) and (2.15), which, to the best of the author's knowledge, are not known.

We can write down the compound probability distribution of the upper and lower bound from Lemma 2.10. The results are given in the following theorem.

Theorem 2.11. *Let $(i, j) \in \Omega$ and $t \in \mathbb{R}^+$. Assume that F follows the statistical model given (2.5) and let $T(i, j)$ and $H_1(i, j)$ be defined as in (2.8) and (2.7). Let $V_1, V_2 \in \mathcal{H}_1(i, j)$. Assume V_1 is such, that $\|\Delta^+ V_1(i, j)\| = \sqrt{2}c$ and V_2 such, that $\|\Delta^+ V_2(i, j)\| = \sqrt{8}c$. Then the following equalities hold:*

$$\begin{aligned} & \mathbb{P}_{V_1}(\|\Delta^+ F(i, j)\| \leq t) \\ &= \frac{1}{\sqrt{2\pi\sigma^2}} \int_0^{\frac{t}{\sigma}} x \exp\left(-\frac{x^2}{2}\right) \int_{-\infty}^{\infty} \exp\left(-\frac{(c-\eta)^2}{\sigma^2} - \frac{\eta^2}{2\sigma^2}\right) I_0\left(\frac{\sqrt{2}x}{\sigma}(c-\eta)\right) d\eta dx \end{aligned} \quad (2.20)$$

$$\begin{aligned} & \mathbb{P}_{V_2}(\|\Delta^+ F(i, j)\| \leq t) \\ &= \frac{1}{\sqrt{2\pi\sigma^2}} \int_0^{\frac{t}{\sigma}} x \exp\left(-\frac{x^2}{2}\right) \int_{-\infty}^{\infty} \exp\left(-\frac{(2c-\eta)^2}{\sigma^2} - \frac{\eta^2}{2\sigma^2}\right) I_0\left(\frac{\sqrt{2}x}{\sigma}(2c-\eta)\right) d\eta dx \end{aligned} \quad (2.21)$$

Proof. From the analysis of possible combinations of $|V(i+1, j) - V(i, j)|$ and $|V(i, j+1) - V(i, j)|$ in Table 1 we can deduce the equivalences

$$\begin{aligned} |V(i+1, j) - V(i, j)| &= |V(i, j+1) - V(i, j)| = c \Leftrightarrow \|\Delta^+ V(i, j)\| = \sqrt{2}c, \\ |V(i+1, j) - V(i, j)| &= |V(i, j+1) - V(i, j)| = 2c \Leftrightarrow \|\Delta^+ V(i, j)\| = \sqrt{8}c. \end{aligned}$$

We start with the first equality and proceed as in the proof of Theorem 2.8.

$$\begin{aligned} & \mathbb{P}_{V_1}(\|\Delta^+ F(i, j)\| \leq t) \\ &= \mathbb{P}_{V_1}\left((c + V_1(i+1, j) + \varepsilon_{i+1, j} - c - V_1(i, j) - \varepsilon_{i, j})^2 \right. \\ &\quad \left. + (c + V_1(i, j+1) + \varepsilon_{i, j+1} - c - V_1(i, j) - \varepsilon_{i, j})^2 \leq t^2\right) \\ &= \mathbb{P}_{V_1}\left((V_1(i+1, j) - V_1(i, j) + \varepsilon_{i+1, j} - \varepsilon_{i, j})^2 \right. \\ &\quad \left. + (V_1(i, j+1) - V_1(i, j) + \varepsilon_{i, j+1} - \varepsilon_{i, j})^2 \leq t^2\right). \end{aligned}$$

We can replace $\varepsilon_{i+1,j}$ and $\varepsilon_{i,j}$ by $-\varepsilon_{i+1,j}$ and $-\varepsilon_{i,j}$ or $\varepsilon_{i,j+1}$ and $\varepsilon_{i,j}$ by $-\varepsilon_{i,j+1}$ and $-\varepsilon_{i,j}$, respectively, without changing the probability. Thus, we can assume without loss of generality

$$V_1(i+1, j) - V_1(i, j) = V_1(i, j+1) - V_1(i, j) = c.$$

This yields

$$\mathbb{P}_{V_1} \left(\|\Delta^+ F(i, j)\| \leq t \right) = \mathbb{P}_{V_1} \left((c + \varepsilon_{i+1,j} - \varepsilon_{i,j})^2 + (c + \varepsilon_{i,j+1} - \varepsilon_{i,j})^2 \leq t^2 \right).$$

We define the following random variables

$$\begin{aligned} \xi &= c - \varepsilon_{i,j} \sim \mathcal{N}(c, \sigma^2), \\ X_1 &= \xi + \varepsilon_{i+1,j} \sim \mathcal{N}(\xi_1, \sigma^2), \\ X_2 &= \xi + \varepsilon_{i,j+1} \sim \mathcal{N}(\xi_2, \sigma^2) \end{aligned}$$

and obtain

$$\mathbb{P}_{V_1} \left(\|\Delta^+ F(i, j)\| \leq t \right) = \mathbb{P}_{V_1} \left(\sqrt{\left(\frac{X_1}{\sigma}\right)^2 + \left(\frac{X_2}{\sigma}\right)^2} \leq \frac{t}{\sigma} \right).$$

Since X_1 and X_2 are independent, the square root inside has a non-central Chi distribution with two degrees of freedom and non-centrality parameter

$$\lambda = \sqrt{\left(\frac{c - \varepsilon_{i,j}}{\sigma}\right)^2 + \left(\frac{c - \varepsilon_{i,j}}{\sigma}\right)^2} = \frac{\sqrt{2}|c - \varepsilon_{i,j}|}{\sigma}.$$

This yields

$$\sqrt{\left(\frac{X_1}{\sigma}\right)^2 + \left(\frac{X_2}{\sigma}\right)^2} \sim \chi_2 \left(\frac{\sqrt{2}|c - \varepsilon_{i,j}|}{\sigma} \right).$$

Since $\varepsilon_{i,j}$ is a normal distributed random variable with zero mean and standard deviation σ , we have a compound probability distribution:

$$\mathbb{P}_{V_1} \left((\|\Delta^+ F(i, j)\| \leq t) \right)$$

$$\begin{aligned}
&= \mathbb{P}_{V_1} \left(\sqrt{\left(\frac{X_1}{\sigma}\right)^2 + \left(\frac{X_2}{\sigma}\right)^2} \leq \frac{t}{\sigma} \right) \\
&= \int_0^{\frac{t}{\sigma}} \int_{-\infty}^{\infty} \underbrace{x \exp\left(-\frac{x^2}{2} - \frac{|c-\eta|^2}{\sigma^2}\right)}_{\text{pdf of } \chi_2\left(\frac{\sqrt{2}|c-\eta|}{\sigma}\right) \text{ for fixed } \eta} I_0\left(\frac{\sqrt{2}|c-\eta|}{\sigma}x\right) \underbrace{\frac{1}{\sqrt{2\pi\sigma^2}} \exp\left(-\frac{\eta^2}{2\sigma^2}\right)}_{\text{pdf of } \mathcal{N}(0, \sigma^2)} d\eta dx \\
&= \frac{1}{\sqrt{2\pi\sigma^2}} \int_0^{\frac{t}{\sigma}} x \exp\left(-\frac{x^2}{2}\right) \int_{-\infty}^{\infty} \exp\left(-\frac{(c-\eta)^2}{\sigma^2} - \frac{\eta^2}{2\sigma^2}\right) I_0\left(\frac{\sqrt{2}x}{\sigma}(c-\eta)\right) d\eta dx,
\end{aligned}$$

where we used the symmetry of I_0 . The second equality can be proven analogously. \square

These results are not as strong as the results from Theorem 2.8, as we do not state the right hand sides of equations (2.20) and (2.21) in terms of well-known functions, but only as integrals. Since the Marcum Q -function is defined as an integral, the function $p_\sigma(t)$ in Theorem 2.8 also involves integrals, making these results only slightly better.

We can simulate random variables V_1 and V_2 as defined in Lemma 2.10 and in this way obtain empirical estimates of upper and lower bounds for the probability of a type II error depending on the standard deviation σ of the noise term in the statistical model (2.5).

Figure 5 shows the result of this simulation for the thresholds $t_{0.05} = 3.5844$ and $t_{0.01} = 4.6017$, that were computed in Section 2.3. A *MATLAB* implementation of the simulation can be found in Appendix C.

Theorem 2.11 also yields a second way to numerically obtain upper and lower bounds for the probability of a type II error by numerically integrating the right hand sides of equations (2.20) and (2.21).

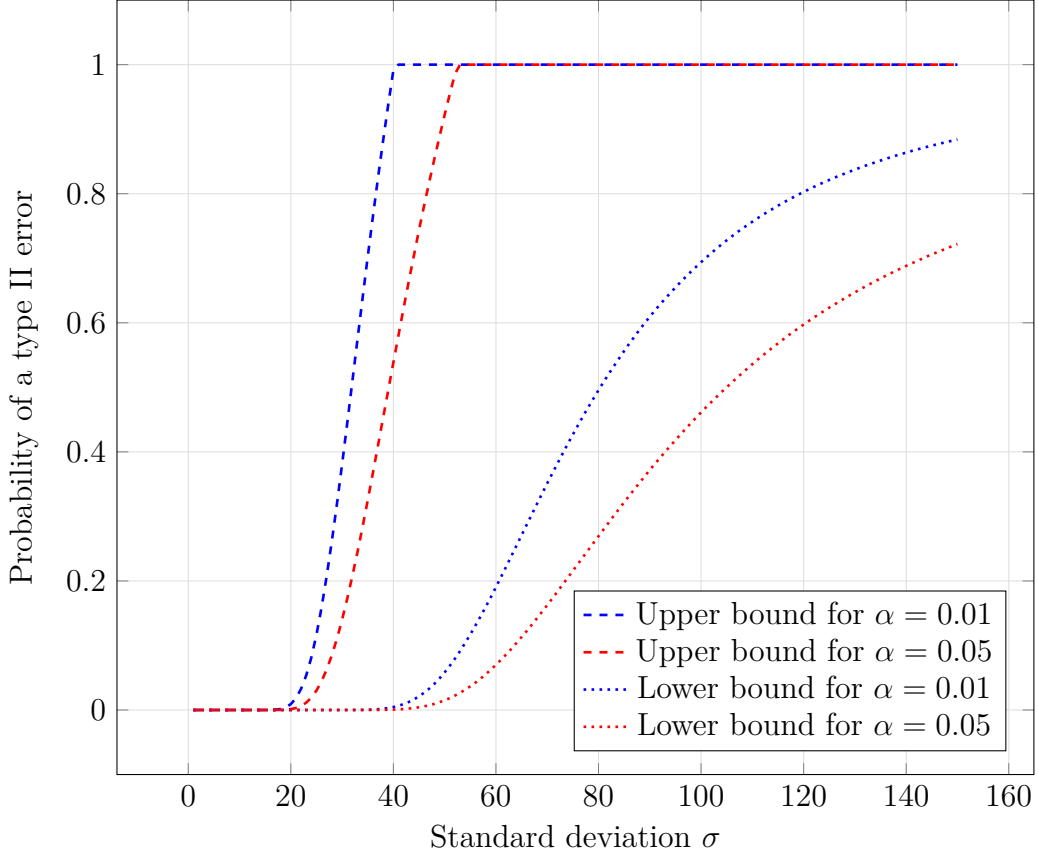


Figure 5: Simulated bounds for the probability of a type II error. We use the thresholds $t_{0.05} = 3.5844$ for $\alpha = 0.05$ and $t_{0.01} = 4.6017$ for $\alpha = 0.01$. (Sample size: 1.000.000)

3 Binary morphological operations

We now introduce morphological operations. Since the output of the testing procedure is binary, it is sufficient to only consider *binary* morphological operations. In particular, we will only study the impact of *binary opening* and *binary closing*. These operations are frequently used in the preprocessing of fingerprint images [BG01; Liu+11] and, as we discuss in Section 3.2, exhibit properties, that make them a versatile tool for the reduction of falsely classified pixels.

Morphological opening and closing are local operations, since they only depend on a limited and fixed number of pixels. In contrast to that, the *con-*

vox hull is a global operation, also commonly used in fingerprint analysis [THG16], depending on all pixels of an image, making it harder to study on a pixel-by-pixel basis.

3.1 Definition of opening & closing

Morphological binary opening and closing are closely related operations. They are both defined as a composition of *binary erosion* and *binary dilation*, defined below. It should be noted, that we focus on morphological operations in image processing and thus the definitions might differ from those in other contexts. The definitions of the basic morphology operations are taken from [Shi10].

Definition 3.1 ([Shi10, p. 64-68]). Let $\Theta, \Psi \subseteq \mathbb{Z}^2$.

1. The *binary erosion* of Θ by Ψ is defined as

$$\Theta \ominus \Psi = \left\{ x \in \mathbb{Z}^2 \mid x + b \in \Theta \text{ for every } b \in \Psi \right\}.$$

2. The *binary dilation* of A by Ψ is defined as

$$\Theta \oplus \Psi = \left\{ c \in \mathbb{Z}^2 \mid c = a + b \text{ for some } a \in \Theta \text{ and } b \in \Psi \right\}.$$

The set Ψ is called a *structuring element*.

Working with images, we extend the definition of binary opening and closing from being operations on subsets of \mathbb{Z}^2 to being operations on matrices $\mathfrak{J} \in \{0, 1\}^{m \times n}$, using, for convenience, the same symbols.

Definition 3.2. Let $m, n \in \mathbb{N}$, $\mathfrak{J} \in \{0, 1\}^{m \times n}$, $\Omega = \{1, \dots, m\} \times \{1, \dots, n\}$ and $\Psi \subseteq \mathbb{Z}^2$, which is called a structuring element. We call

$$\Theta_{\mathfrak{J}} := \{(i, j) \in \Omega \mid \mathfrak{J}(i, j) = 1\} \subseteq \mathbb{Z}^2$$

the *set of non-zero entries* of the binary matrix \mathfrak{J} .

1. The *erosion* of the binary matrix \mathfrak{J} by the structuring element Ψ is defined by

$$(\mathfrak{J} \ominus \Psi)(i, j) = \begin{cases} 1, & \text{if } (i, j) \in \Theta_{\mathfrak{J}} \ominus \Psi, \\ 0, & \text{if } (i, j) \notin \Theta_{\mathfrak{J}} \ominus \Psi, \end{cases} \quad (3.1)$$

for every $(i, j) \in \Omega$.

2. The *dilation* of the binary matrix \mathfrak{J} by the structuring element Ψ is defined by

$$(\mathfrak{J} \oplus \Psi)(i, j) = \begin{cases} 1, & \text{if } (i, j) \in \Theta_{\mathfrak{J}} \oplus \Psi, \\ 0, & \text{if } (i, j) \notin \Theta_{\mathfrak{J}} \oplus \Psi, \end{cases} \quad (3.2)$$

for every $(i, j) \in \Omega$.

By definition, erosion and dilation of a binary matrix are binary matrices as well, i.e. $\mathfrak{J} \ominus \Psi, \mathfrak{J} \oplus \Psi \in \{0, 1\}^{m \times n}$.

We want to express $\mathfrak{J} \ominus \Psi$ and $\mathfrak{J} \oplus \Psi$ in terms of \mathfrak{J} . In [Shi10, p. 65-67] this connection is described with an informal notation. To the best of the author's knowledge, this connection has, surprisingly, not been formalized. This is done in the following lemma.

Lemma 3.3. *Let $m, n \in \mathbb{N}$, $\mathfrak{J} \in \{0, 1\}^{m \times n}$ and $\Psi \subseteq \mathbb{Z}^2$. Let $(i, j) \in \Omega$. Then the following equalities hold:*

$$(\mathfrak{J} \ominus \Psi)(i, j) = \prod_{(k, \ell) \in \Psi} \mathfrak{J}(i + k, j + \ell) \quad (3.3)$$

$$(\mathfrak{J} \oplus \Psi)(i, j) = 1 - \prod_{(k, \ell) \in \Psi} (1 - \mathfrak{J}(i - k, j - \ell)) \quad (3.4)$$

where we extend the matrix \mathfrak{J} to all of \mathbb{Z}^2 by setting $\mathfrak{J}(k, \ell) = 0$ for $(k, \ell) \notin \Omega$.

Proof. Let $\Theta_{\mathfrak{J}}$ be the set of non-zero entries of the binary matrix \mathfrak{J} . By definition of binary erosion and using basic properties of set theory, we obtain

$$\begin{aligned} (\mathfrak{J} \ominus \Psi)(i, j) = 1 &\Leftrightarrow (i, j) \in \Theta_{\mathfrak{J}} \ominus \Psi \\ &\Leftrightarrow \forall (k, \ell) \in \Psi : (i, j) + (k, \ell) \in \Theta_{\mathfrak{J}} \\ &\Leftrightarrow (i, j) \in \bigcap_{(k, \ell) \in \Psi} (\Theta_{\mathfrak{J}} - (k, \ell)) \end{aligned}$$

where we define the sets $\Theta_{\mathfrak{J}} - (k, \ell) := \{a - (k, \ell) \mid a \in \Theta_{\mathfrak{J}}\}$ for any $(k, \ell) \in \mathbb{Z}^2$. The sets $\Theta_{\mathfrak{J}} - (k, \ell)$ are related to the matrix \mathfrak{J} through the equivalence

$$(i, j) \in (\Theta_{\mathfrak{J}} - (k, \ell)) \Leftrightarrow \mathfrak{J}(i + k, j + \ell) = 1. \quad (3.5)$$

Using (3.5), we obtain

$$\begin{aligned} (\mathfrak{J} \ominus \Psi)(i, j) = 1 &\Leftrightarrow (i, j) \in \bigcap_{(k, \ell) \in \Psi} (\Theta_{\mathfrak{J}} - (k, \ell)) \\ &\Leftrightarrow \prod_{(k, \ell) \in \Psi} \mathfrak{J}(i + k, j + \ell) = 1. \end{aligned}$$

The functions on both sides of this equivalence only take values in $\{0, 1\}$. Thus, we end up with

$$(\mathfrak{J} \ominus \Psi)(i, j) = \prod_{(k, \ell) \in \Psi} \mathfrak{J}(i + k, j + \ell).$$

This proves the first equality.

The proof of the second equality is similar. First we use the definition of binary dilation and basic set theory properties to get the equivalence

$$\begin{aligned} (\mathfrak{J} \oplus \Psi)(i, j) = 1 &\Leftrightarrow (i, j) \in \Theta_{\mathfrak{J}} \oplus \Psi \\ &\Leftrightarrow \exists (k, \ell) \in \Psi : (i, j) - (k, \ell) \in \Theta_{\mathfrak{J}} \\ &\Leftrightarrow (i, j) \in \bigcup_{(k, \ell) \in \Psi} (\Theta_{\mathfrak{J}} + (k, \ell)). \end{aligned}$$

The property $(i, j) \in \bigcup_{(k, \ell) \in \Psi} (\Theta_{\mathfrak{J}} + (k, \ell))$ is satisfied, if $\mathfrak{J}(i - k, j - \ell) = 1$ for some $(k, \ell) \in \Psi$. This observation yields the equivalence

$$\begin{aligned} (\mathfrak{J} \oplus \Psi)(i, j) = 1 &\Leftrightarrow (i, j) \in \bigcup_{(k, \ell) \in \Psi} (\Theta_{\mathfrak{J}} + (k, \ell)) \\ &\Leftrightarrow \prod_{(k, \ell) \in \Psi} (1 - \mathfrak{J}(i - k, j - \ell)) = 0. \end{aligned}$$

Since \mathfrak{J} is binary, $\prod_{(k, \ell) \in \Psi} (1 - \mathfrak{J}(i - k, j - \ell))$ only takes values in $\{0, 1\}$.

Hence, we have the equivalence

$$\begin{aligned} (\mathfrak{J} \oplus \Psi)(i, j) = 1 &\Leftrightarrow \prod_{(k, \ell) \in \Psi} (1 - \mathfrak{J}(i - k, j - \ell)) = 0 \\ &\Leftrightarrow 1 - \prod_{(k, \ell) \in \Psi} (1 - \mathfrak{J}(i - k, j - \ell)) = 1. \end{aligned}$$

Again, since both sides only take values in $\{0, 1\}$, this yields a full equality

$$(\mathfrak{J} \oplus \Psi)(i, j) = 1 - \prod_{(k, \ell) \in \Psi} (1 - \mathfrak{J}(i - k, j - \ell)).$$

□

Remark 3.4. The extension of \mathfrak{J} to all of \mathbb{Z}^2 is necessary, because in the products on the right hand sides of equations (3.3) and (3.4), we might reach indices outside of Ω , if (i, j) is close to the boundary of the image.

After having defined binary erosion and dilation, we now can define binary opening and closing. Again, we start by defining it for subsets of \mathbb{Z}^2 and then proceed to define it for binary matrices $\mathfrak{J} \in \{0, 1\}^{m \times n}$.

Definition 3.5 ([Shi10, p. 68-69]). Let $\Theta, \Psi \subseteq \mathbb{Z}^2$.

1. The *binary opening* of Θ by a structuring element Ψ is defined as

$$\Theta \circ \Psi = (\Theta \ominus \Psi) \oplus \Psi.$$

2. The *binary closing* of Θ by a structuring element Ψ is defined as

$$\Theta \bullet \Psi = (\Theta \oplus \Psi) \ominus \Psi.$$

The definitions for matrices are done the same way, as they were done for erosion and dilation of binary matrices.

Definition 3.6. Let $m, n \in \mathbb{N}$, $\mathfrak{J} \in \{0, 1\}^{m \times n}$, $\Psi \subseteq \mathbb{Z}^2$, which is called a structuring element, and $\Theta_{\mathfrak{J}}$ be the set of non-zero entries of \mathfrak{J} .

1. The *opening* of the binary matrix \mathfrak{J} by the structuring element Ψ is defined by

$$(\mathfrak{J} \circ \Psi)(i, j) = \begin{cases} 1, & \text{if } (i, j) \in \Theta_{\mathfrak{J}} \circ \Psi, \\ 0, & \text{if } (i, j) \notin \Theta_{\mathfrak{J}} \circ \Psi, \end{cases} \quad (3.6)$$

for every $(i, j) \in \Omega$.

2. The *closing* of the binary matrix \mathfrak{J} by the structuring element Ψ is defined by

$$(\mathfrak{J} \bullet \Psi)(i, j) = \begin{cases} 1, & \text{if } (i, j) \in \Theta_{\mathfrak{J}} \bullet \Psi, \\ 0, & \text{if } (i, j) \notin \Theta_{\mathfrak{J}} \bullet \Psi, \end{cases} \quad (3.7)$$

for every $(i, j) \in \Omega$.

We need to show, that opening and closing of a binary matrix are also concatenations of erosion and dilation of binary matrices.

Lemma 3.7. *Let $m, n \in \mathbb{N}$, $\mathfrak{J} \in \{0, 1\}^{m \times n}$ and $\Psi \subseteq \mathbb{Z}^2$. We have the following connections between opening and closing and erosion and dilation of binary matrices:*

$$(\mathfrak{J} \circ \Psi) = (\mathfrak{J} \ominus \Psi) \oplus \Psi \quad (3.8)$$

$$(\mathfrak{J} \bullet \Psi) = (\mathfrak{J} \oplus \Psi) \ominus \Psi \quad (3.9)$$

Proof. To prove these relations, we first show, that $\Theta_{\mathfrak{J} \circ \Psi} = \Theta_{\mathfrak{J}} \ominus \Psi$ and $\Theta_{\mathfrak{J} \oplus \Psi} = \Theta_{\mathfrak{J}} \oplus \Psi$. By definition of the set of non-zero entries of a binary matrix, we have

$$\begin{aligned} \Theta_{\mathfrak{J} \circ \Psi} &= \{(i, j) \in \Omega \mid (\mathfrak{J} \circ \Psi)(i, j) = 1\} \\ &= \{(i, j) \in \Omega \mid (i, j) \in \Theta_{\mathfrak{J}} \circ \Psi\} \\ &= \Theta_{\mathfrak{J}} \ominus \Psi. \end{aligned}$$

The second equality is proven analogously.

Using this equality, we obtain

$$(\mathfrak{J} \circ \Psi)(i, j) = 1 \Leftrightarrow (i, j) \in \Theta_{\mathfrak{J}} \circ \Psi$$

$$\begin{aligned}
&\Leftrightarrow (i, j) \in (\Theta_{\mathfrak{J}} \ominus \Psi) \oplus \Psi \\
&\Leftrightarrow (i, j) \in \Theta_{\mathfrak{J} \ominus \Psi} \oplus \Psi \\
&\Leftrightarrow ((\mathfrak{J} \ominus \Psi) \oplus \Psi)(i, j) = 1
\end{aligned}$$

and thus prove the first relation. The proof of the second relation is analogous. \square

After we established this connection, we can use the equalities deduced in Lemma 3.3 for erosion and dilation to derive similar equalities for opening and closing of a binary matrix.

Lemma 3.8. *Let $m, n \in \mathbb{N}$, $\mathfrak{J} \in \{0, 1\}^{m \times n}$ and $\Psi \subseteq \mathbb{Z}^2$. Let $(i, j) \in \Omega$. Then the following equalities hold:*

$$(\mathfrak{J} \circ \Psi)(i, j) = 1 - \prod_{(k, \ell) \in \Psi} \left(1 - \left(\prod_{(\tilde{k}, \tilde{\ell}) \in \Psi} \mathfrak{J}(i - k + \tilde{k}, j - \ell + \tilde{\ell}) \right) \right) \quad (3.10)$$

$$(\mathfrak{J} \bullet \Psi)(i, j) = \prod_{(k, \ell) \in \Psi} \left(1 - \prod_{(\tilde{k}, \tilde{\ell}) \in \Psi} (1 - \mathfrak{J}(i + k - \tilde{k}, j + \ell - \tilde{\ell})) \right) \quad (3.11)$$

where by convention matrix entries of \mathfrak{J} that lie outside of Ω are set to be $\mathfrak{J}(k, \ell) = 0$.

Proof. We can use the previous lemma, as well as equations (3.4) and (3.3) to obtain the first equality

$$\begin{aligned}
(\mathfrak{J} \circ \Psi)(i, j) &= ((\mathfrak{J} \ominus \Psi) \oplus \Psi)(i, j) \\
&= 1 - \prod_{(k, \ell) \in \Psi} (1 - (\mathfrak{J} \ominus \Psi)(i - k, j - \ell)) \\
&= 1 - \prod_{(k, \ell) \in \Psi} \left(1 - \left(\prod_{(\tilde{k}, \tilde{\ell}) \in \Psi} \mathfrak{J}(i - k + \tilde{k}, j - \ell + \tilde{\ell}) \right) \right).
\end{aligned}$$

Using the same lemma and equations also yields the second equality

$$\begin{aligned}
(\mathfrak{J} \bullet \Psi)(i, j) &= ((\mathfrak{J} \oplus \Psi) \ominus \Psi)(i, j) \\
&= \prod_{(k, \ell) \in \Psi} (\mathfrak{J} \oplus \Psi)(i + k, j + \ell)
\end{aligned}$$

$$= \prod_{(k,\ell) \in \Psi} \left(1 - \prod_{(\tilde{k},\tilde{\ell}) \in \Psi} (1 - \mathfrak{I}(i+k-\tilde{k}, j+\ell-\tilde{\ell})) \right).$$

This finishes the proof. \square

Using the previous lemma, we can deduce the following equalities of sets of matrices $\mathfrak{I} \in \{0,1\}^{m \times n}$.

Lemma 3.9. *Let $m, n \in \mathbb{N}$ and $\Psi \subseteq \mathbb{Z}^2$. Let $(i, j) \in \Omega$. Then the following equalities hold:*

$$\begin{aligned} & \left\{ \mathfrak{I} \in \{0,1\}^{m \times n} \mid (\mathfrak{I} \circ \Psi)(i, j) = 1 \right\} \\ &= \bigcup_{(k,\ell) \in \Psi} \bigcap_{(\tilde{k},\tilde{\ell}) \in \Psi} \left\{ \mathfrak{I} \in \{0,1\}^{m \times n} \mid \mathfrak{I}(i-k+\tilde{k}, j-\ell+\tilde{\ell}) = 1 \right\} \end{aligned} \quad (3.12)$$

$$\begin{aligned} & \left\{ \mathfrak{I} \in \{0,1\}^{m \times n} \mid (\mathfrak{I} \bullet \Psi)(i, j) = 1 \right\} \\ &= \bigcap_{(k,\ell) \in \Psi} \bigcup_{(\tilde{k},\tilde{\ell}) \in \Psi} \left\{ \mathfrak{I} \in \{0,1\}^{m \times n} \mid \mathfrak{I}(i+k-\tilde{k}, j+\ell-\tilde{\ell}) = 1 \right\} \end{aligned} \quad (3.13)$$

Proof. Using equation (3.10), we obtain the equality

$$\begin{aligned} & \left\{ \mathfrak{I} \in \{0,1\}^{m \times n} \mid (\mathfrak{I} \circ \Psi)(i, j) = 1 \right\} \\ &= \left\{ \mathfrak{I} \in \{0,1\}^{m \times n} \mid 1 - \prod_{(k,\ell) \in \Psi} \left(1 - \left(\prod_{(\tilde{k},\tilde{\ell}) \in \Psi} \mathfrak{I}(i-k+\tilde{k}, j-\ell+\tilde{\ell}) \right) \right) = 1 \right\} \\ &= \left\{ \mathfrak{I} \in \{0,1\}^{m \times n} \mid \prod_{(k,\ell) \in \Psi} \left(1 - \left(\prod_{(\tilde{k},\tilde{\ell}) \in \Psi} \mathfrak{I}(i-k+\tilde{k}, j-\ell+\tilde{\ell}) \right) \right) = 0 \right\}. \end{aligned}$$

Consider, that $\prod_{(k,\ell) \in \Psi} \left(1 - \left(\prod_{(\tilde{k},\tilde{\ell}) \in \Psi} \mathfrak{I}(i-k+\tilde{k}, j-\ell+\tilde{\ell}) \right) \right) = 0$, if and only if $1 - \left(\prod_{(\tilde{k},\tilde{\ell}) \in \Psi} \mathfrak{I}(i-k+\tilde{k}, j-\ell+\tilde{\ell}) \right) = 0$ for any $(k, \ell) \in \Psi$. Thus, we obtain

$$\begin{aligned} & \left\{ \mathfrak{I} \in \{0,1\}^{m \times n} \mid (\mathfrak{I} \circ \Psi)(i, j) = 1 \right\} \\ &= \left\{ \mathfrak{I} \in \{0,1\}^{m \times n} \mid \prod_{(k,\ell) \in \Psi} \left(1 - \left(\prod_{(\tilde{k},\tilde{\ell}) \in \Psi} \mathfrak{I}(i-k+\tilde{k}, j-\ell+\tilde{\ell}) \right) \right) = 0 \right\} \end{aligned}$$

$$\begin{aligned}
&= \bigcup_{(k,\ell) \in \Psi} \left\{ \mathfrak{I} \in \{0,1\}^{m \times n} \mid 1 - \left(\prod_{(\tilde{k},\tilde{\ell}) \in \Psi} \mathfrak{I}(i-k+\tilde{k}, j-\ell+\tilde{\ell}) \right) = 0 \right\} \\
&= \bigcup_{(k,\ell) \in \Psi} \left\{ \mathfrak{I} \in \{0,1\}^{m \times n} \mid \prod_{(\tilde{k},\tilde{\ell}) \in \Psi} \mathfrak{I}(i-k+\tilde{k}, j-\ell+\tilde{\ell}) = 1 \right\}.
\end{aligned}$$

For fixed $(k, \ell) \in \Psi$, we have $\prod_{(\tilde{k}, \tilde{\ell}) \in \Psi} \mathfrak{I}(i-k+\tilde{k}, j-\ell+\tilde{\ell}) = 1$, if and only if $\mathfrak{I}(i-k+\tilde{k}, j-\ell+\tilde{\ell}) = 1$ for all $(\tilde{k}, \tilde{\ell}) \in \Psi$. This yields

$$\begin{aligned}
&\left\{ \mathfrak{I} \in \{0,1\}^{m \times n} \mid (\mathfrak{I} \circ \Psi)(i, j) = 1 \right\} \\
&= \bigcup_{(k,\ell) \in \Psi} \left\{ \mathfrak{I} \in \{0,1\}^{m \times n} \mid \prod_{(\tilde{k},\tilde{\ell}) \in \Psi} \mathfrak{I}(i-k+\tilde{k}, j-\ell+\tilde{\ell}) = 1 \right\} \\
&= \bigcup_{(k,\ell) \in \Psi} \bigcap_{(\tilde{k},\tilde{\ell}) \in \Psi} \left\{ \mathfrak{I} \in \{0,1\}^{m \times n} \mid \mathfrak{I}(i-k+\tilde{k}, j-\ell+\tilde{\ell}) = 1 \right\},
\end{aligned}$$

proving the first equality. The second equality can be proven analogously. \square

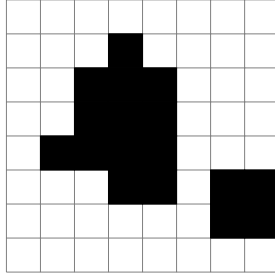
3.2 Examples

In the following Figures, we display examples of binary opening and closing to depict the effects these operators have on a binary image. Note, that pixels with value one are black and pixels with value zero are white. For convenience, we display the original image as light gray.

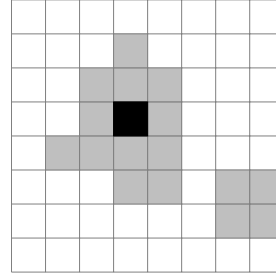
In Figure 6 we see an example of binary morphological opening, whose effect we want to examine. We use a 3×3 pixel structuring element. Edges of the larger connected region are smoothed, making morphological opening a versatile tool for simplifying edges and outlier elimination, see [Shi10, p. 69].

Figure 7 shows an example of binary morphological closing with a 3×3 pixel structuring element. The gaps between the pixels are filled. Hence, morphological closing is frequently used as a tool to fill gaps in binary images, see [Shi10, p. 69].

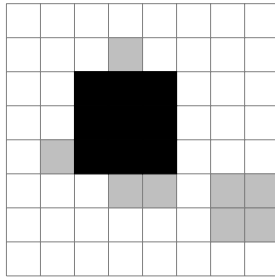
Altogether, both morphological opening and closing are effective tools to smooth edges. Morphological opening removes outliers and simplifies edges.



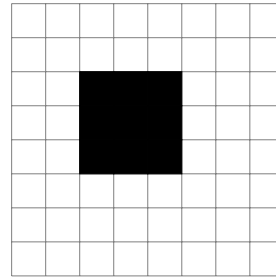
(a) Binary image.



(b) Result of binary erosion of 6a with a 3×3 pixel structuring element. The light gray pixels are set to zero.



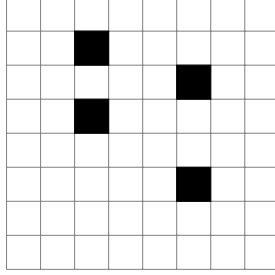
(c) Binary dilation of the black pixel in 6b with a 3×3 pixel structuring element. The original image is displayed as light gray.



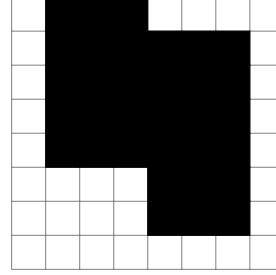
(d) Result of opening of 6a with a 3×3 pixel structuring element. Outliers have been eliminated and edges have been smoothed.

Figure 6: Example of binary morphological opening using a 3×3 pixel structuring element.

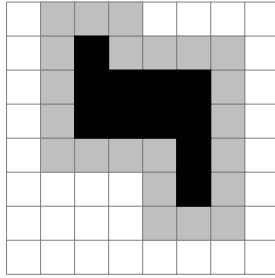
Closing fills gaps. The operators are dual in the sense, that the complement of the complement's closing is opening of the original set with the same structuring element and vice versa.



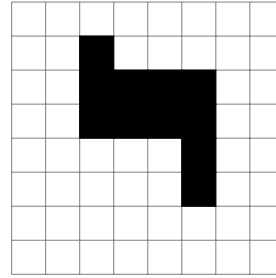
(a) Binary image.



(b) Binary dilation of 7a with a 3×3 pixel structuring element.



(c) Result of binary erosion of 7b with a 3×3 pixel structuring element. The light gray pixels are set to zero again.



(d) Result of closing of 7a with a 3×3 pixel structuring element. The gaps between pixels have been filled.

Figure 7: Example of binary morphological closing using a 3×3 pixel structuring element.

4 Main results

In the following, we consider the effect of morphological opening and closing on the upper bounds for the error probabilities in the statistical test developed in Section 2.2. Note, that under morphological opening and closing we have $\Theta \circ \Psi \subseteq \Theta \subseteq \Theta \bullet \Psi$ for any structuring element Ψ . From this fact we deduce, that morphological opening will lower the probability of a type I error, but increase the probability of a type II error. Morphological closing, on the other hand, has the opposite effect. While this serves as a qualitative argument for the employment of these operators, we aim at quantifying this change of the probabilities by proving upper bounds for the error probabilities after morphological opening and closing have been applied.

We use a square structuring element, since we have the prior information,

that the region of interest in the image is rectangular.

The changes of the upper bound for the probability of a type I error after opening and after opening and closing with a square structuring element are quantified in the following theorem.

Theorem 4.1. *Let $m, n \in \mathbb{N}$, $c \in \mathbb{R} \setminus \{0\}$ and $\Omega = \{1, \dots, m\} \times \{1, \dots, n\}$.*

Assume that F follows the statistical model given in (2.5).

For a statistical significance $\alpha \in (0, 1)$, let t_α be a threshold, such that $\mathbb{P}_V(\|\Delta^+ F(i, j)\| \geq t_\alpha) \leq \alpha$ for every $(i, j) \in \Omega$ and $V \in \mathcal{H}_0^+(i, j)$ and $\mathbb{P}_V(\|\Delta^- F(i, j)\| \geq t_\alpha) \leq \alpha$ for every $(i, j) \in \Omega$ and $V \in \mathcal{H}_0^-(i, j)$, cf. (2.10) and (2.11).

Let \mathfrak{I}_α be the random binary image defined by

$$\mathfrak{I}_\alpha(i, j) = \mathbb{1}_{\{T(i, j) \geq t_\alpha\}}$$

for all $(i, j) \in \Omega$.

Let $(i, j) \in \Omega$ and let $T(i, j)$ be the test statistic defined in (2.8) and $H_0(i, j)$ be the null hypothesis defined in (2.6).

Let $\varphi \in \mathbb{N}$ be odd and define the set $\Phi_\varphi = \left\{-\frac{\varphi-1}{2}, -\frac{\varphi-3}{2}, \dots, \frac{\varphi-3}{2}, \frac{\varphi-1}{2}\right\}$ and the structuring element $\Psi_\varphi = \Phi_\varphi \times \Phi_\varphi$. Then for $V \in \mathcal{H}_0(i, j)$ the following inequalities hold:

$$\mathbb{P}_V((\mathfrak{I}_\alpha \circ \Psi_\varphi)(i, j) = 1) \leq \varphi \alpha^{\frac{\varphi+1}{2}} \quad (4.1)$$

$$\mathbb{P}_V((\mathfrak{I}_\alpha \bullet \Psi_\varphi)(i, j) = 1) \leq \varphi^2 \alpha \quad (4.2)$$

$$\mathbb{P}_V(((\mathfrak{I}_\alpha \circ \Psi_\varphi) \bullet \Psi_\varphi)(i, j) = 1) \leq \varphi^3 \alpha^{\frac{\varphi+1}{2}} \quad (4.3)$$

Proof. We start with the proof of inequality (4.1). We aim to find an upper bound for the probability

$$\mathbb{P}_V((\mathfrak{I}_\alpha \circ \Psi_\varphi)(i, j) = 1)$$

for $V \in \mathcal{H}_0(i, j)$.

As discussed in Section 2.1, any matrix $V \in \mathcal{V}_c^{m, n}$ is uniquely defined by the top left corner (κ_1, λ_1) and bottom right corner (κ_2, λ_2) of the ROI $\Lambda =$

$\{\kappa_1, \dots, \kappa_2\} \times \{\lambda_1, \dots, \lambda_2\}$ contained in V , where Λ is defined as in Definition 2.1.

Since $V \in \mathcal{H}_0(i, j)$ we have $(i, j) \notin \Lambda$, implying, that $i < \kappa_1$ or $j < \lambda_1$ or $i > \kappa_2$ or $j > \lambda_2$, see Figure 3. These four cases are not mutually exclusive. As deducted in Section 2.2, the first two cases imply $\|\Delta^- V(i, j)\| = 0$ and the latter two imply $\|\Delta^+ V(i, j)\| = 0$.

Based on this knowledge, we can split up the sets $\mathcal{H}_0^+(i, j)$ and $\mathcal{H}_0^-(i, j)$ as defined in (2.10) and (2.11) by defining the sets

$$\begin{aligned}\mathcal{H}_0^{(I)}(i, j) &:= \left\{ V \in \mathcal{V}_c^{m, n} \mid V(\tilde{i}, \tilde{j}) = 0 \text{ for all } (\tilde{i}, \tilde{j}) \in \{1, \dots, i\} \times \{1, \dots, n\} \right\}, \\ \mathcal{H}_0^{(II)}(i, j) &:= \left\{ V \in \mathcal{V}_c^{m, n} \mid V(\tilde{i}, \tilde{j}) = 0 \text{ for all } (\tilde{i}, \tilde{j}) \in \{1, \dots, m\} \times \{1, \dots, j\} \right\}, \\ \mathcal{H}_0^{(III)}(i, j) &:= \left\{ V \in \mathcal{V}_c^{m, n} \mid V(\tilde{i}, \tilde{j}) = 0 \text{ for all } (\tilde{i}, \tilde{j}) \in \{i, \dots, m\} \times \{1, \dots, n\} \right\}, \\ \mathcal{H}_0^{(IV)}(i, j) &:= \left\{ V \in \mathcal{V}_c^{m, n} \mid V(\tilde{i}, \tilde{j}) = 0 \text{ for all } (\tilde{i}, \tilde{j}) \in \{1, \dots, m\} \times \{j, \dots, n\} \right\}.\end{aligned}$$

These sets correspond to the regions displayed in Figure 3. Note, that $\mathcal{H}_0^-(i, j) = \mathcal{H}_0^{(I)}(i, j) \cup \mathcal{H}_0^{(II)}(i, j)$ and $\mathcal{H}_0^+(i, j) = \mathcal{H}_0^{(III)}(i, j) \cup \mathcal{H}_0^{(IV)}(i, j)$. Furthermore, this implies $\mathcal{H}_0(i, j) = \mathcal{H}_0^{(I)}(i, j) \cup \mathcal{H}_0^{(II)}(i, j) \cup \mathcal{H}_0^{(III)}(i, j) \cup \mathcal{H}_0^{(IV)}(i, j)$.

W.l.o.g. due to symmetry, we assume the first case, i.e. $V \in \mathcal{H}_0^{(I)}(i, j)$. It follows, that

$$\|\Delta^- V(i, 1)\| = \dots = \|\Delta^- V(i, n)\| = 0.$$

implying $V \in \bigcap_{j=1}^n \mathcal{H}_0^-(i, j)$.

In a first step, we use equation (3.12) and the fact, that $\Psi_\varphi = \Phi_\varphi \times \Phi_\varphi$ to write the left hand side of inequality (4.1) as

$$\begin{aligned}\mathbb{P}_V((\mathfrak{I}_\alpha \circ \Psi_\varphi)(i, j) = 1) \\ &= \mathbb{P}_V \left(\bigcup_{(k, \ell) \in \Psi_\varphi} \bigcap_{(\tilde{k}, \tilde{\ell}) \in \Psi_\varphi} \left\{ \mathfrak{I}_\alpha(i - k + \tilde{k}, j - \ell + \tilde{\ell}) = 1 \right\} \right) \\ &= \mathbb{P}_V \left(\bigcup_{k, \ell \in \Phi_\varphi} \bigcap_{\tilde{k}, \tilde{\ell} \in \Phi_\varphi} \left\{ \mathfrak{I}_\alpha(i - k + \tilde{k}, j - \ell + \tilde{\ell}) = 1 \right\} \right).\end{aligned}$$

Using sub-additivity we can bound this from above by writing it as a sum over $\ell \in \Phi_\varphi$ to obtain

$$\begin{aligned} & \mathbb{P}_V((\mathfrak{I}_\alpha \circ \Psi_\varphi)(i, j) = 1) \\ & \leq \sum_{\ell \in \Phi_\varphi} \mathbb{P}_V \left(\bigcup_{k \in \Phi_\varphi} \bigcap_{\tilde{k}, \tilde{\ell} \in \Phi_\varphi} \left\{ \mathfrak{I}_\alpha(i - k + \tilde{k}, j - \ell + \tilde{\ell}) = 1 \right\} \right). \end{aligned}$$

By dropping every term except for $\tilde{k} = k$ in the inner intersection, we obtain

$$\begin{aligned} & \mathbb{P}_V((\mathfrak{I}_\alpha \circ \Psi_\varphi)(i, j) = 1) \\ & \leq \sum_{\ell \in \Phi_\varphi} \mathbb{P}_V \left(\bigcup_{k \in \Phi_\varphi} \bigcap_{\tilde{k}=k, \tilde{\ell} \in \Phi_\varphi} \left\{ \mathfrak{I}_\alpha(i - k + \tilde{k}, j - \ell + \tilde{\ell}) = 1 \right\} \right) \\ & = \sum_{\ell \in \Phi_\varphi} \mathbb{P}_V \left(\bigcup_{k \in \Phi_\varphi} \bigcap_{\tilde{\ell} \in \Phi_\varphi} \left\{ \mathfrak{I}_\alpha(i, j - \ell + \tilde{\ell}) = 1 \right\} \right). \end{aligned}$$

The events inside the probability do not depend on $k \in \Phi_\varphi$ anymore, which yields

$$\bigcup_{k \in \Phi_\varphi} \bigcap_{\tilde{\ell} \in \Phi_\varphi} \left\{ \mathfrak{I}_\alpha(i, j - \ell + \tilde{\ell}) = 1 \right\} = \bigcap_{\tilde{\ell} \in \Phi_\varphi} \left\{ \mathfrak{I}_\alpha(i, j - \ell + \tilde{\ell}) = 1 \right\}.$$

Plugging this in, we obtain

$$\mathbb{P}_V((\mathfrak{I}_\alpha \circ \Psi_\varphi)(i, j) = 1) \leq \sum_{\ell \in \Phi_\varphi} \mathbb{P}_V \left(\bigcap_{\tilde{\ell} \in \Phi_\varphi} \left\{ \mathfrak{I}_\alpha(i, j - \ell + \tilde{\ell}) = 1 \right\} \right).$$

We have defined the binary \mathfrak{I}_α by setting $\mathfrak{I}_\alpha(i, j) = \mathbf{1}_{\{T(i, j) \geq t_\alpha\}}$. Using this definition and the definition of $T(i, j)$ we can rewrite the upper bound in the above inequality as

$$\sum_{\ell \in \Phi_\varphi} \mathbb{P}_V \left(\bigcap_{\tilde{\ell} \in \Phi_\varphi} \left\{ \mathfrak{I}_\alpha(i, j - \ell + \tilde{\ell}) = 1 \right\} \right)$$

$$\begin{aligned}
&= \sum_{\ell \in \Phi_\varphi} \mathbb{P}_V \left(\bigcap_{\tilde{\ell} \in \Phi_\varphi} \{T(i, j - \ell + \tilde{\ell}) \geq t_\alpha\} \right) \\
&= \sum_{\ell \in \Phi_\varphi} \mathbb{P}_V \left(\bigcap_{\tilde{\ell} \in \Phi_\varphi} \left(\{\|\Delta^+ F(i, j - \ell + \tilde{\ell})\| \geq t_\alpha\} \cap \{\|\Delta^- F(i, j - \ell + \tilde{\ell})\| \geq t_\alpha\} \right) \right).
\end{aligned}$$

In the case $V \in \mathcal{H}_0^{(I)}(i, j) \subseteq \mathcal{H}_0^-(i, j)$, the values of $\|\Delta^+ V(i, j - \ell + \tilde{\ell})\|$ are unknown. Thus, we do not know the distribution of the random variables $\|\Delta^+ F(i, j - \ell + \tilde{\ell})\|$ and we drop the events $\{\|\Delta^+ F(i, j - \ell + \tilde{\ell})\| \geq t_\alpha\}$ to obtain

$$\begin{aligned}
&\mathbb{P}_V((\mathfrak{I}_\alpha \circ \Psi_\varphi)(i, j) = 1) \\
&\leq \sum_{\ell \in \Phi_\varphi} \mathbb{P}_V \left(\bigcap_{\tilde{\ell} \in \Phi_\varphi} \left(\{\|\Delta^+ F(i, j - \ell + \tilde{\ell})\| \geq t_\alpha\} \cap \{\|\Delta^- F(i, j - \ell + \tilde{\ell})\| \geq t_\alpha\} \right) \right) \\
&\leq \sum_{\ell \in \Phi_\varphi} \mathbb{P}_V \left(\bigcap_{\tilde{\ell} \in \Phi_\varphi} \{\|\Delta^- F(i, j - \ell + \tilde{\ell})\| \geq t_\alpha\} \right).
\end{aligned}$$

Define a subset $\tilde{\Phi}_\varphi = \left\{ -\frac{\varphi-1}{2}, -\frac{\varphi-5}{2}, \dots, \frac{\varphi-5}{2}, \frac{\varphi-1}{2} \right\}$ of Φ_φ . Since $\Delta^- F(i, j)$ only depends on the pixels (i, j) , $(i-1, j)$ and $(i, j-1)$, the set $\{\|\Delta^- F(i, j - \ell + \tilde{\ell})\| \mid \tilde{\ell} \in \tilde{\Phi}_\varphi\}$ is a set of independent random variables for fixed $\ell \in \Phi_\varphi$, see Figure 8.

We drop the terms in $\Phi_\varphi \setminus \tilde{\Phi}_\varphi$ and use the independence to obtain

$$\begin{aligned}
\mathbb{P}_V((\mathfrak{I}_\alpha \circ \Psi_\varphi)(i, j) = 1) &\leq \sum_{\ell \in \Phi_\varphi} \mathbb{P}_V \left(\bigcap_{\tilde{\ell} \in \Phi_\varphi} \{\|\Delta^- F(i, j - \ell + \tilde{\ell})\| \geq t_\alpha\} \right) \\
&\leq \sum_{\ell \in \Phi_\varphi} \mathbb{P}_V \left(\bigcap_{\tilde{\ell} \in \tilde{\Phi}_\varphi} \{\|\Delta^- F(i, j - \ell + \tilde{\ell})\| \geq t_\alpha\} \right) \\
&= \sum_{\ell \in \Phi_\varphi} \prod_{\tilde{\ell} \in \tilde{\Phi}_\varphi} \mathbb{P}_V(\|\Delta^- F(i, j - \ell + \tilde{\ell})\| \geq t_\alpha).
\end{aligned}$$

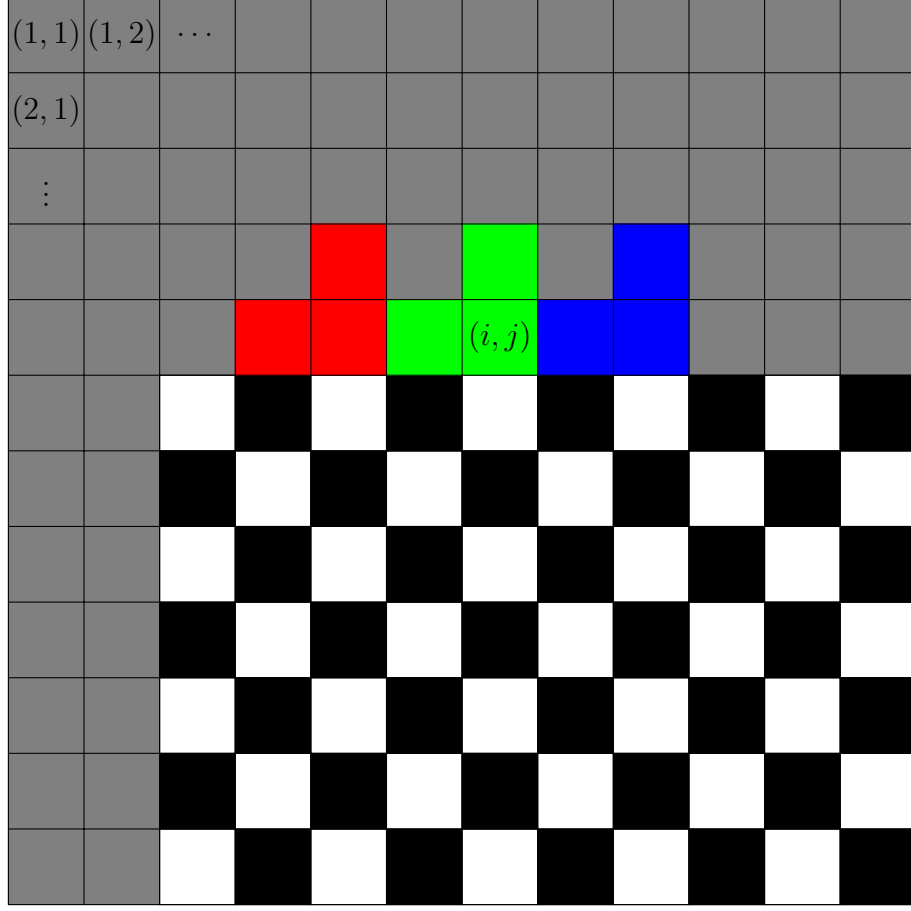


Figure 8: The random variable $\|\Delta^- F(i, j)\|$ only depends on the green pixels, $\|\Delta^- F(i, j - 2)\|$ depends on the red pixels and $\|\Delta^- F(i, j + 2)\|$ on the blue pixels. Since these are all distinct from another, the random variables are independent.

Since $V \in \mathcal{H}_0^{(I)}(i, j)$, we have

$$V \in \bigcap_{\tilde{j}=1}^n \mathcal{H}_0^-(i, \tilde{j}) \subseteq \bigcap_{\ell \in \Phi_\varphi, \tilde{\ell} \in \tilde{\Phi}_\varphi} \mathcal{H}_0^-(i, j - \ell + \tilde{\ell}).$$

By assumption, $\mathbb{P}_V(\|\Delta^- F(i, j)\| \geq t_\alpha) \leq \alpha$ for $V \in \mathcal{H}_0^-(i, j)$ yielding the upper bound

$$\mathbb{P}_V((\mathcal{I}_\alpha \circ \Psi_\varphi)(i, j) = 1) \leq \sum_{\ell \in \Phi_\varphi} \prod_{\tilde{\ell} \in \tilde{\Phi}_\varphi} \mathbb{P}_V(\|\Delta^- F(i, j - \ell + \tilde{\ell})\| \geq t_\alpha)$$

$$\begin{aligned}
&\leq \sum_{\ell \in \Phi_\varphi} \prod_{\tilde{\ell} \in \tilde{\Phi}_\varphi} \alpha \\
&= |\Phi_\varphi| \alpha^{|\tilde{\Phi}_\varphi|} \\
&= \varphi \alpha^{\frac{\varphi+1}{2}}.
\end{aligned}$$

This proves the first inequality for $V \in \mathcal{H}_0^{(I)}(i, j)$. The other three cases can be proven analogously by swapping the roles of k or \tilde{k} with ℓ or $\tilde{\ell}$, respectively and/or by replacing Δ^- by Δ^+ . This finishes the proof of the first inequality.

For the proof of the second and third inequality, we exploit our prior knowledge on V again. As already stated in the proof of the first inequality, we have, that $H_0(i, j)$ is equivalent to $(i, j) \notin \Lambda$, which is equivalent to at least one of the cases $V \in \mathcal{H}_0^{(I)}(i, j), V \in \mathcal{H}_0^{(II)}(i, j), V \in \mathcal{H}_0^{(III)}(i, j)$ or $V \in \mathcal{H}_0^{(IV)}(i, j)$.

Again, we assume the first case, i.e. $V \in \mathcal{H}_0^{(I)}(i, j)$. This implies, that the null hypotheses $H_0(\tilde{i}, 1), \dots, H_0(\tilde{i}, n)$ are true for all $\tilde{i} \in \{1, \dots, i\}$. It also implies

$$\|\Delta^- V(\tilde{i}, 1)\| = \dots = \|\Delta^- V(\tilde{i}, n)\| = 0$$

for all $\tilde{i} \in \{1, \dots, i\}$.

Set $k_0 = -\frac{\varphi-1}{2}$ and $\ell_0 = 0$. Then $(k_0, \ell_0) \in \Psi_\varphi$ and we get that the null hypotheses $H_0(i + k_0 - \tilde{k}, j + \ell_0 - \tilde{\ell})$ are true for all $\tilde{k}, \tilde{\ell} \in \Phi_\varphi$. Hence, we have $V \in \cap_{\tilde{k}, \tilde{\ell} \in \Phi_\varphi} \mathcal{H}_0(i + k_0 - \tilde{k}, j + \ell_0 - \tilde{\ell})$ as well as $\|\Delta^- V(i + k_0 - \tilde{k}, j + \ell_0 - \tilde{\ell})\| = 0$ for all $\tilde{k}, \tilde{\ell} \in \Phi_\varphi$.

Let $\mathfrak{K}_\alpha \in \{\mathfrak{I}_\alpha, \mathfrak{I}_\alpha \circ \Psi_\varphi\}$. We use equation (3.13) and $\Psi_\varphi = \Phi_\varphi \times \Phi_\varphi$ to expand $\mathbb{P}_V((\mathfrak{K}_\alpha \bullet \Psi_\varphi)(i, j) = 1)$ as

$$\begin{aligned}
&\mathbb{P}_V((\mathfrak{K}_\alpha \bullet \Psi_\varphi)(i, j) = 1) \\
&= \mathbb{P}_V \left(\bigcap_{(k, \ell) \in \Psi_\varphi} \bigcup_{(\tilde{k}, \tilde{\ell}) \in \Psi_\varphi} \{\mathfrak{K}_\alpha(i + k - \tilde{k}, j + \ell - \tilde{\ell}) = 1\} \right) \\
&= \mathbb{P}_V \left(\bigcap_{k, \ell \in \Phi_\varphi} \bigcup_{\tilde{k}, \tilde{\ell} \in \Phi_\varphi} \{\mathfrak{K}_\alpha(i + k - \tilde{k}, j + \ell - \tilde{\ell}) = 1\} \right).
\end{aligned}$$

By dropping every term in the intersection except for $k = k_0$ and $\ell = \ell_0$ we can bound this from above by

$$\begin{aligned} \mathbb{P}_V((\mathfrak{K}_\alpha \bullet \Psi_\varphi)(i, j) = 1) &= \mathbb{P}_V \left(\bigcap_{k, \ell \in \Phi_\varphi} \bigcup_{\tilde{k}, \tilde{\ell} \in \Phi_\varphi} \left\{ \mathfrak{K}_\alpha(i + k - \tilde{k}, j + \ell - \tilde{\ell}) = 1 \right\} \right) \\ &\leq \mathbb{P}_V \left(\bigcup_{\tilde{k}, \tilde{\ell} \in \Phi_\varphi} \left\{ \mathfrak{K}_\alpha(i + k_0 - \tilde{k}, j + \ell_0 - \tilde{\ell}) = 1 \right\} \right) \\ &= \mathbb{P}_V \left(\bigcup_{\tilde{k}, \tilde{\ell} \in \Phi_\varphi} \left\{ \mathfrak{K}_\alpha(i + k_0 - \tilde{k}, j - \tilde{\ell}) = 1 \right\} \right). \end{aligned}$$

Using sub-additivity to write this as the sum over all $\tilde{k}, \tilde{\ell} \in \Phi_\varphi$ yields

$$\mathbb{P}_V((\mathfrak{K}_\alpha \bullet \Psi_\varphi)(i, j) = 1) \leq \sum_{\tilde{k}, \tilde{\ell} \in \Phi_\varphi} \mathbb{P}_V \left(\mathfrak{K}_\alpha(i + k_0 - \tilde{k}, j - \tilde{\ell}) = 1 \right).$$

As discussed, we have $V \in \bigcap_{\tilde{k}, \tilde{\ell} \in \Phi_\varphi} \mathcal{H}_0(i + k_0 - \tilde{k}, j - \tilde{\ell})$. In the case $\mathfrak{K}_\alpha = \mathfrak{I}_\alpha$, we get the upper bound

$$\begin{aligned} \mathbb{P}_V((\mathfrak{K}_\alpha \bullet \Psi_\varphi)(i, j) = 1) &\leq \sum_{\tilde{k}, \tilde{\ell} \in \Phi_\varphi} \mathbb{P}_V \left(\mathfrak{I}_\alpha(i + k_0 - \tilde{k}, j - \tilde{\ell}) = 1 \right) \\ &\leq \sum_{\tilde{k}, \tilde{\ell} \in \Phi_\varphi} \alpha \\ &= \varphi^2 \alpha, \end{aligned}$$

which proves the second inequality.

In the case $\mathfrak{K}_\alpha = \mathfrak{I}_\alpha \circ \Psi_\varphi$, we can use inequality (4.1) to get the upper bound

$$\begin{aligned} \mathbb{P}_V((\mathfrak{K}_\alpha \bullet \Psi_\varphi)(i, j) = 1) &\leq \sum_{\tilde{k}, \tilde{\ell} \in \Phi_\varphi} \mathbb{P}_V \left((\mathfrak{I}_\alpha \circ \Psi_\varphi)(i + k_0 - \tilde{k}, j - \tilde{\ell}) = 1 \right) \\ &\leq \sum_{\tilde{k}, \tilde{\ell} \in \Phi_\varphi} \varphi \alpha^{\frac{\varphi+1}{2}} \\ &= \varphi^3 \alpha^{\frac{\varphi+1}{2}}. \end{aligned}$$

This proves the second and third inequality for $V \in \mathcal{H}_0^{(I)}(i, j)$. The other

cases are proven analogously by taking $k_0 = 0, \ell_0 = -\frac{\varphi-1}{2}$ in the second case, $k_0 = \frac{\varphi-1}{2}, \ell_0 = 0$ in the third case and $k_0 = 0, \ell_0 = \frac{\varphi-1}{2}$ in the fourth case. In the second and fourth case, the roles of Δ^+ and Δ^- are swapped. This finishes the proof of the second and third inequality and thus the proof of the theorem. \square

Remark 4.2. The bounds in Theorem 4.1 hold for all background pixels. This means, they also hold for the worst case, i.e. pixels, that lie adjacent to the region of interest, see Figure 8.

Remark 4.3. We require the threshold t_α in Theorem 4.1 to satisfy stronger conditions than $\mathbb{P}_V(T(i, j) \geq t_\alpha) \leq \alpha$ for every $V \in \mathcal{H}_0(i, j)$. Since the methods developed in Section 2.3 yield thresholds, that meet these stronger requirements, we use them to achieve better bounds in Theorem 4.1. Inequality 4.2 also holds for less assumptions than stated in Theorem 4.1, but this generalization is not needed in our case.

Let us consider the probability of a type II error in the statistical test. In Section 2.4 we numerically calculated bounds for this probability. Similar to the previous theorem, we aim at quantifying the change of the upper bound after morphological opening and closing are applied.

We will need the additional assumption, that the region of interest is sufficiently large, i.e. larger than the structuring element. Otherwise, even if there are no errors in the binarization through the statistical test, morphological opening will classify all pixels as background and thus the probability of a type II error cannot be bounded anymore.

Theorem 4.4. *Let $m, n \in \mathbb{N}$, $c \in \mathbb{R} \setminus \{0\}$ and $\Omega = \{1, \dots, m\} \times \{1, \dots, n\}$. Assume that F follows the statistical model given in (2.5). Let t be a threshold, such that*

$$\mathbb{P}_V(T(i, j) \leq t) \leq \beta$$

for some $\beta \in (0, 1)$ and all $(i, j) \in \Omega$ and $V \in \mathcal{H}_1(i, j)$, cf. (2.17).

Let \mathfrak{I} be the random binary image defined by

$$\mathfrak{I}(i, j) = \mathbb{1}_{\{T(i, j) \geq t\}}$$

for all $(i, j) \in \Omega$.

Let $(i, j) \in \Omega$ and let $T(i, j)$ be the test statistic defined in (2.8) and $H_1(i, j)$ be the alternative hypothesis defined in (2.7).

Let $\varphi \in \mathbb{N}$ be odd and define the set $\Phi_\varphi = \left\{-\frac{\varphi-1}{2}, -\frac{\varphi-3}{2}, \dots, \frac{\varphi-3}{2}, \frac{\varphi-1}{2}\right\}$ and the structuring element $\Psi_\varphi = \Phi_\varphi \times \Phi_\varphi$.

Denote by $\Lambda = \{\kappa_1, \dots, \kappa_2\} \times \{\lambda_1, \dots, \lambda_2\}$ the ROI contained in V . Let $\min\{\kappa_2 - \kappa_1 + 1, \lambda_2 - \lambda_1 + 1\} \geq \varphi$. Then for $V \in \mathcal{H}_1(i, j)$ the following inequalities hold:

$$\mathbb{P}_V((\mathfrak{I} \circ \Psi_\varphi)(i, j) = 0) \leq \varphi^2 \beta \quad (4.4)$$

$$\mathbb{P}_V((\mathfrak{I} \bullet \Psi_\varphi)(i, j) = 0) \leq \beta \quad (4.5)$$

$$\mathbb{P}_V(((\mathfrak{I} \circ \Psi_\varphi) \bullet \Psi_\varphi)(i, j) = 0) \leq \varphi^2 \beta \quad (4.6)$$

Proof. We start by proving inequality (4.4). We use a similar approach as in Theorem 4.1 by finding indices $(k_0, \ell_0) \in \Psi_\varphi$, such that the alternative hypotheses $H_1(i - k_0 + \tilde{k}, j - \ell_0 + \tilde{\ell})$ are true for all $\tilde{k}, \tilde{\ell} \in \Phi_\varphi$. Figure 9 shows, that we can find such indices even for the case of a corner pixel. A constructive proof can be found in Appendix A.

The alternative hypotheses $H_1(i - k_0 + \tilde{k}, j - \ell_0 + \tilde{\ell})$ being true for all $\tilde{k}, \tilde{\ell} \in \Phi_\varphi$ implies $V \in \bigcap_{\tilde{k}, \tilde{\ell} \in \Phi_\varphi} \mathcal{H}_1(i - k_0 + \tilde{k}, j - \ell_0 + \tilde{\ell})$.

We start by using equation (3.12) and $\Psi_\varphi = \Phi_\varphi \times \Phi_\varphi$ to write the left hand side of inequality (4.4) as

$$\begin{aligned} \mathbb{P}_V((\mathfrak{I} \circ \Psi_\varphi)(i, j) = 0) &= \mathbb{P}_V \left(\bigcap_{(k, \ell) \in \Psi_\varphi} \bigcup_{(\tilde{k}, \tilde{\ell}) \in \Psi_\varphi} \{\mathfrak{I}(i - k + \tilde{k}, j - \ell + \tilde{\ell}) = 0\} \right) \\ &= \mathbb{P}_V \left(\bigcap_{k, \ell \in \Phi_\varphi} \bigcup_{\tilde{k}, \tilde{\ell} \in \Phi_\varphi} \{\mathfrak{I}(i - k + \tilde{k}, j - \ell + \tilde{\ell}) = 0\} \right). \end{aligned}$$

We drop every term in the intersection except $k = k_0, \ell = \ell_0$ to bound this

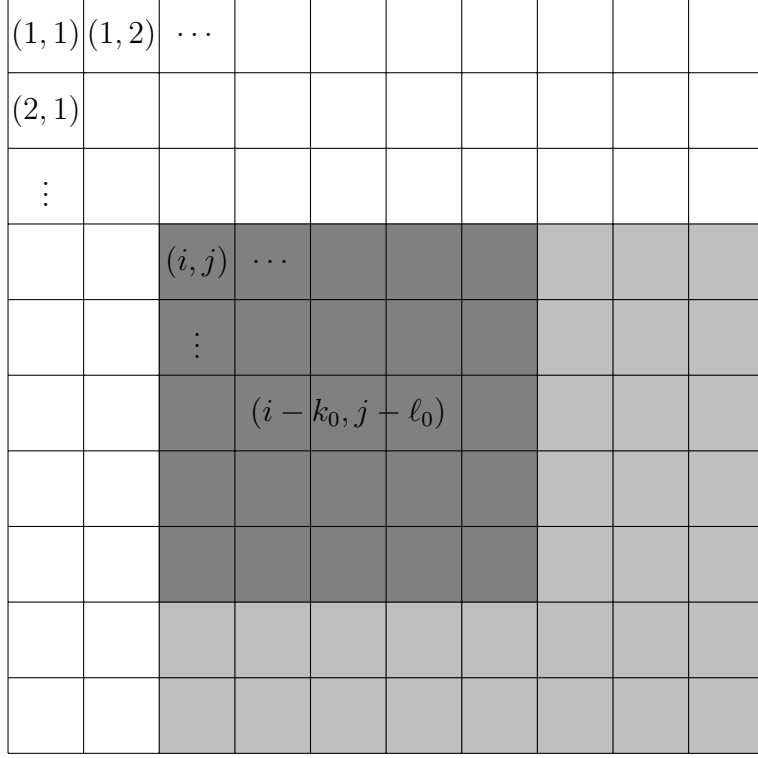


Figure 9: White pixels represent background, light gray pixels represent foreground. The indices $(k_0, \ell_0) \in \Psi_\varphi$ are chosen, such that for all $\tilde{k}, \tilde{\ell} \in \Phi_\varphi$ the pixels $(i - k_0 + \tilde{k}, j - \ell_0 + \tilde{\ell})$ belong to the foreground. These pixels are marked as dark gray.

by

$$\begin{aligned} \mathbb{P}_V((\mathcal{I} \circ \Psi_\varphi)(i, j) = 0) &= \mathbb{P}_V \left(\bigcap_{k, \ell \in \Phi_\varphi} \bigcup_{\tilde{k}, \tilde{\ell} \in \Phi_\varphi} \{ \mathcal{I}(i - k + \tilde{k}, j - \ell + \tilde{\ell}) = 0 \} \right) \\ &\leq \mathbb{P}_V \left(\bigcup_{\tilde{k}, \tilde{\ell} \in \Phi_\varphi} \{ \mathcal{I}(i - k_0 + \tilde{k}, j - \ell_0 + \tilde{\ell}) = 0 \} \right). \end{aligned}$$

We use sub-additivity to write this as the sum over all $\tilde{k}, \tilde{\ell} \in \Phi_\varphi$ and obtain

$$\mathbb{P}_V((\mathcal{I} \circ \Psi_\varphi)(i, j) = 0) \leq \sum_{\tilde{k}, \tilde{\ell} \in \Phi_\varphi} \mathbb{P}_V(\mathcal{I}(i - k_0 + \tilde{k}, j - \ell_0 + \tilde{\ell}) = 0).$$

Using the fact, that $V \in \cap_{\tilde{k}, \tilde{\ell} \in \Phi_\varphi} \mathcal{H}_1(i - k_0 + \tilde{k}, j - \ell_0 + \tilde{\ell})$ as well as the definition of \mathfrak{J} and the choice of the threshold t we get the upper bound

$$\begin{aligned}
\mathbb{P}_V((\mathfrak{J} \circ \Psi_\varphi)(i, j) = 0) &\leq \sum_{\tilde{k}, \tilde{\ell} \in \Phi_\varphi} \mathbb{P}_V(\mathfrak{J}(i - k_0 + \tilde{k}, j - \ell_0 + \tilde{\ell}) = 0) \\
&= \sum_{\tilde{k}, \tilde{\ell} \in \Phi_\varphi} \mathbb{P}_V(T(i - k_0 + \tilde{k}, j - \ell_0 + \tilde{\ell}) \leq t) \\
&\leq \sum_{\tilde{k}, \tilde{\ell} \in \Phi_\varphi} \beta \\
&= |\Phi_\varphi|^2 \beta \\
&= \varphi^2 \beta.
\end{aligned}$$

This finishes the proof of the first inequality.

For the proof of the second and third inequality, let $\mathfrak{K} \in \{\mathfrak{J}, \mathfrak{J} \circ \Psi_\varphi\}$. By the properties of morphological closing we have $(\mathfrak{K} \bullet \Psi_\varphi)(i, j) \geq \mathfrak{K}(i, j)$, yielding

$$\mathbb{P}_V((\mathfrak{K} \bullet \Psi_\varphi)(i, j) = 0) \leq \mathbb{P}_V(\mathfrak{K}(i, j) = 0).$$

In the case $\mathfrak{K} = \mathfrak{J}$, we obtain

$$\mathbb{P}_V((\mathfrak{K} \bullet \Psi_\varphi)(i, j) = 0) \leq \mathbb{P}_V(\mathfrak{J}(i, j) = 0) = \mathbb{P}_V(T(i, j) \leq t) \leq \beta.$$

In the case $\mathfrak{K} = \mathfrak{J} \circ \Psi_\varphi$, we can apply inequality (4.4), since $V \in \mathcal{H}_1(i, j)$, and obtain the upper bound

$$\begin{aligned}
\mathbb{P}_V((\mathfrak{K} \bullet \Psi_\varphi)(i, j) = 0) &\leq \mathbb{P}_V((\mathfrak{J} \circ \Psi_\varphi)(i, j) = 0) \\
&\leq \varphi^2 \beta.
\end{aligned}$$

This proves the second and third inequality and thus finishes the proof. \square

Remark 4.5. The bounds in the previous theorem hold for all pixels within the region of interest, i.e. also for the edges and corners of the region of interest.

For pixels with a sufficient distance from the edges of the region of interest,

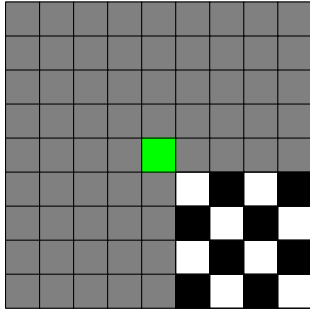
we can also prove the upper bound

$$\mathbb{P}_V (((\mathfrak{I} \circ \Psi_\varphi) \bullet \Psi_\varphi)(i, j) = 0) \leq \varphi^{10} \beta^4.$$

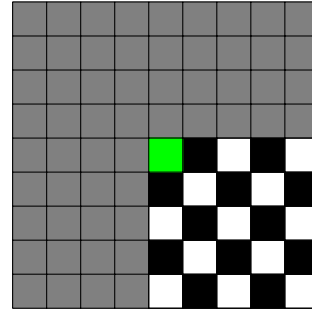
A proof can be found in Appendix A. This only improves the bound for very small values of β .

5 Simulation results

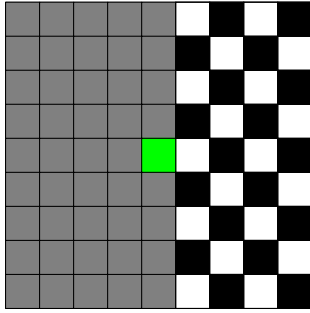
To simulate the error rates of the statistical test and the subsequent application of morphological opening and closing, we create six different types of images, depending on the position of the pixel (i, j) with respect to the region of interest, see Figure 10.



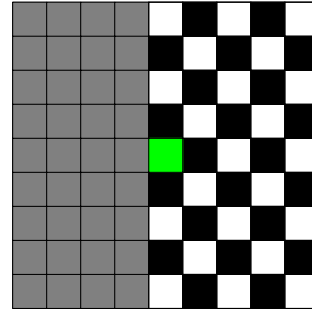
(a) Background pixel at the corner of the ROI.



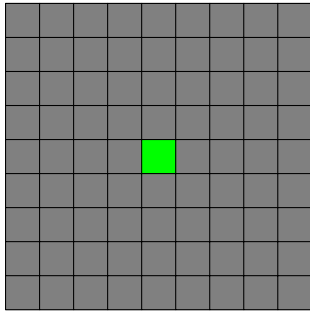
(b) Foreground pixel at the corner of the ROI.



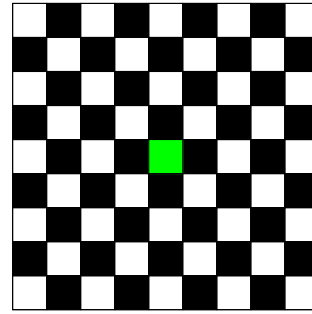
(c) Background pixel at the edge of the ROI.



(d) Foreground pixel at the edge of the ROI.



(e) Background pixel surrounded by background.



(f) Foreground pixel surrounded by foreground.

Figure 10: Position of the simulated pixels with respect to the ROI.

The six different simulated types include the best and worst case for identification of a background and foreground pixel, respectively. For both background and foreground pixels to be identified correctly, it is ideal, if the pixel is only surrounded by other background or foreground pixels, see Figures 10e and 10f. For a background pixel to be correctly identified, the worst case is, if the pixel is located at the edge of the region of interest, see Figure 10c. Similarly, the worst case for a foreground pixel to be correctly identified is to be located at the corner of the region of interest, see Figure 10b.

While other positions of the pixel (i, j) with respect to the region of interest are possible, our simulations cover the best and worst cases. The error rates for other cases lie between those of the extreme cases.

The images are constructed around the pixel according to the target position of the pixel. This is achieved by creating the image V as an image with side length $2\varphi + 3$ and setting the values of V , such that the pixel $(\varphi + 2, \varphi + 2)$ has the desired position with respect to the region of interest, where φ is the side length of the used structuring element.

For our simulations we cover four different approaches to extracting the ROI. In the first one, we only perform the statistical test developed in Section 2.2. For the second and third approach, we apply morphological opening or closing subsequently to the statistical test, respectively. The last approach covers the application of opening to the outcome of the statistical test and subsequent closing.

We want to bound the probability of a type I error below the statistical significance α for all of these four methods. To this end, we use an adjusted statistical significance $\tilde{\alpha}$ to calculate the threshold $t_{\tilde{\alpha}}$ for the statistical test depending on the morphological operations we perform subsequently to the statistical test, see Table 2.

Then, by inequalities (4.1), (4.2) and (4.3), the probability of a type I error is bounded by α for all approaches.

For each type of image and each of the four methods, we randomly generate 1000 noise terms and add it to the image with standard deviations σ ranging from 1 to 150. For each of the four approaches, we determine the error rate by dividing the the number of times the pixel is falsely identified by the

Morphological operations	Adjusted statistical significance $\tilde{\alpha}$
-	$\tilde{\alpha} = \alpha$
Opening	$\tilde{\alpha} = \left(\frac{\alpha}{\varphi}\right)^{\frac{2}{\varphi+1}}$
Closing	$\tilde{\alpha} = \frac{\alpha}{\varphi^2}$
Opening, closing	$\tilde{\alpha} = \left(\frac{\alpha}{\varphi^3}\right)^{\frac{2}{\varphi+1}}$

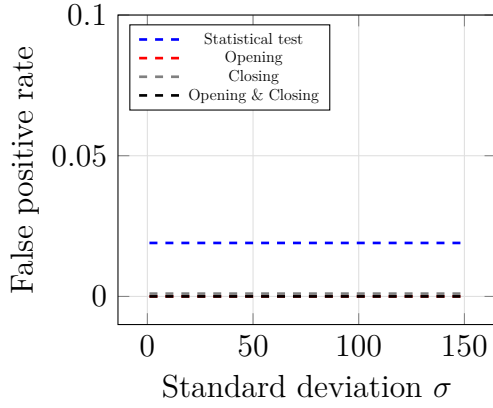
Table 2: Adjusted statistical significance for the statistical test depending on the morphological operations performed subsequently to the statistical test.

number of generated noise terms.

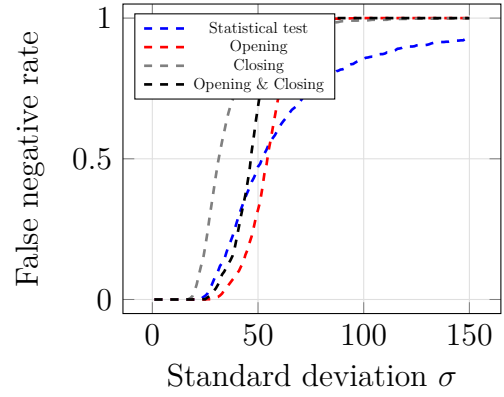
In Figure 11 the error rates for $\alpha = 0.05$ and $\varphi = 7$ are displayed.

We see, that for a background pixel the false positive rate is below the target statistical significance of 0.05 for all approaches and all simulated positions. Only in Figure 11c the false positive rate is close to α for small values of σ , but drops, as σ increases. We also note, that for all simulated positions of a background pixel, the binarization through the statistical test has by far the highest error rate, although we chose adjusted statistical significances to bound the false positive rate below 0.05 for all used methods. This is explained by the fact, that inequalities (2.16), (4.1), (4.2) and (4.3) are only upper bounds. These simulation results indicate, that they are not sharp and an improvement is possible.

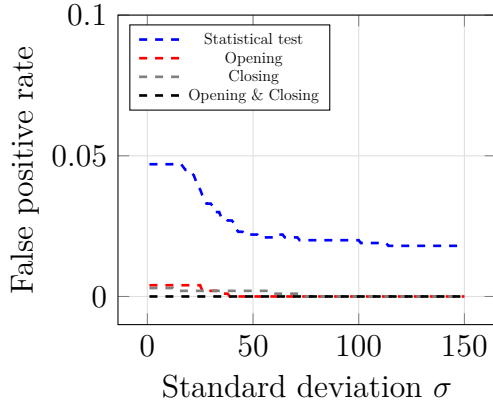
For the simulated positions of foreground pixels, the error rates are zero for small standard deviations for all methods. In the worst case, the false negative rate is zero only up to around $\sigma = 25$, see Figure 11b. In the best case, the false negative rate stays close to zero up to around $\sigma = 50$, see Figure 11f. For all simulated positions, the false negative rate increases, as the standard deviation increases. Eventually, the approach without application of morphological operations has the lowest false negative rate. Improvements of the aforementioned inequalities could change this, as a more accurately chosen adjusted statistical significance $\tilde{\alpha}$ would lower the false negative rate.



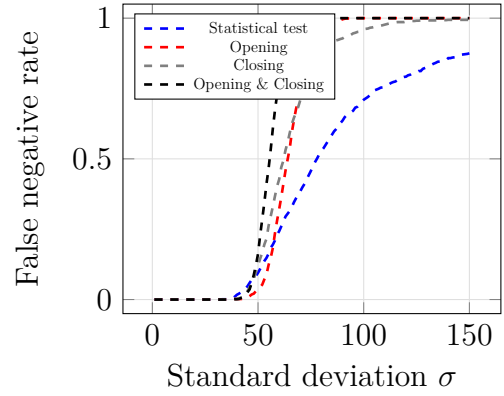
(a) Background pixel at the corner of the ROI.



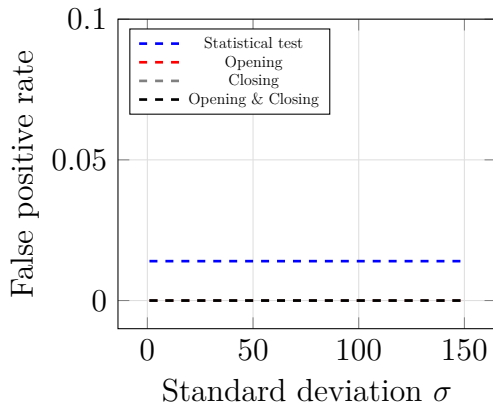
(b) Foreground pixel at the corner of the ROI.



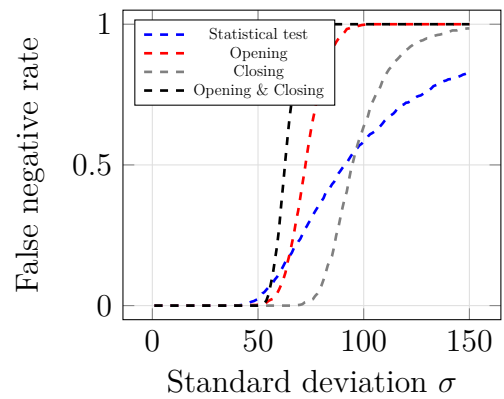
(c) Background pixel at the edge of the ROI.



(d) Foreground pixel at the edge of the ROI.



(e) Background pixel surrounded by background.



(f) Foreground pixel surrounded by foreground.

Figure 11: Error rates for all four ROI extraction approaches. The x -axes display the standard deviation σ and the y -axes the error rate ($\alpha = 0.05, \varphi = 7$).

Figure 12 provides a closer look at the false negative rates in Figure 11. We zoom in on the range of standard deviations, where the error rates change the most.

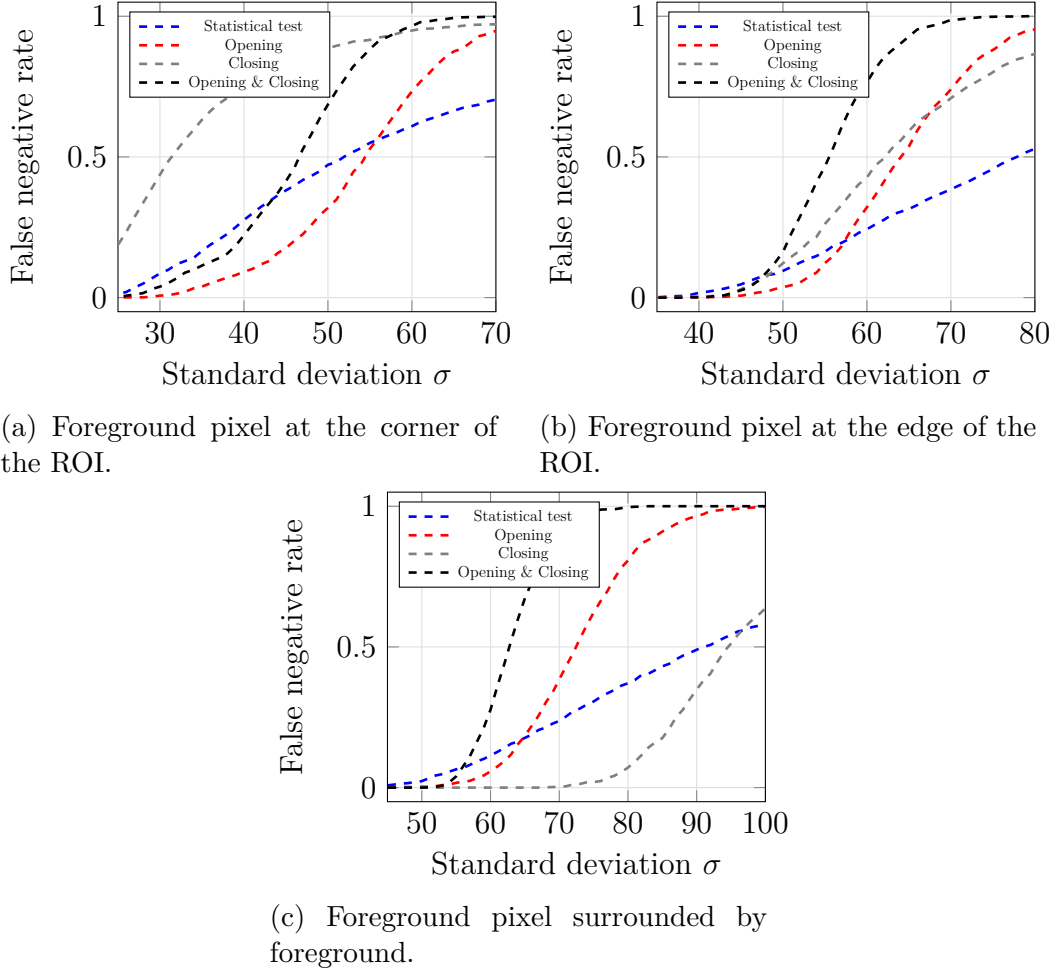


Figure 12: Closer look at the false negative rates in Figure 11.

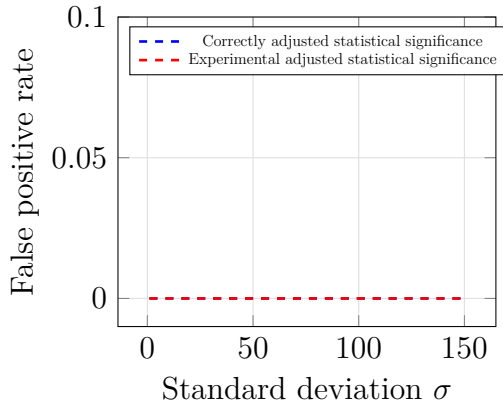
In the case of a foreground pixel at the corner of the ROI, we see, that only applying morphological opening after the statistical test provides the lowest false negative rate for $\sigma \leq 56$, see Figure 12a. On the other hand, applying morphological closing has the highest false negative rate. This is counterintuitive at first, as we use closing to decrease the false negative rate and opening can only worsen the false negative rate. But, as the pixel is located at the corner of the ROI, morphological opening and closing rarely

change the outcome of the statistical test. Thus, the observed false negative rates are due to the threshold in the statistical test being the lowest for $\tilde{\alpha} = \left(\frac{\alpha}{\varphi}\right)^{\frac{2}{\varphi+1}}$ and the highest for $\tilde{\alpha} = \frac{\alpha}{\varphi^2}$. For $\sigma > 56$ morphological opening changes the outcome of the statistical test more frequently, as type II errors in the statistical test become more numerous. Thus, the false negative rate, when applying opening after the statistical test, becomes higher than the false negative rate, when only the statistical test is performed.

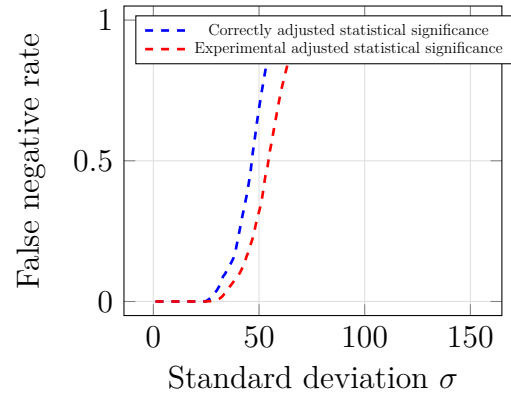
For a foreground pixel at the edge of the ROI, the statistical test alone has the lowest false negative rate for $\sigma > 57$ for the same reason as above. When comparing the four approaches, the positive effect of closing on the false negative rate becomes visible in this case, see Figure 12b. For $\sigma > 46$ the application of closing offers a lower false negative rate than that of opening & closing. For $\sigma > 67$ the false negative rate of closing falls below that of opening. At these points, the positive effect of closing on the number of type II errors surpasses the effect that the lower threshold based on the adjusted statistical significance has.

When considering a foreground pixel, that is only surrounded by other foreground pixels, closing comes into full effect, see Figure 12c. For $\sigma \leq 96$, closing offers the best false negative rate. Only performing the statistical test has a lower false negative rate for higher standard deviations, which is due to more numerous type II errors, that are not fixed by closing anymore. Here, again, the higher threshold for closing, based on the adjusted statistical significance, leads to a worse false negative rate.

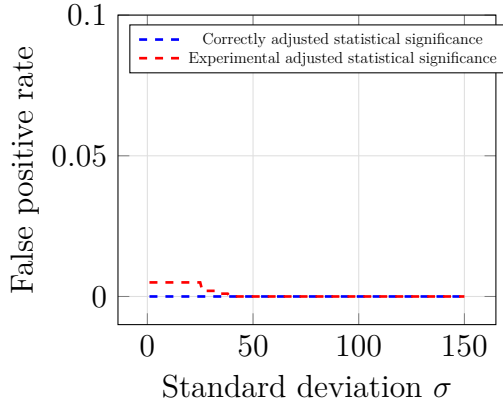
In all three cases, the false negative rates behave similarly, when comparing the statistical test, opening and opening & closing. Opening always performs better than opening & closing. Both perform better than the statistical test alone up to a certain σ . This behaviour is due to the different thresholds based on the adjusted statistical significances and the increase in type II errors, as the standard deviation of the noise terms increases. The performance of closing highly depends on the position of the pixel within the ROI. It can lead to the worst false negative rate for a corner pixel and the best false negative rate for a pixel only surrounded by other foreground pixels.



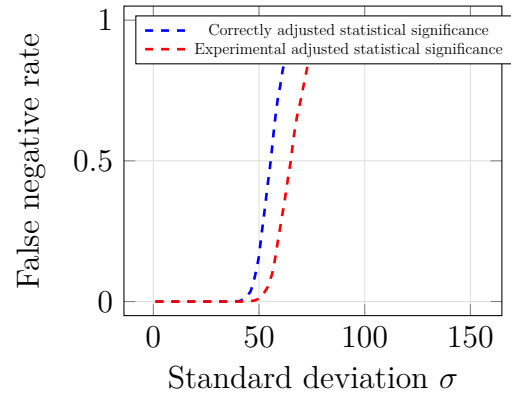
(a) Background pixel at the corner of the ROI.



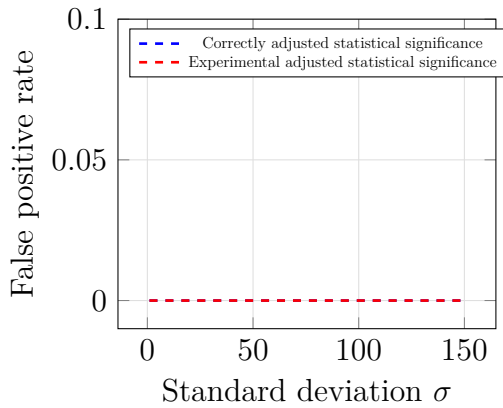
(b) Foreground pixel at the corner of the ROI.



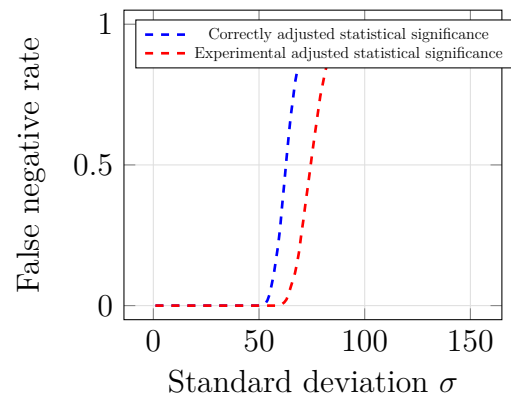
(c) Background pixel at the edge of the ROI.



(d) Foreground pixel at the edge of the ROI.



(e) Background pixel surrounded by background.



(f) Foreground pixel surrounded by foreground.

Figure 13: Comparison of the correctly adjusted statistical significance for opening & closing and the adjusted statistical significance for opening being used for opening & closing ($\alpha = 0.05$, $\varphi = 7$).

As we have found evidence, that improvements in the upper bounds (4.1), (4.2) and (4.3) could be possible, we are interested, how significant these improvements can be. To this end, we use the adjusted statistical significances for opening $\tilde{\alpha} = \left(\frac{\alpha}{\varphi}\right)^{\frac{2}{\varphi+1}}$ and for opening & closing $\tilde{\alpha} = \left(\frac{\alpha}{\varphi^3}\right)^{\frac{2}{\varphi+1}}$ and use them for the statistical test, but perform opening and subsequent closing in both cases. The results of this experimental approach are displayed in Figure 13. For the simulated background pixels, only the error rate only changes in the worst case. It is slightly higher for the experimental approach, but does not get close to the intended upper bound of 0.05. We notice, that for the simulated foreground pixels, the error rates are significantly lower in the experimental approach. The difference between the two adjusted statistical significances is the factor φ^2 . Since dropping this factor barely has an effect on the false positive rates, we expect that in inequalities (4.1) and (4.3) higher exponents are possible.

Simulations for other values of φ as well as for $\alpha = 0.01$ can be found in Appendix B. The code used for the simulation can be found in Appendix C.

6 Discussion

In this thesis we consider how the upper bounds for the error probabilities of a statistical test change, when morphological opening and closing are applied. To this end, we examine a simplified model and develop a thresholding method to extract the region of interest. The simplified model and thresholding method are designed, such that the probability of a type I error can be bounded by a given statistical significance. This is achieved by computing a suitable threshold based on the target statistical significance.

Theorems 4.1 and 4.4 quantify upper bounds for the error probabilities after morphological opening and closing are applied to the outcome of the statistical test. The upper bounds are stated in terms of the structuring element and the upper bounds for the error probabilities before morphological operations are applied. This was done by exploiting the prior knowledge, that the region of interest is rectangular and has a chessboard pattern.

In particular, we were able to obtain the exponent $\frac{\varphi+1}{2}$ in inequality (4.1) through the choice of the structuring element. For a background pixel to be falsely identified as foreground after opening, at least $\frac{\varphi+1}{2}$ many pixels background pixels have to be falsely categorized by the binarization through the statistical test. This is the *minimum number of independent points in a structuring element* that can lead to a false categorization of a background pixel.

A different shaped structuring element could lead to no improvements of the error probabilities. To see this, consider a diamond shaped structuring element. A background pixel at the edge of the region of interest, cf. Figure 10c, that is falsely classified by the statistical test, would not be correctly identified as a background pixel, when morphological opening with a diamond shaped structuring element is applied. Thus, the upper bound of this probability in this case does not decrease through application of morphological opening. Hence, we see, that the choice of the structuring element is substantial.

Since we only considered the categorization of a single pixel, a natural next step would be an expansion beyond the scope of this thesis by applying tech-

niques from the field of multiple testing. When researching the connection between multiple testing and morphological operations, one might consider more morphological operators. Namely, the convex hull operator is of high interest in the extraction of the region of interest of a fingerprint.

Generalizations of the results from Sections 2.2 and 2.3 to convex regions of interest with a chessboard pattern are possible. For the reasons described above, the choice of the structuring element for a convex region of interest is a question to ponder on. Advances could be achieved in conjunction with multiple testing techniques, since the choice of the structuring element is mainly a limiting factor for pixels close to the edge of the region of interest, which form only a subset of the total pixels in the image.

References

- [AB96] "Felix Abramovich and Yoav Benjamini". "Adaptive thresholding of wavelet coefficients". In: *Computational Statistics & Data Analysis* "22".4 ("1996"), "351 –361". ISSN: "0167-9473". DOI: "[https://doi.org/10.1016/0167-9473\(96\)00003-5](https://doi.org/10.1016/0167-9473(96)00003-5)". URL: "<http://www.sciencedirect.com/science/article/pii/0167947396000035>".
- [BG01] Asker Bazen and Sabih Gerez. "Segmentation of Fingerprint Images". In: 12 (Dec. 2001).
- [GR07] I.S. Gradshteyn and I.M. Ryzhik. *Table of Integrals, Series, and Products*. 7th. Academic Press, 2007.
- [Hen00] E. R. Henry. "Classification and uses of finger prints". In: (1900).
- [Liu+11] Eryun Liu et al. "Fingerprint segmentation based on an AdaBoost classifier". In: *Frontiers of Computer Science in China* 5 (June 2011), pp. 148–157. DOI: 10.1007/s11704-011-9134-x.
- [Mal+09] Davide Maltoni et al. *Handbook of fingerprint recognition*. Springer Science & Business Media, 2009.

- [Nut74] Albert H. Nuttall. “Some integrals involving the Q_M -function”. In: (1974).
- [Olv+10] Frank Olver et al. *NIST Handbook of Mathematical Functions*. Jan. 2010.
- [Shi10] Frank Y Shih. *Image processing and pattern recognition: fundamentals and techniques*. John Wiley & Sons, 2010.
- [THG16] Duy Hoang Thai, Stephan Huckemann, and Carsten Gottschlich. “Filter Design and Performance Evaluation for Fingerprint Image Segmentation”. In: *PLOS ONE* 11.5 (May 2016), pp. 1–31. DOI: 10.1371/journal.pone.0154160. URL: <https://doi.org/10.1371/journal.pone.0154160>.
- [Wat66] G.N. Watson. *A treatise on the theory of Bessel functions*. 2nd. Cambridge University Press, 1966.

A Additional proofs

Theorem A.1. *Let $\alpha, \beta > 0$. Denote by I_0 the modified Bessel function of the first kind [GR07, p. 910-911]. Then*

$$\int_0^\infty \exp(-\alpha\eta^2) I_0(\beta\eta) d\eta = \frac{\sqrt{\pi}}{2\sqrt{\alpha}} \exp\left(\frac{\beta^2}{8\alpha}\right) I_0\left(\frac{\beta^2}{8\alpha}\right). \quad (\text{A.1})$$

Proof. We note, that by substituting $\phi = \pi - \theta$ and $\zeta = -\eta$ we obtain the equality

$$\begin{aligned} & \int_0^\pi \int_0^\infty \exp(-\alpha\eta^2) \exp(\beta\eta \cos \theta) d\eta d\theta \\ &= \int_0^\pi \int_{-\infty}^0 \exp(-\alpha\zeta^2) \exp(-\beta\zeta \cos(\pi - \phi)) d\zeta d\phi \\ &= \int_0^\pi \int_{-\infty}^0 \exp(-\alpha\zeta^2) \exp(\beta\zeta \cos \phi) d\zeta d\phi. \end{aligned}$$

We start the proof by using the integral representation of the modified Bessel function of the first kind [Wat66, p. 181], which yields

$$\begin{aligned} \int_0^\infty \exp(-\alpha\eta^2) I_0(\beta\eta) d\eta &= \int_0^\infty \exp(-\alpha\eta^2) \int_0^\pi \exp(\beta\eta \cos \theta) d\theta d\eta \\ &= \int_0^\pi \int_0^\infty \exp(-\alpha\eta^2) \exp(\beta\eta \cos \theta) d\eta d\theta. \end{aligned}$$

Using the equality from above, we obtain

$$\int_0^\infty \exp(-\alpha\eta^2) I_0(\beta\eta) d\eta = \frac{1}{2} \int_0^\pi \int_{-\infty}^\infty \exp(-\alpha\eta^2) \exp(\beta\eta \cos \theta) d\eta d\theta.$$

Completing the square inside the exponential function then yields

$$\begin{aligned} & \int_0^\infty \exp(-\alpha\eta^2) I_0(\beta\eta) d\eta \\ &= \frac{1}{2} \int_0^\pi \int_{-\infty}^\infty \exp\left(-\alpha\left(\eta^2 - \frac{\beta\eta}{\alpha} \cos \theta\right)\right) d\eta d\theta \\ &= \frac{1}{2} \int_0^\pi \exp\left(\frac{\beta^2}{4\alpha} \cos^2 \theta\right) \int_{-\infty}^\infty \exp\left(-\alpha\left(\eta - \frac{\beta}{2\alpha} \cos \theta\right)^2\right) d\eta d\theta. \end{aligned}$$

The inner integral is a Gaussian integral and evaluates to $\sqrt{\frac{\pi}{\alpha}}$. Thus, we obtain

$$\int_0^\infty \exp(-\alpha\eta^2) I_0(\beta\eta) d\eta = \frac{\sqrt{\pi}}{2\sqrt{\alpha}} \int_0^\pi \exp\left(\frac{\beta^2}{4\alpha} \cos^2 \theta\right) d\theta.$$

Using the relation $\cos^2 \theta = \frac{1}{2} (1 + \cos 2\theta)$ and subsequently substituting $\phi = 2\theta$ yields

$$\begin{aligned} \int_0^\infty \exp(-\alpha\eta^2) I_0(\beta\eta) d\eta &= \frac{\sqrt{\pi}}{2\sqrt{\alpha}} \exp\left(\frac{\beta^2}{8\alpha}\right) \int_0^\pi \exp\left(\frac{\beta^2}{8\alpha} \cos 2\theta\right) d\theta \\ &= \frac{\sqrt{\pi}}{2\sqrt{\alpha}} \exp\left(\frac{\beta^2}{8\alpha}\right) \frac{1}{2} \int_0^{2\pi} \exp\left(\frac{\beta^2}{8\alpha} \cos \phi\right) d\phi. \end{aligned}$$

To proceed, we substitute $\vartheta = 2\pi - \phi$ to obtain the equality

$$\begin{aligned} \int_\pi^{2\pi} \exp\left(\frac{\beta^2}{8\alpha} \cos \phi\right) d\phi &= \int_0^\pi \exp\left(\frac{\beta^2}{8\alpha} \cos (2\pi - \vartheta)\right) d\vartheta \\ &= \int_0^\pi \exp\left(\frac{\beta^2}{8\alpha} \cos \vartheta\right) d\vartheta. \end{aligned}$$

Using this equality, we obtain

$$\begin{aligned} \int_0^\infty \exp(-\alpha\eta^2) I_0(\beta\eta) d\eta &= \frac{\sqrt{\pi}}{2\sqrt{\alpha}} \exp\left(\frac{\beta^2}{8\alpha}\right) \int_0^\pi \exp\left(\frac{\beta^2}{8\alpha} \cos \phi\right) d\phi \\ &= \frac{\sqrt{\pi}}{2\sqrt{\alpha}} \exp\left(\frac{\beta^2}{8\alpha}\right) I_0\left(\frac{\beta^2}{8\alpha}\right) \end{aligned}$$

This finishes the proof. □

Theorem A.2. Let $m, n \in \mathbb{N}$, $c \in \mathbb{R} \setminus \{0\}$ and $\Omega = \{1, \dots, m\} \times \{1, \dots, n\}$. Assume that F follows the statistical model given in (2.5) and let $T(i, j)$ be the test statistic as defined in (2.8) and $H_1(i, j)$ be the alternative hypothesis as defined in (2.7). Let t be a threshold, such that

$$\mathbb{P}_V(T(i, j) \leq t) \leq \beta$$

for all $V \in \mathcal{H}_1(i, j)$. Let \mathfrak{I} be the binary image defined by

$$\mathfrak{I}(i, j) = \mathbb{1}_{\{T(i, j) \geq t\}} \quad (\text{A.2})$$

for all $(i, j) \in \Omega$.

Let $\varphi \in \mathbb{N}$ be odd. Let $\Phi_\varphi = \{-\frac{\varphi-1}{2}, -\frac{\varphi-3}{2}, \dots, \frac{\varphi-3}{2}, \frac{\varphi-1}{2}\}$ and $\Psi_\varphi = \Phi_\varphi \times \Phi_\varphi$ be a structuring element.

Denote by $\Lambda = \{\kappa_1, \dots, \kappa_2\} \times \{\lambda_1, \dots, \lambda_2\}$ the ROI contained in V . Let $\min\{\kappa_2 - \kappa_1 + 1, \lambda_2 - \lambda_1 + 1\} \geq \varphi$. Let $V \in \mathcal{H}_1(i, j)$ and $(i, j) \in \Omega$ be such, that

$$\begin{aligned} i - 2\varphi + 2 &\geq \kappa_1, \\ i + 2\varphi - 2 &\leq \kappa_2, \\ j - 2\varphi + 2 &\geq \lambda_1, \\ j + 2\varphi - 2 &\leq \lambda_2. \end{aligned} \quad (\text{A.3})$$

Then the following inequality holds:

$$\mathbb{P}_V(((\mathfrak{I} \circ \Psi_\varphi) \bullet \Psi_\varphi)(i, j) = 0) \leq \varphi^{10} \beta^4 \quad (\text{A.4})$$

Proof. The assumptions on $(i, j) \in \Omega$ assure, that the alternative hypotheses $H_1(i + k - \tilde{k} - r + \tilde{r}, j + \ell - \tilde{\ell} - s + \tilde{s})$ are true for all $k, \ell, r, s, \tilde{k}, \tilde{\ell}, \tilde{r}, \tilde{s} \in \Phi_\varphi$. Using equalities (3.12) and (3.13) and $\Psi_\varphi = \Phi_\varphi \times \Phi_\varphi$ yields

$$\begin{aligned} &\mathbb{P}_V(((\mathfrak{I} \circ \Psi_\varphi) \bullet \Psi_\varphi)(i, j) = 0) \\ &= \mathbb{P}_V \left(\bigcup_{(k, \ell) \in \Psi_\varphi} \bigcap_{(\tilde{k}, \tilde{\ell}) \in \Psi_\varphi} \bigcap_{(r, s) \in \Psi_\varphi} \bigcup_{(\tilde{r}, \tilde{s}) \in \Psi_\varphi} \{\mathfrak{I}(i + k - \tilde{k} - r + \tilde{r}, j + \ell - \tilde{\ell} - s + \tilde{s}) = 0\} \right) \end{aligned}$$

$$= \mathbb{P}_V \left(\bigcup_{k, \ell \in \Phi_\varphi} \bigcap_{\tilde{k}, \tilde{\ell} \in \Phi_\varphi} \bigcap_{r, s \in \Phi_\varphi} \bigcup_{\tilde{r}, \tilde{s} \in \Phi_\varphi} \{\mathfrak{I}(i + k - \tilde{k} - r + \tilde{r}, j + \ell - \tilde{\ell} - s + \tilde{s}) = 0\} \right).$$

By sub-additivity we obtain

$$\begin{aligned} & \mathbb{P}_V ((\mathfrak{I} \circ \Psi_\varphi) \bullet \Psi_\varphi)(i, j) = 0) \\ &= \mathbb{P}_V \left(\bigcup_{k, \ell \in \Phi_\varphi} \bigcap_{\tilde{k}, \tilde{\ell} \in \Phi_\varphi} \bigcap_{r, s \in \Phi_\varphi} \bigcup_{\tilde{r}, \tilde{s} \in \Phi_\varphi} \{\mathfrak{I}(i + k - \tilde{k} - r + \tilde{r}, j + \ell - \tilde{\ell} - s + \tilde{s}) = 0\} \right) \\ &\leq \sum_{k, \ell \in \Phi_\varphi} \mathbb{P}_V \left(\bigcap_{\tilde{k}, \tilde{\ell} \in \Phi_\varphi} \bigcap_{r, s \in \Phi_\varphi} \bigcup_{\tilde{r}, \tilde{s} \in \Phi_\varphi} \{\mathfrak{I}(i + k - \tilde{k} - r + \tilde{r}, j + \ell - \tilde{\ell} - s + \tilde{s}) = 0\} \right). \end{aligned}$$

We can pull the two intersections together and get

$$\begin{aligned} & \mathbb{P}_V ((\mathfrak{I} \circ \Psi_\varphi) \bullet \Psi_\varphi)(i, j) = 0) \\ &\leq \sum_{k, \ell \in \Phi_\varphi} \mathbb{P}_V \left(\bigcap_{\tilde{k}, \tilde{\ell} \in \Phi_\varphi} \bigcap_{r, s \in \Phi_\varphi} \bigcup_{\tilde{r}, \tilde{s} \in \Phi_\varphi} \{\mathfrak{I}(i + k - \tilde{k} - r + \tilde{r}, j + \ell - \tilde{\ell} - s + \tilde{s}) = 0\} \right) \\ &= \sum_{k, \ell \in \Phi_\varphi} \mathbb{P}_V \left(\bigcap_{\tilde{k}, \tilde{\ell}, r, s \in \Phi_\varphi} \bigcup_{\tilde{r}, \tilde{s} \in \Phi_\varphi} \{\mathfrak{I}(i + k - \tilde{k} - r + \tilde{r}, j + \ell - \tilde{\ell} - s + \tilde{s}) = 0\} \right). \end{aligned}$$

We drop every term in the intersection besides $r + \tilde{k}, s + \tilde{\ell} \in \{-(\varphi - 1), \varphi - 1\}$.

This yields

$$\begin{aligned} & \mathbb{P}_V ((\mathfrak{I} \circ \Psi_\varphi) \bullet \Psi_\varphi)(i, j) = 0) \\ &\leq \sum_{k, \ell \in \Phi_\varphi} \mathbb{P}_V \left(\bigcap_{\tilde{k}, \tilde{\ell}, r, s \in \Phi_\varphi} \bigcup_{\tilde{r}, \tilde{s} \in \Phi_\varphi} \{\mathfrak{I}(i + k - \tilde{k} - r + \tilde{r}, j + \ell - \tilde{\ell} - s + \tilde{s}) = 0\} \right) \\ &\leq \sum_{k, \ell \in \Phi_\varphi} \mathbb{P}_V \left(\bigcap_{r + \tilde{k}, s + \tilde{\ell} \in \{-(\varphi - 1), \varphi - 1\}} \bigcup_{\tilde{r}, \tilde{s} \in \Phi_\varphi} \{\mathfrak{I}(i + k - \tilde{k} - r + \tilde{r}, j + \ell - \tilde{\ell} - s + \tilde{s}) = 0\} \right). \end{aligned}$$

The sets $\bigcup_{\tilde{r}, \tilde{s} \in \Phi_\varphi} \{\mathfrak{I}(i + k - \tilde{k} - r + \tilde{r}, j + \ell - \tilde{\ell} - s + \tilde{s}) = 0\}$ are mutually independent for $r + \tilde{k}, s + \tilde{\ell} \in \{-(\varphi - 1), \varphi - 1\}$ and fixed $k, \ell \in \Phi_\varphi$, see

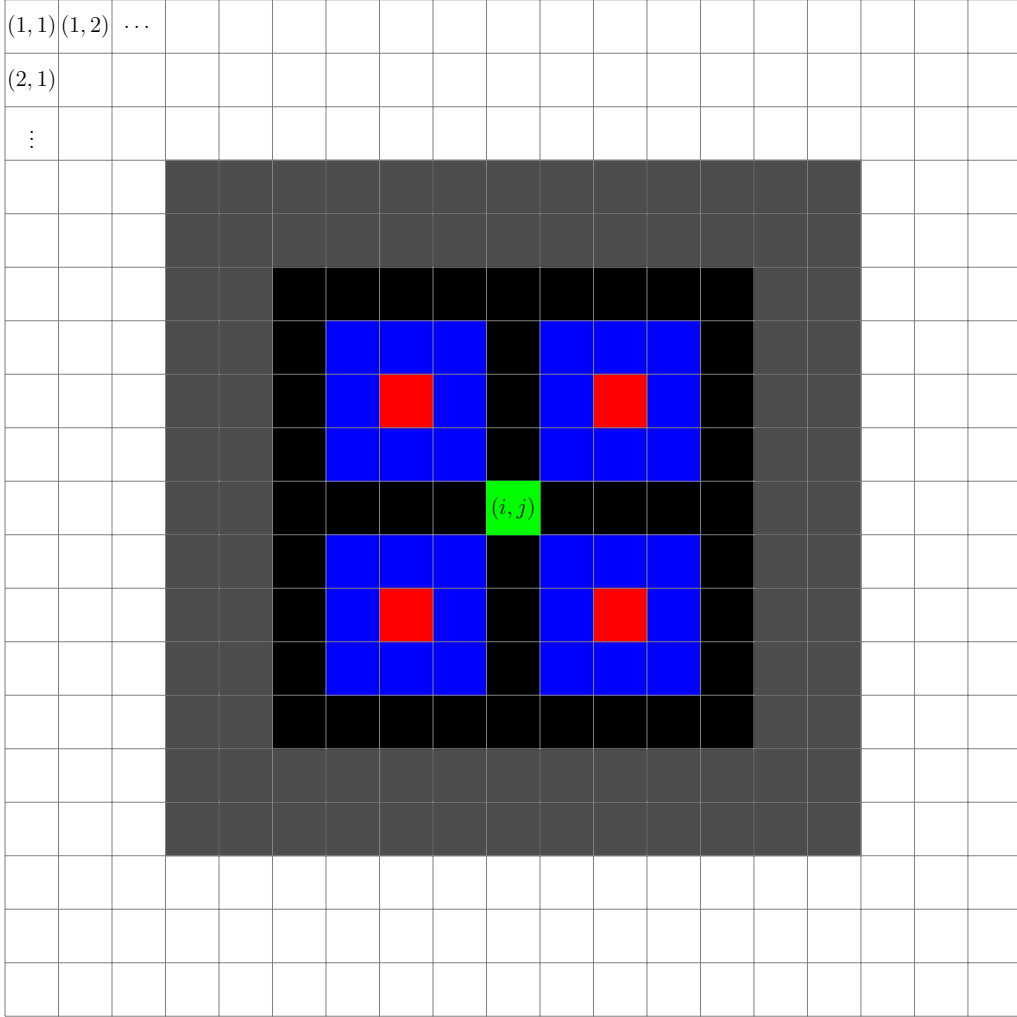


Figure 14: The black area are the pixels that contribute to $(\mathcal{I} \circ \Psi_\varphi) \bullet \Psi_\varphi(i, j)$. The blue squares are mutually independent. The red pixels are the pixels that we reduce the intersection in the proof to.

Figure 14. Thus we obtain

$$\begin{aligned}
& \mathbb{P}_V((\mathcal{I} \circ \Psi_\varphi) \bullet \Psi_\varphi)(i, j) = 0) \\
& \leq \sum_{k, \ell \in \Phi_\varphi} \mathbb{P}_V \left(\bigcap_{r+\tilde{k}, s+\tilde{\ell} \in \{-(\varphi-1), \varphi-1\}} \bigcup_{\tilde{r}, \tilde{s} \in \Phi_\varphi} \{\mathcal{I}(i+k-\tilde{k}-r+\tilde{r}, j+\ell-\tilde{\ell}-s+\tilde{s}) = 0\} \right) \\
& = \sum_{k, \ell \in \Phi_\varphi} \prod_{r+\tilde{k}, s+\tilde{\ell} \in \{-(\varphi-1), \varphi-1\}} \mathbb{P}_V \left(\bigcup_{\tilde{r}, \tilde{s} \in \Phi_\varphi} \{\mathcal{I}(i+k-\tilde{k}-r+\tilde{r}, j+\ell-\tilde{\ell}-s+\tilde{s}) = 0\} \right).
\end{aligned}$$

Again, by using sub-additivity, we get

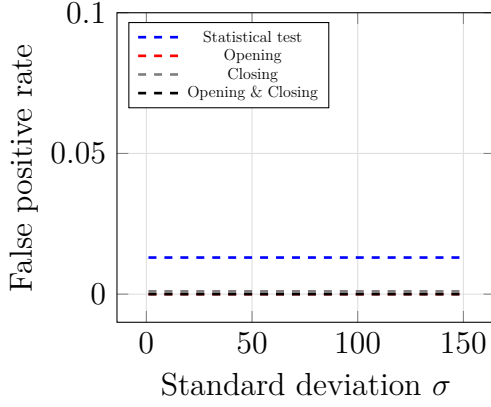
$$\begin{aligned}
& \mathbb{P}_V((\mathfrak{I} \circ \Psi_\varphi) \bullet \Psi_\varphi)(i, j) = 0) \\
& \leq \sum_{k, \ell \in \Phi_\varphi} \prod_{r + \tilde{k}, s + \tilde{\ell} \in \{-(\varphi-1), \varphi-1\}} \mathbb{P}_V \left(\bigcup_{\tilde{r}, \tilde{s} \in \Phi_\varphi} \{\mathfrak{I}(i + k - \tilde{k} - r + \tilde{r}, j + \ell - \tilde{\ell} - s + \tilde{s}) = 0\} \right) \\
& = \sum_{k, \ell \in \Phi_\varphi} \prod_{r + \tilde{k}, s + \tilde{\ell} \in \{-(\varphi-1), \varphi-1\}} \sum_{\tilde{r}, \tilde{s} \in \Phi_\varphi} \mathbb{P}_V \left(\{\mathfrak{I}(i + k - \tilde{k} - r + \tilde{r}, j + \ell - \tilde{\ell} - s + \tilde{s}) = 0\} \right).
\end{aligned}$$

We have assumed, that $(i, j) \in \Omega$ is such, that the alternative hypotheses $H_1(i + k - \tilde{k} - r + \tilde{r}, j + \ell - \tilde{\ell} - s + \tilde{s})$ are true for all $k, \ell, r, s, \tilde{k}, \tilde{\ell}, \tilde{r}, \tilde{s} \in \Phi_\varphi$. Using this assumption and the fact, that $\mathbb{P}_V(T(i, j) \leq t) \leq \beta$ for $\mathcal{H}_1(i, j)$ we obtain

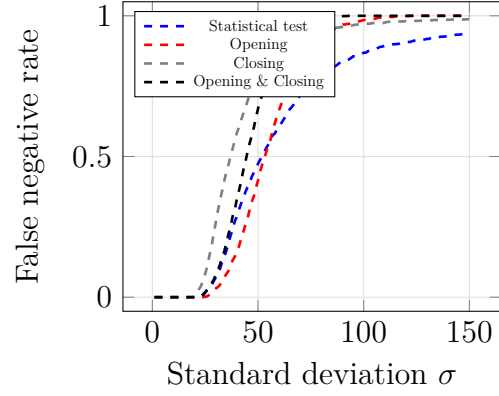
$$\begin{aligned}
& \mathbb{P}_V((\mathfrak{I} \circ \Psi_\varphi) \bullet \Psi_\varphi)(i, j) = 0) \\
& \leq \sum_{k, \ell \in \Phi_\varphi} \prod_{r + \tilde{k}, s + \tilde{\ell} \in \{-(\varphi-1), \varphi-1\}} \sum_{\tilde{r}, \tilde{s} \in \Phi_\varphi} \mathbb{P}_V \left(\{\mathfrak{I}(i + k - \tilde{k} - r + \tilde{r}, j + \ell - \tilde{\ell} - s + \tilde{s}) = 0\} \right) \\
& \leq \sum_{k, \ell \in \Phi_\varphi} \prod_{r + \tilde{k}, s + \tilde{\ell} \in \{-(\varphi-1), \varphi-1\}} \sum_{\tilde{r}, \tilde{s} \in \Phi_\varphi} \beta \\
& = \sum_{k, \ell \in \Phi_\varphi} \prod_{r + \tilde{k}, s + \tilde{\ell} \in \{-(\varphi-1), \varphi-1\}} \varphi^2 \beta \\
& = \sum_{k, \ell \in \Phi_\varphi} (\varphi^2 \beta)^4 \\
& = \varphi^2 (\varphi^2 \beta)^4 \\
& = \varphi^{10} \beta^4.
\end{aligned}$$

This finishes the proof. □

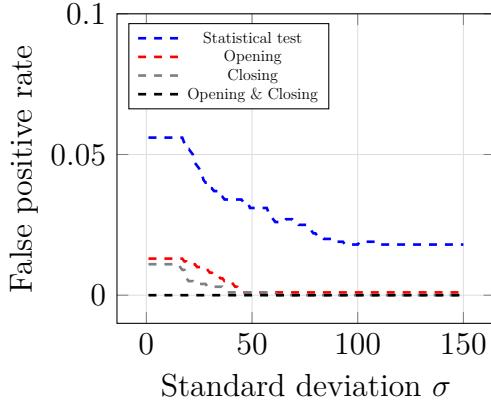
B Simulations



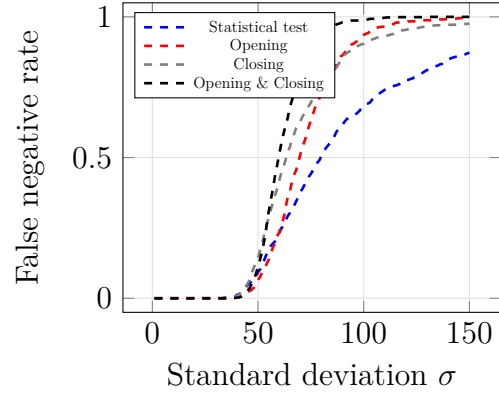
(a) Background pixel at the corner of the ROI.



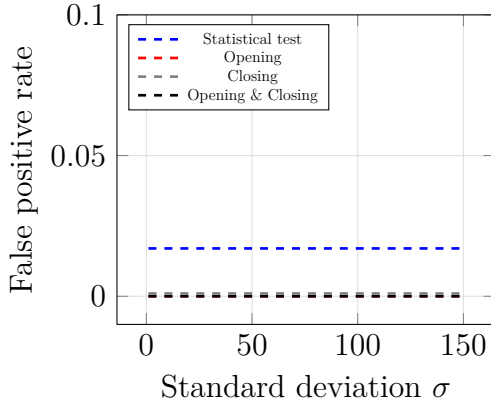
(b) Foreground pixel at the corner of the ROI.



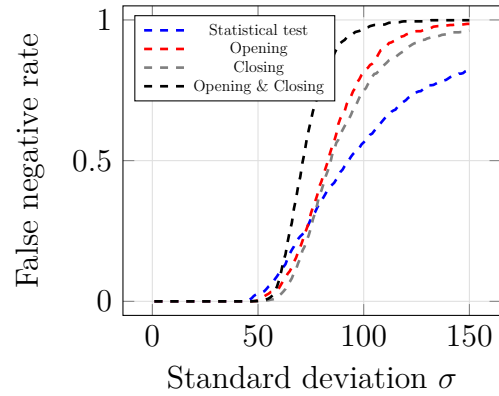
(c) Background pixel at the edge of the ROI.



(d) Foreground pixel at the edge of the ROI.

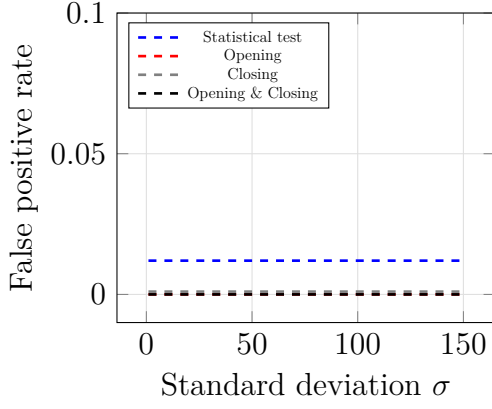


(e) Background pixel surrounded by background.

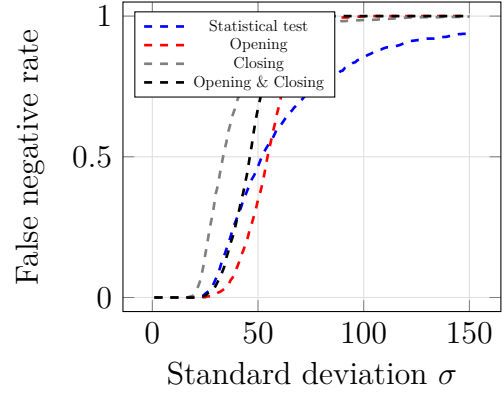


(f) Foreground pixel surrounded by foreground.

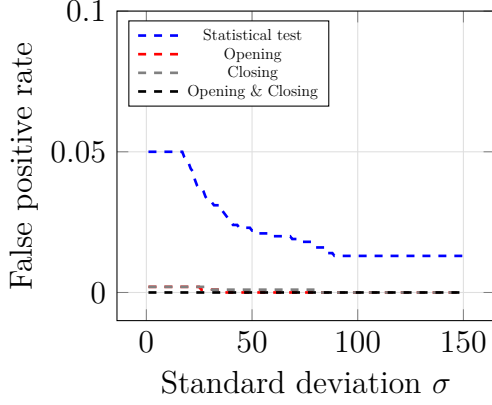
Figure 15: Error rates for all four ROI extraction approaches. The x -axes display the standard deviation σ and the y -axes the error rate ($\alpha = 0.05, \varphi = 3$).



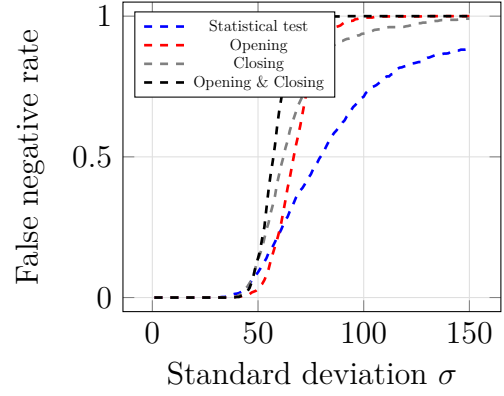
(a) Background pixel at the corner of the ROI.



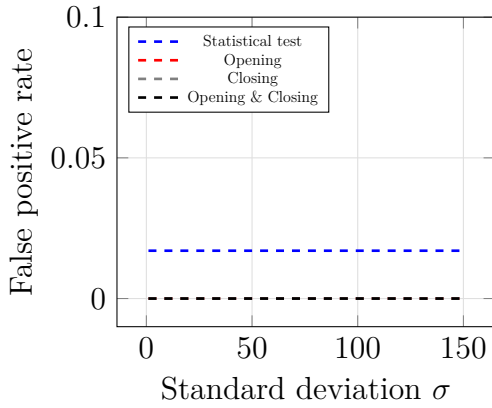
(b) Foreground pixel at the corner of the ROI.



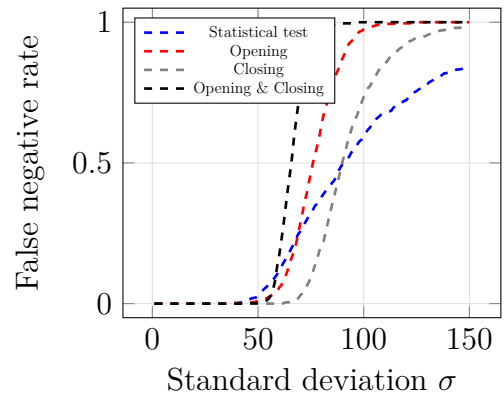
(c) Background pixel at the edge of the ROI.



(d) Foreground pixel at the edge of the ROI.

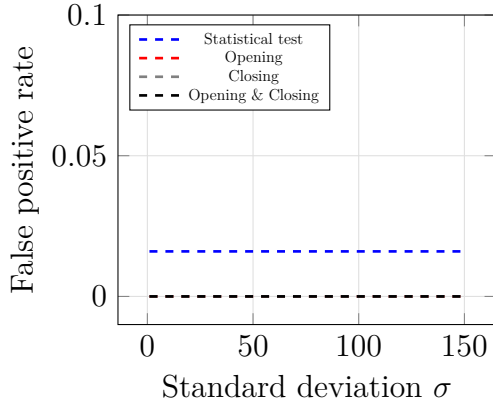


(e) Background pixel surrounded by background.

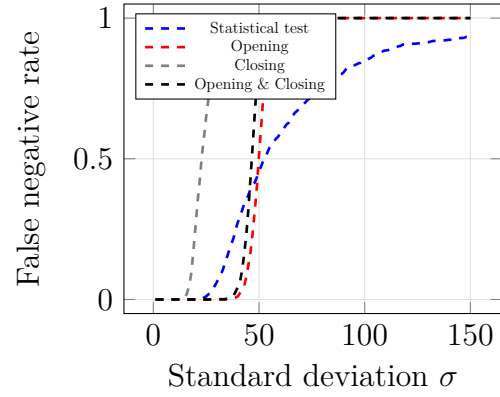


(f) Foreground pixel surrounded by foreground.

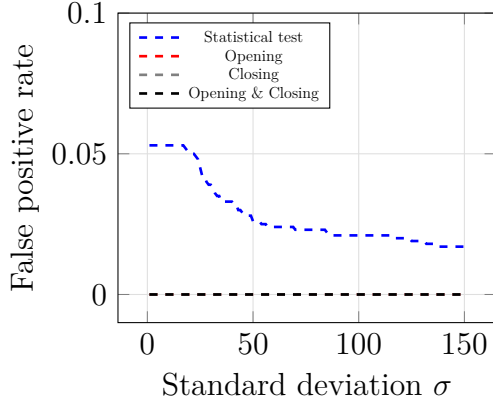
Figure 16: Error rates for all four ROI extraction approaches. The x -axes display the standard deviation σ and the y -axes the error rate ($\alpha = 0.05, \varphi = 5$).



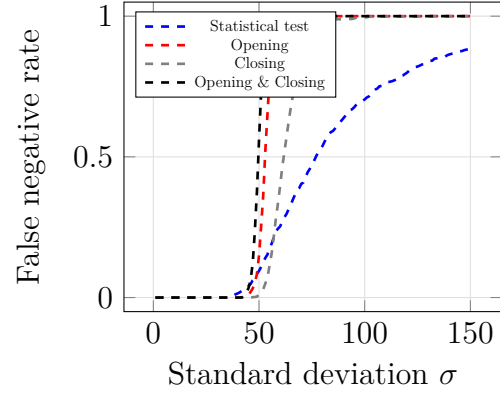
(a) Background pixel at the corner of the ROI.



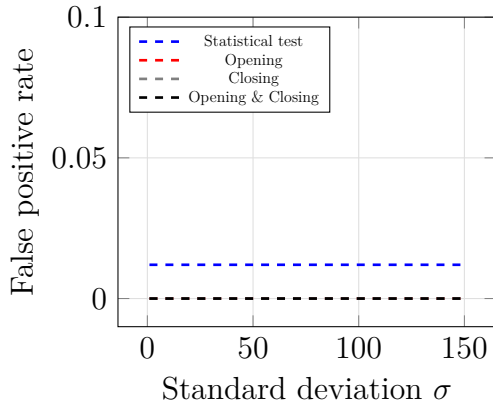
(b) Foreground pixel at the corner of the ROI.



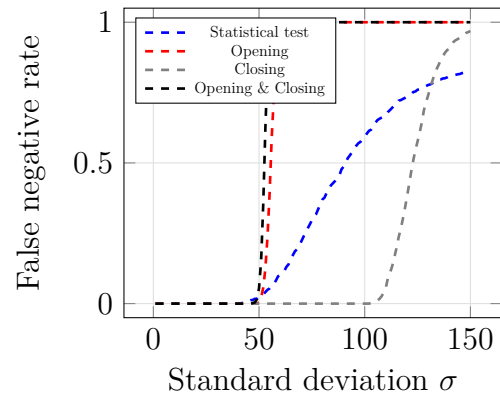
(c) Background pixel at the edge of the ROI.



(d) Foreground pixel at the edge of the ROI.

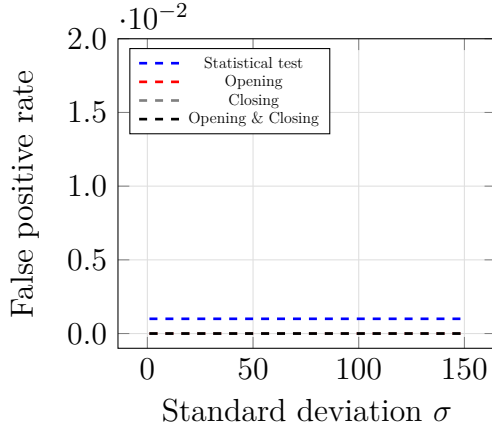


(e) Background pixel surrounded by background.

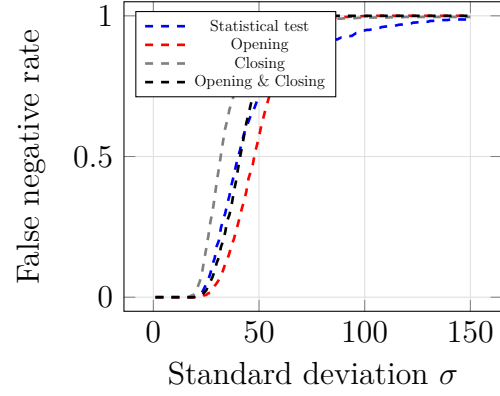


(f) Foreground pixel surrounded by foreground.

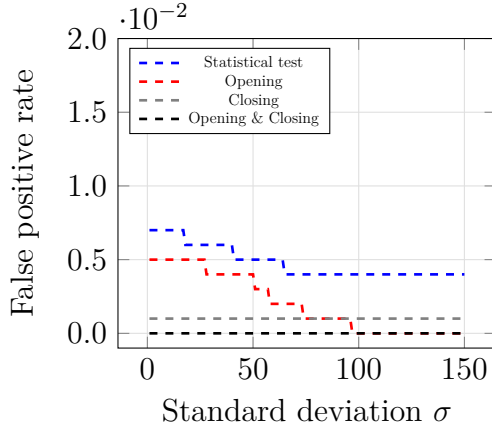
Figure 17: Error rates for all four ROI extraction approaches. The x -axes display the standard deviation σ and the y -axes the error rate ($\alpha = 0.05, \varphi = 99$).



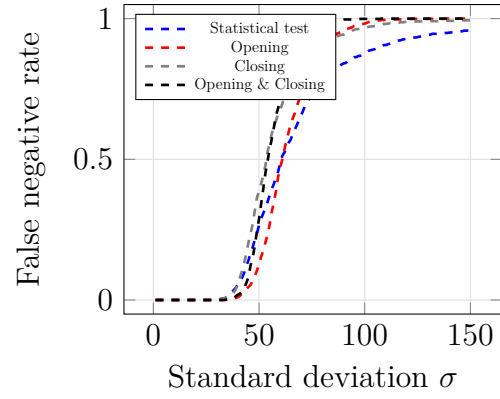
(a) Background pixel at the corner of the ROI.



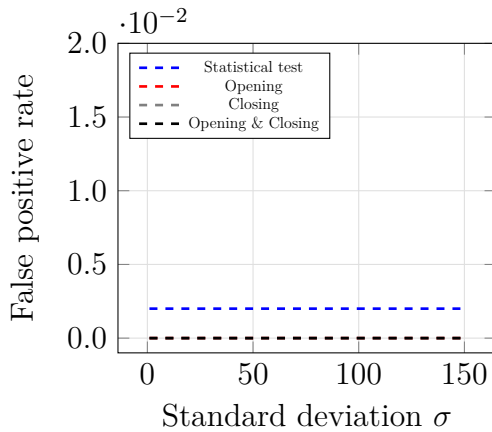
(b) Foreground pixel at the corner of the ROI.



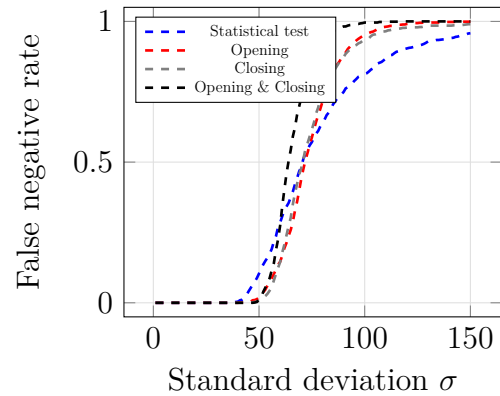
(c) Background pixel at the edge of the ROI.



(d) Foreground pixel at the edge of the ROI.

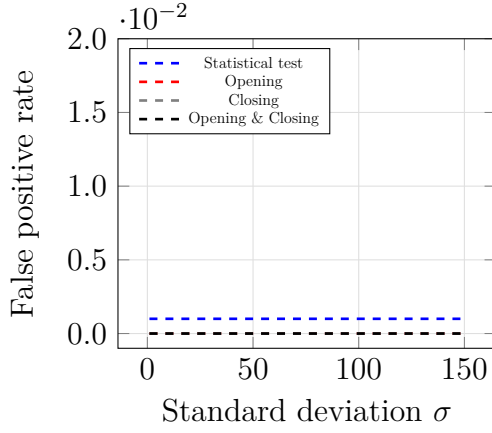


(e) Background pixel surrounded by background.

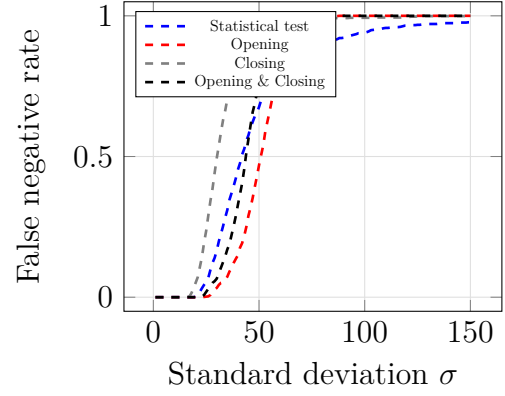


(f) Foreground pixel surrounded by foreground.

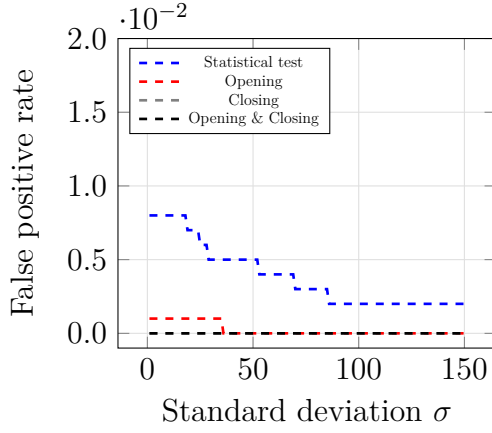
Figure 18: Error rates for all four ROI extraction approaches. The x -axes display the standard deviation σ and the y -axes the error rate ($\alpha = 0.01, \varphi = 3$).



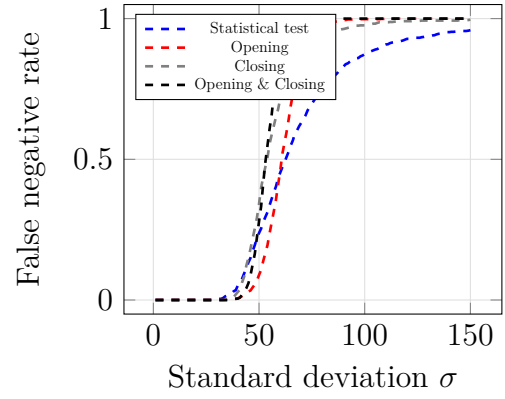
(a) Background pixel at the corner of the ROI.



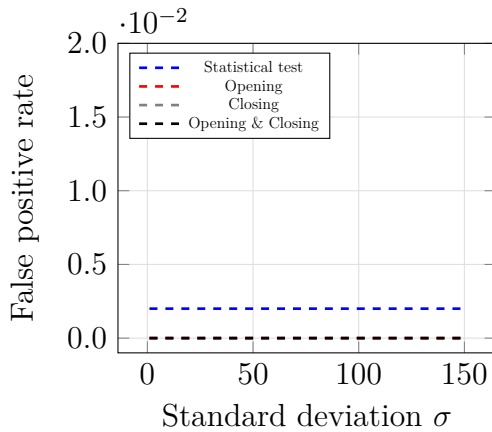
(b) Foreground pixel at the corner of the ROI.



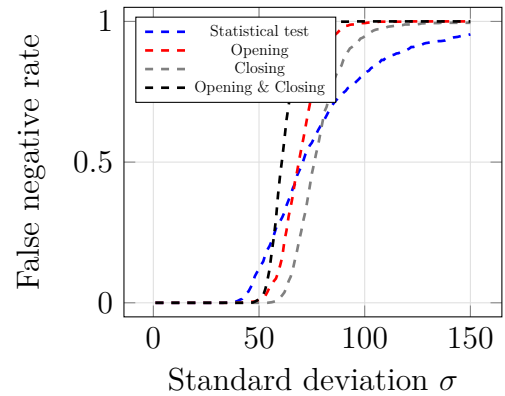
(c) Background pixel at the edge of the ROI.



(d) Foreground pixel at the edge of the ROI.

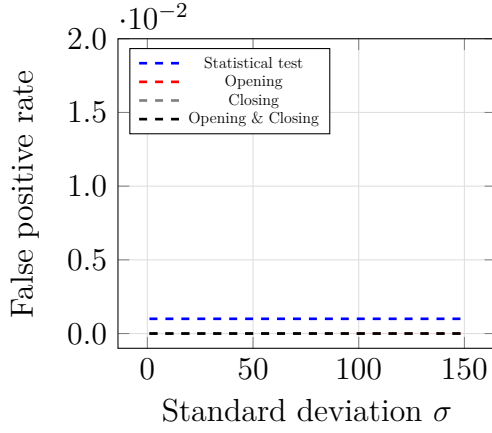


(e) Background pixel surrounded by background.

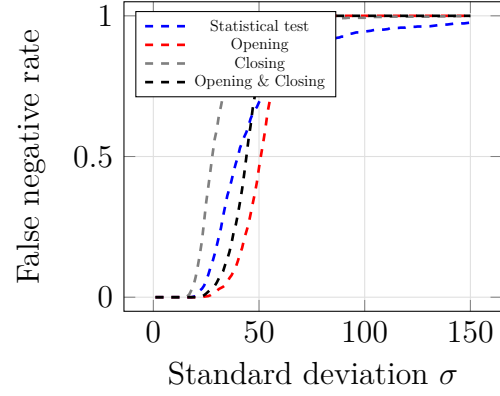


(f) Foreground pixel surrounded by foreground.

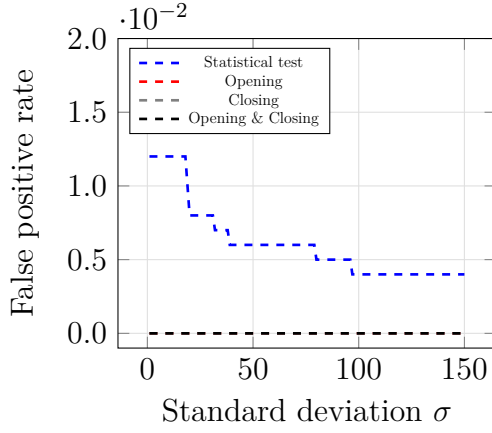
Figure 19: Error rates for all four ROI extraction approaches. The x -axes display the standard deviation σ and the y -axes the error rate ($\alpha = 0.01, \varphi = 5$).



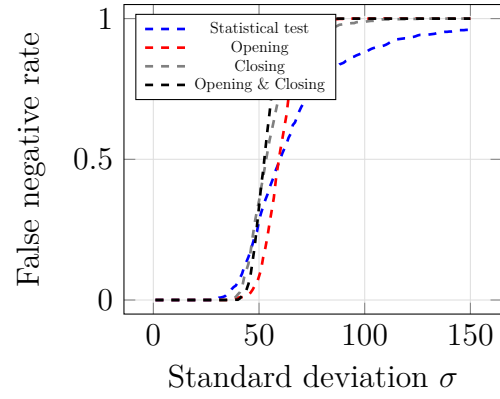
(a) Background pixel at the corner of the ROI.



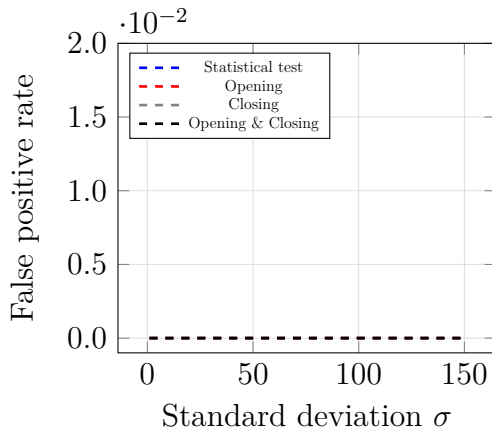
(b) Foreground pixel at the corner of the ROI.



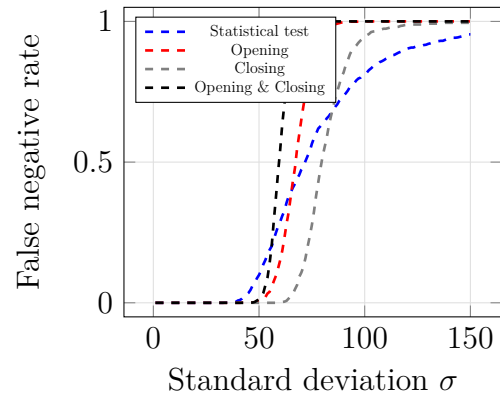
(c) Background pixel at the edge of the ROI.



(d) Foreground pixel at the edge of the ROI.

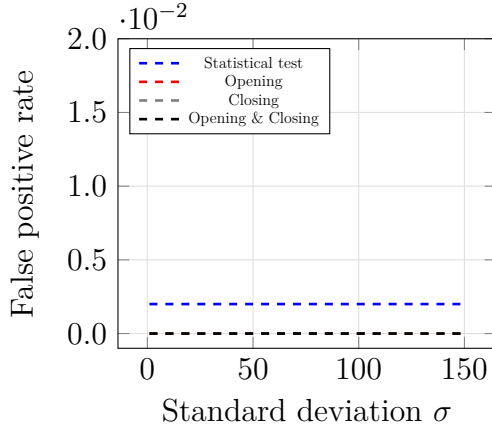


(e) Background pixel surrounded by background.

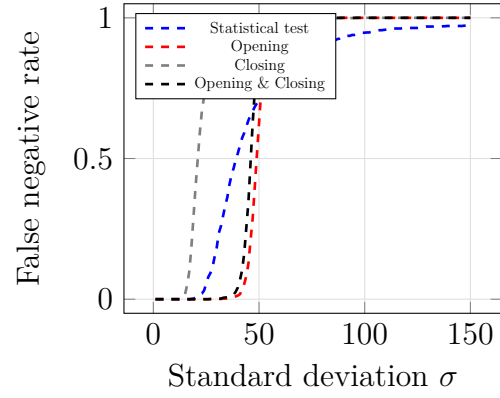


(f) Foreground pixel surrounded by foreground.

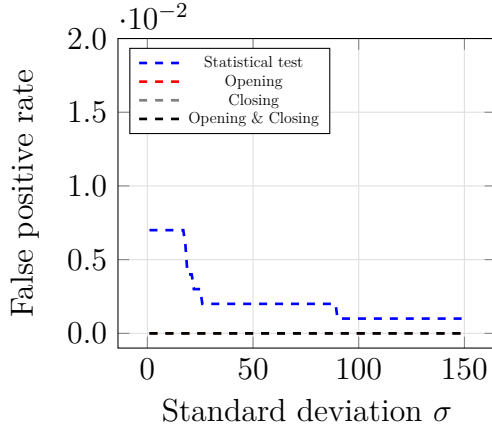
Figure 20: Error rates for all four ROI extraction approaches. The x -axes display the standard deviation σ and the y -axes the error rate ($\alpha = 0.01, \varphi = 7$).



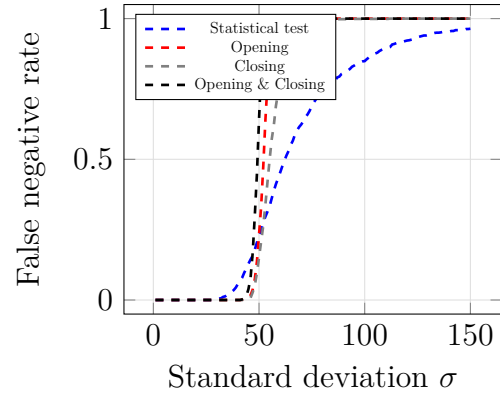
(a) Background pixel at the corner of the ROI.



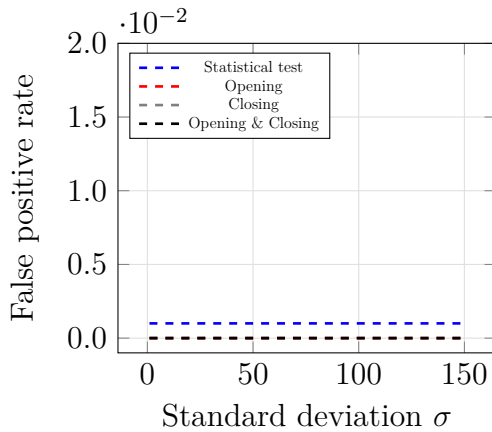
(b) Foreground pixel at the corner of the ROI.



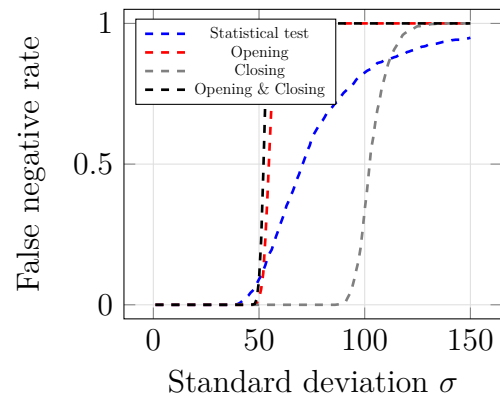
(c) Background pixel at the edge of the ROI.



(d) Foreground pixel at the edge of the ROI.



(e) Background pixel surrounded by background.



(f) Foreground pixel surrounded by foreground.

Figure 21: Error rates for all four ROI extraction approaches. The x -axes display the standard deviation σ and the y -axes the error rate ($\alpha = 0.01, \varphi = 99$).

C Algorithms

```
1 function [t, alpha_real] = Threshold(alpha, increment)
2
3 % Set initial guess for t:
4 t = 0;
5 alpha_real = 1;
6
7 while alpha_real >= alpha
8     t = t + increment;
9     alpha_real = 1 - CDF(t, 1);
10 end
11
12 end
13
14 function y = CDF(x, sigma)
15
16 % Initialize output array:
17 y = zeros(size(x));
18
19 % Compute pdf values:
20 for i = 1 : size(x, 1)
21     for j = 1 : size(x, 2)
22         y(i, j) = (1 / sqrt(3)) * ( 3 / 2 - (3 / 2) * exp(-x(i,
23             j)^2 / (3 * sigma^2)) * besseli(0, x(i, j)^2 / (6 * sigma^2))
24             ) - sqrt(3) ...
25             - ((2 - sqrt(3)) / 2) * marcumq(sqrt((2 - sqrt(3)) /
26                 6) * (x(i, j) / sigma), sqrt((2 + sqrt(3)) / 6) * (x(i, j) /
27                 sigma)) ...
28             + ((2 + sqrt(3)) / 2) * marcumq(sqrt((2 + sqrt(3)) /
29                 6) * (x(i, j) / sigma), sqrt((2 - sqrt(3)) / 6) * (x(i, j) /
30                 sigma));
31     end
32 end
33 end
```

Listing 1: *MATLAB* implementation of a trial and error algorithm to find a threshold for the statistical test.

```

1 function [lowerBound, upperBound] = PowerSim(t_alpha, nr_noise,
    max_sigma, c_bg)
2
3 % Simulate random variable:
4 RV = RVSim(nr_noise, max_sigma, c_bg);
5
6 % Initialize output vectors:
7 lowerBound = zeros(1, max_sigma);
8 upperBound = zeros(1, max_sigma);
9
10 % Estimate lower and upper bound for the probability of a type
    II error:
11 for sigma = 1: max_sigma
12     lowerBound(1, sigma) = sum(RV.( 'D2c2c' )(:, sigma) <= sigma *
        t_alpha) / nr_noise;
13     upperBound(1, sigma) = min(2 * sum(RV.( 'Dcc' )(:, sigma) <=
        sigma * t_alpha) / nr_noise, 1);
14 end
15
16 end
17
18 function RV = RVSim(nr_noise, max_sigma, c_bg)
19
20 % Initialize structure to save results:
21 RV = struct;
22
23 % Initialize matrices to store simulation results:
24 RV.( 'dcc' ) = zeros(nr_noise, max_sigma);
25 RV.( 'd2c2c' ) = zeros(nr_noise, max_sigma);
26
27 % Generate realizations of a standard normal distribution:
28 eps1 = randn(nr_noise, 1);
29 eps2 = randn(nr_noise, 1);
30 eps = randn(nr_noise, 1);
31
32 for sigma = 1 : max_sigma
33     % Calculate random variables:
34     RV.( 'Dcc' )(:, sigma) = sqrt((c_bg + sigma * eps1 - sigma *
        eps).^2 + (c_bg + sigma * eps2 - sigma * eps).^2);

```

```

35     RV.( 'D2c2c' ) (:, sigma) = sqrt((2 * c_bg + sigma * eps1 -
      sigma * eps).^2 + (2 * c_bg + sigma * eps2 - sigma * eps).^2)
      ;
36 end
37
38 end

```

Listing 2: *MATLAB* implementation of simulation algorithm to simulate upper and lower bounds for the probability of a type II error in the statistical test.

```

1 function I = ROI_Detection(F, t_alpha, sigma)
2 % F: square, noisy input image that contains a rectangular ROI
3 % t_alpha: threshold based on statistical significance alpha
4 % sigma: standard deviation of the noise
5
6 % Determine height and width of the input picture:
7 [m, n] = size(F);
8
9 % Calculate the euclidean norm of the vertical and horizontal
10 % discrete
11 % derivatives:
12 D_plus = discreteDerivative(F, m, n, 'plus');
13 D_minus = discreteDerivative(F, m, n, 'minus');
14
15 % Calculate test statistic:
16 T = min(D_plus, D_minus);
17
18 % Create thresholded binary matrix:
19 I = T >= t_alpha * sigma;
20
21 end
22
23 function D = discreteDerivative(F, m, n, direction)
24 % Determine direction of discrete derivative:
25 switch direction
26     case 'plus'
27         shift = 0;
28     case 'minus'
29         shift = 1;
30
31 end
32
33 % Initialize d1, d2:
34 % d1: vertical discrete derivative
35 % d2: horizontal discrete derivative
36 D1 = ones(m, n);
37 D2 = ones(m, n);
38
39 % Calculate d1:
40 D1(1 + shift : m - 1 + shift, :) = F(2 - shift : m - shift, :) -

```

```

39     F(1 + shift : m - 1 + shift , :);
40 D1((1 - shift) * m + shift , :) = F(shift * m + (1 - shift), :) -
    F((1 - shift) * m + shift , :);
41 % Calculate d2:
42 D2(:, 1 + shift : n - 1 + shift) = F(:, 2 - shift : n - shift) -
    F(:, 1 + shift : n - 1 + shift);
43 D2(:, (1 - shift) * n + shift) = F(:, shift * n + (1 - shift)) -
    F(:, (1 - shift) * n + shift);
44
45 % Calculate d as the euclidean norm of d1 and d2:
46 D = sqrt(D1.^2 + D2.^2);
47
48 end

```

Listing 3: *MATLAB* implementation of the testing procedure to test for a rectangular region of interest with a chessboard pattern.


```

1 % Set parent folder to store the .csv files:
2 folder = '/space/fbms/dblank';
3
4 % Reset RNG seed:
5 rng('default')
6
7 %
8
9 % Set number of noises to generate:
10 nr_noise = 1000;
11
12 % Set statistical significances to consider:
13 alphas = [0.01 0.05];
14
15 % Set side lengths of the structuring element to consider:
16 phis = [3 5 7 99];
17
18 % Set maximal standard deviation of the noise:
19 max_sigma = 150;
20
21 % Set background grayscale value:
22 c_bg = 127.5;
23
24 % Set increment size for threshold algorithm:
25 increment = 0.0001;
26
27 %
28
29 % Define array to loop over different positions of the pixels:
30 pixelPositions = {'background_corner', 'background_edge', '
    background_free', 'foreground_corner', 'foreground_edge', '
    foreground_free'};
31 correctVals = [0 0 0 1 1 1];
32
33 %

```

```

34
35 % Determine range of standard deviations:
36 sigma_range = 1 : max_sigma;
37
38 % Loop over background and foreground pixels:
39 parfor p = 1 : size(pixelPositions, 2)
40
41     % Determine what pixel position simulate:
42     pixelPos = pixelPositions{p};
43
44     % Determine correct value based on pixel position:
45     correctVal = correctVals(p);
46
47     % Loop over side lengths of the structuring element:
48     for phi = phis
49
50         % Define structuring element:
51         SE = strel('square', phi);
52
53         % Initialize image around the pixel:
54         V = ones(2 * phi + 3, 2 * phi + 3) * c_bg;
55
56         % Set top left corner of the ROI based position of the
57         % pixel to simulate (Simulated pixel is [phi + 2 phi +
58         2]):
59         switch pixelPos
60             case 'background_corner'
61                 tlc = [phi + 3 phi + 3];
62             case 'background_edge'
63                 tlc = [1 phi + 3];
64             case 'background_free'
65                 tlc = [2 * phi + 3 2 * phi + 3];
66             case 'foreground_corner'
67                 tlc = [phi + 2 phi + 2];
68             case 'foreground_edge'
69                 tlc = [1 phi + 2];
70             case 'foreground_free'

```

```

70         tlc = [1 1];
71     end
72
73     % Set bottom right corner of the ROI (always
74     % [2 * phi + 3, 2 * phi + 3]):
75     brc = [2 * phi + 3 2 * phi + 3];
76
77     % Determine modulus of the top left corner of the ROI:
78     mod_tlc = mod(tlc(1) + tlc(2), 2);
79
80     % Generate ROI pattern:
81     for i = tlc(1) : brc(1)
82         for j = tlc(2) : brc(2)
83             if mod(i + j, 2) == mod_tlc
84                 V(i, j) = 2 * c_bg;
85             elseif mod(i + j, 2) ~= mod_tlc
86                 V(i, j) = 0;
87             end
88         end
89     end
90
91     % Loop over statistical significances:
92     for alpha = alphas
93
94         % Calculate different statistical significances:
95         alpha_bin = alpha;
96         alpha_o = power(alpha / phi, 2 / (phi + 1));
97         alpha_c = alpha / phi^2;
98         alpha_oc = power(alpha / phi^3, 2 / (phi + 1));
99
100        % Calculate thresholds based on alphas:
101        [t_bin, alpha_bin] = Threshold(alpha_bin, increment)
102        ;
103        [t_o, alpha_o] = Threshold(alpha_o, increment);
104        [t_c, alpha_c] = Threshold(alpha_c, increment);
105        [t_oc, alpha_oc] = Threshold(alpha_oc, increment);
106
107        % Initialize counter for errors:
108        err = zeros(max_sigma, 4);

```

```

108         err_test = zeros(max_sigma, 1);
109
110     % Repeat for multiple different randomly generated
noises:
111     for k = 1 : nr_noise
112
113         % Create standard normally distributed noise:
114         eps = randn(2 * phi + 3, 2 * phi + 3);
115
116         % Loop over a range of standard deviations:
117         for sigma = 1 : max_sigma
118
119             % Add noise to the image:
120             F = V + sigma * eps;
121
122             % Perform binarization:
123             I_bin = ROI_Detection(F, t_bin, sigma);
124
125             % Perform binary opening:
126             I_o = ROI_Detection(F, t_o, sigma);
127             I_o = imopen(I_o, SE);
128
129             % Perform binary closing:
130             I_c = ROI_Detection(F, t_c, sigma);
131             I_c = imclose(I_c, SE);
132
133             % Perform binary opening & closing:
134             I_oc = ROI_Detection(F, t_oc, sigma);
135             I_oc = imopen(I_oc, SE);
136             I_oc = imclose(I_oc, SE);
137
138             % Count errors:
139             err(sigma, 1) = err(sigma, 1) + (I_bin(phi +
2, phi + 2) ~= correctVal);
140             err(sigma, 2) = err(sigma, 2) + (I_o(phi +
2, phi + 2) ~= correctVal);
141             err(sigma, 3) = err(sigma, 3) + (I_c(phi +
2, phi + 2) ~= correctVal);
142             err(sigma, 4) = err(sigma, 4) + (I_oc(phi +

```

```

143     2, phi + 2) ~= correctVal);
144
145         % Try test procedure (t_o for I_oc):
146         I_test = imclose(I_o, SE);
147         err_test(sigma, 1) = err_test(sigma, 1) + (
148         I_test(phi + 2, phi + 2) ~= correctVal);
149
150     end
151
152     %
153
154     % Write to .csv file:
155     csvwrite(strcat(folder, '/alpha', num2str(alpha), '/
156     phi', num2str(phi), '/', pixelPos, '.csv'), [sigma_range' (
157     err(:, 1) / nr_noise) (err(:, 2) / nr_noise) (err(:, 3) /
158     nr_noise) (err(:, 4) / nr_noise)])
159     csvwrite(strcat(folder, '/alpha', num2str(alpha), '/
160     phi', num2str(phi), '/', pixelPos, '_test.csv'), [sigma_range
161     ' (err_test(:, 1) / nr_noise)])
162
163     end
164
165 end
166
167 end

```

Listing 4: *MATLAB* implementation of the algorithm determining the error rates for the different pixel positions.